Order Number: 42423

Université de Lille

Doctoral School **Sciences Pour l'Ingénieur**

University Department **CRIStAL**

Thesis defended by

Ibrahim ABDALLAH

on **23rd November, 2017**

In partial fulfilment of the requirements for the PhD degree from Université de Lille

Academic Field **Automatics et industrial computer science**

Event-Driven Hybrid Bond Graph

Application: Hybrid Renewable Energy System for Hydrogen Production and Storage

Thesis supervised by Belkacem OULD BOUAMAMA — Supervisor
Anne-Lise GEHIN — Co-Supervisor

Committee members

Referees	Wolfgang BORUTZKY	Professor at Bonn-Rhein-Sieg University -Germany
	Christophe TURPIN	CR-HDR CNRS Université de Toulouse -France
Examiners	Marie-Cécile PÉRA	Professor at Université de Franche Comté -France
	Dominique SAUTER	Professor at Université de Lorraine -France
	Aziz NAAMANE	HDR Lecturer at Université Aix-Marseille -France
Guest	Claire BUGNER	Chargée de mission au Conseil régional Hauts-de-France

Université de Lille

Doctoral School **Sciences Pour l'Ingénieur**

University Department **CRIStAL**

Thesis defended by

Ibrahim ABDALLAH

on **23rd November, 2017**

In partial fulfilment of the requirements for the PhD degree from Université de Lille

Academic Field **Automatics et industrial computer science**

Event-Driven Hybrid Bond Graph

Application: Hybrid Renewable Energy System for Hydrogen Production and Storage

Thesis supervised by	Belkacem Ould Bouamama	Supervisor
	Anne-Lise Gehin	Co-Supervisor

Committee members

Referees	Wolfgang Borutzky	Professor at Bonn-Rhein-Sieg University -Germany
	Christophe Turpin	CR-HDR CNRS Université de Toulouse -France
Examiners	Marie-Cécile Péra	Professor at Université de Franche Comté -France
	Dominique Sauter	Professor at Université de Lorraine -France
	Aziz Naamane	HDR Lecturer at Université Aix-Marseille -France
Guest	Claire Bugner	Chargée de mission au Conseil régional Hauts-de-France

Université de Lille

École doctorale **Sciences Pour l'Ingénieur**

Unité de recherche **CRIStAL**

Thèse présentée par

Ibrahim ABDALLAH

Soutenue le **23 novembre 2017**

En vue de l'obtention du grade de docteur de l'Université de Lille

Discipline **Automatique et informatique industrielle**

Bond Graph hybride piloté par événements

Application : Système d'énergie renouvelable hybride pour la production et le stockage de l'hydrogène

Thèse dirigée par	Belkacem Ould Bouamama	directeur
	Anne-Lise Gehin	co-encadrante

Composition du jury

Rapporteurs	Wolfgang Borutzky	professeur au Bonn-Rhein-Sieg University -Germany
	Christophe Turpin	CR-HDR CNRS Université de Toulouse -France
Examinateurs	Marie-Cécile Péra	professeur à l'Université de Franche Comté -France
	Dominique Sauter	professeur à l'Université de Lorraine -France
	Aziz Naamane	MCF HDR à l'Université Aix-Marseille -France
Invitée	Claire Bugner	Chargée de mission au Conseil régional Hauts-de-France

Keywords: hybrid systems, renewable energy, hybrid bond graph, supervision, power and energy management

Mots clés : systèmes hybrides, énergies renouvelables, bond graph hybrides, supervision, gestion de la puissance et de l'énergie

This thesis has been prepared at

CRIStAL
Centre de Recherche en Informatique, Signal et Automatique de Lille
CNRS UMR 9189
Avenue Paul Langevin
59650 Villeneuve d'Ascq

The enchanting charms of this sublime science reveal only to those who have the courage to go deeply into it.

Carl Friedrich Gauss

I would rather have questions that can't be answered than answers that can't be questioned.

Richard Feynman

Event-Driven Hybrid Bond Graph

Application: Hybrid Renewable Energy System for Hydrogen Production and Storage

Abstract

From a general perspective, this research work constitutes a general contribution towards a simpler modelling and diagnosis of the multidisciplinary hybrid systems. Hybrid renewable energy systems where hydrogen, as an energy vector, is used to store the surplus of the renewable power fits perfectly under this description. Such system gathers different energetic components which are needed to be connected or disconnected according to different operating conditions. These different switching configurations generate different operating modes and depend on the intermittency of the primary sources, the production needs, the storage capacities and the operational availability of the different material resources that constitute the system. The switching behaviour engenders a variable dynamic which is hard to be expressed mathematically without investigating all the operating modes. This modelling difficulty is transmitted to affect all the model-based tasks such as the diagnosis and the operating mode management. To solve this problematic, a new modelling tool, called event-driven hybrid bond graph, is developed. Entirely graphic, the proposed formalism allows a multidisciplinary global modelling for all the operating modes of the hybrid system at once. By separating the continuous dynamic driven by the bond graph, from the discrete states modelled by an integrated automaton, the proposed approach simplifies the management of the operating modes. The model issued using this methodology is also well-adapted to perform a robust diagnosis which is achievable without referring back to the analytical description of the model. The operating mode management, when associated with the on-line diagnosis, allows the implementation of reconfiguration strategies and protection protocols when faults are detected. This thesis is written in 5 chapters. After a general introduction that presents the context and the problematic, the first chapter presents the state of art of the modelling and the diagnosis of the multi-sources systems. The proposed event-driven hybrid bond graph is detailed in chapter 2. The third chapter introduces the diagnosis and the operating mode management. Chapter 4 presents the application and chapter 5 is preserved for the general conclusion.

CRIStAL

Centre de Recherche en Informatique, Signal et Automatique de Lille – CNRS UMR 9189 – Avenue Paul Langevin – 59650 Villeneuve d'Ascq

Bond Graph hybride piloté par événements

Application : Système d'énergie renouvelable hybride pour la production et le stockage de l'hydrogène

Résumé

Ce travail de thèse constitue, d'un point de vue général, une contribution à la modélisation et au diagnostic des systèmes multi-domaines hybrides. Il est appliqué à la supervision des systèmes multi-sources de production d'énergie propre où l'hydrogène est utilisé comme moyen de stockage. Un tel système associe des composantes énergétiques de nature différente et fait l'objet de commutations produites par la connexion et la déconnection d'un ou plusieurs composants. Ces commutations génèrent différents modes de fonctionnement et sont liées à l'intermittence des sources primaires, aux besoins de production, aux capacités de stockage et à la disponibilité opérationnelle des ressources matérielles qui constituent le système. La présence de ces commutations engendre une dynamique variable qui est classiquement difficile à exprimer mathématiquement sans exploiter tous les modes. Ces difficultés de modélisation se propagent pour affecter toutes les tâches dépendantes du modèle comme le diagnostic et la gestion de modes de fonctionnement. Pour résoudre ces problématiques, un nouvel outil, appelé, Bond Graph Hybride piloté par événements a été développé. Entièrement graphique, le formalisme proposé permet une modélisation interdisciplinaire globale du système quel que soit son mode de fonctionnement. En séparant la dynamique continue gérée par le Bond Graph Hybride des états discrets modélisés par un automate intégré au formalisme, l'approche proposée simplifie la gestion des modes de fonctionnement. Le modèle issu de cette méthodologie est également bien adapté au diagnostic robuste, réalisable sans recourir aux équations analytiques. Cette gestion des modes de fonctionnement associée au diagnostic robuste permet l'implémentation de stratégies de reconfiguration et de protection en présence de défaillances. Le mémoire de thèse est décomposé en cinq chapitres. Après une introduction générale qui présente le contexte et la problématique, le premier chapitre présente un état de l'art sur la modélisation et la supervision des systèmes multi-sources. Le BGH piloté par événement est détaillé dans le deuxième chapitre. Le troisième chapitre est consacré au diagnostic et à la gestion des modes de fonctionnement. Le quatrième chapitre présente l'application et le cinquième donne une conclusion générale.

Acknowledgments/remerciements

Ce mémoire résume mes travaux de recherche effectués dans le cadre de ma thèse de doctorat au Centre de Recherche en Informatique, Signal et Automatique de Lille (CRIStAL). Il me semble essentiel de remercier tous ceux qui ont contribué à l'aboutissement de ce projet.

Je remercie tout d'abord la direction de CRIStAL et l'université de Lille de m'avoir accueilli au sein de leurs équipes de recherches.

Mes remerciements vont aussi pour les différents financeurs, particulièrement l'université de Lille, la région Hauts-de-France et Polytech de Lille, qui, au travers de leur soutien matériel, ont reconnu mon travail et m'ont fait confiance.

Ce travail n'aurait pu être bien réalisé sans l'aide de mes superviseurs: Monsieur Belkacem Ould Bouamama et Madame Anne-Lise Gehin. Je sais tout gré pour leur encadrement, leurs conseils, leur patience ainsi que pour l'aide apportée au développement et à la rédaction de ce document ainsi que les autres publications.

Je tiens à remercier vivement Monsieur Wolfgang Borutzky, professeur à l'université Bonn-Rhein-Sieg et Monsieur Christophe Turpin, chargé de recherche HDR CNRS à l'université de Toulouse, d'avoir accepté d'être les rapporteurs de ce mémoire de thèse. Je remercie également les membres du jury, Madame Marie-Cécile Péra, professeur à l'université de Franche Comté, Monsieur Dominique Sauter, professeur à l'université de Lorraine, Monsieur Aziz Naamane, professeur à l'université Aix-Marseille et Madame Claire Bugner, chargée de mission au Conseil régional Hauts-de-France.

Je tiens à remercier profondément tous ceux qui m'ont encouragé pendant mon parcours, surtout ma mère qui a éveillé en moi l'intérêt et la curiosité envers la science et sans oublier mon père et mon frère pour son immense soutien.

J'adresse aussi mes remerciements à ma grande famille de mes amis en France et au Liban, je suis très reconnaissant pour leur soutien, pour tous les bons moments, les fêtes, les vacances que l'on a passés ensemble. Je remercie mes collègues à l'université libanaise surtout mes colocataires les parisiens Youssef et Georges. Je remercie aussi Alexandre, Théo, Alaa, Jad (na2), Ribal, Marie, Jean-Baptiste, Mathilde et Nathalie. Je n'oublie pas de mentionner Sbeity et Akhdar ainsi que l'équipe et les voisins dans la résidence Reeflex Nemer, Jad, Jean, Serge, Mahmoud, Christian, Mohamad, Sami, Ali, Khoder, Mahdi, Ayman et Nicolas. Finalement, merci à tous mes collègues au CRIStAL, particulièrement Joëlle, Beranger, Yuqi, Houria, Adel et Gerardo...

Un grand merci à tous.

Acronyms

ARR	Analytical Redundancy Relation.
BD	Block Diagram.
BG	Bond Graph.
BGD	Bond Graph Diagnoser.
DES	Discrete Event System.
DFIG	Double Fed Induction Generator.
DS	Dynamical System.
EDHBG	Event-Driven Hybrid Bond Graph.
EEC	Equivelant Electrical Circuit.
EL	Electrolyser.
EMR	Energetic Macroscopic Representation.
FC	Fuel Cell.
FDI	Fault Detection and Isolation.
FFC	Feeder-Flow Control.
FSM	Fault Signature Matrix.
GARR	Global Analytical Redundancy Relation.
HA	Hybrid Automaton.
HBG	Hybrid Bond Graph.
HBGD	Hybrid Bond Graph Diagnoser.
HDS	Hybrid Dynamical Systems.
HEV	Hybrid Electrical Vehicule.
HPN	Hybrid Petri Net.
HRES	Hybrid Renewable Energy System.
LFT	Linear Fractional Transformation.
LG	Linear Graph.
MBD	Model-Based Diagnosis.
MPN	Mixed Petri Net.
MPP	Maximum Power Point.
Mppt	Maximum Power Point Tracking.
OC	Operating Condition.
ODE	Ordinary Differential Equation.
OM	Operating Mode.
OMM	Operating Mode Management.
PEM	Proton Exchange Membrane.
PMG	Permanent Magnet Generator.
PN	Petri Net.

PV	Solar Photovoltaic Panel.
RE	Renewable Energy.
SDG	Signed Direct Graph.
SoC	State of Charge.
SSE	State-Space Equations.
STC	Standard Conditions.
STG	Standard Temperature and Irradiation.
UC	Ultra-Capacitor.
UG	Utility Grid.
UPC	Unit Power Control.
WT	Wind Turbine.

Table of content

List of Tables

List of Figures

General Introduction

PhD thesis framework

The research results summarized in this PhD thesis are obtained at CRIStAL (Centre de Recherche en Informatique, Signal et Automatique de Lille, CNRS UMR 9189) under the supervision of Professor Belkacem Ould Bouamama and Doctor Anne-Lise Gehin. This work is performed in the framework of a global project concerning the domain of the sustainable energy development. It is supported by the University of Lille, the school Polytech Lille and the region Hauts-de-France. This support is manifested through funding the subventions of the PhD grant and covering the cost of the experimental platform.

General context

Today electricity production and the transport sectors represent the major contributors in inducing the global warming [1]. Due to the fast growing in the energy demand, this energy-pollution dilemma pushes more than ever toward an energy transition using clean energy sources. Solar and wind energies, as the most abundant energy sources, represent sustainable clean alternatives to confront the increasing climate change and pollution problems. However, despite their long-term sustainability, these sources are not permanently available and they do not provide stable power. Their power production depends on variant factors such as the random conditions of the ambient environment, the weather, the day-night and seasonal cycles. The fact that the majority of renewable sources does not provide a stable power over daily-time basis emphasizes the need of a power storage unit. Moreover, due to the seasonal intermittency between the solar and the wind energy as shown by Fig. 1, combining both sources contributes in increasing the overall seasonal reliability of the system.

For the local storage units, different techniques can be used to store the surplus

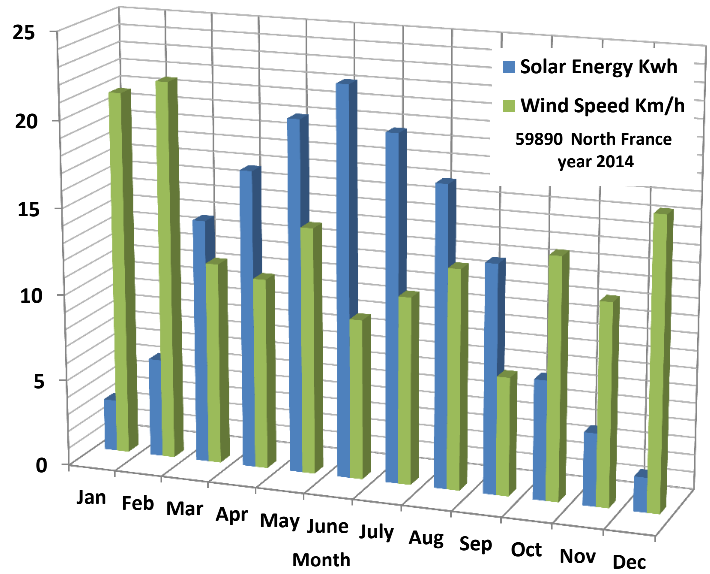

Figure 1 – Wind and Solar energy seasonal intermittency in north of France [2]

of the generated power by the renewable sources. In fact, each storage technology is characterized by two main criteria: the energy and the power capacities. The energy capacity is defined as the total amount of energy that can be stored in the conventional size of the concerned storage. Capacitors, for example, are known for their small energy capacity, while batteries are used to store much more energy. The power capacity defines how fast the stored energy can be recovered. In this case, capacitors are high power storage devices while batteries tolerate medium power.

Fig. 2 illustrates the main power/energy storage options used in the Hybrid Renewable Energy System (HRES). The figure shows the classification of the storage techniques according to their power and energy capacities. The choice of the storage techniques depends on the system objectives. Of course, the batteries are the most widely used storage technology in the HRES. They represent a fair trade between the capacity and the power oriented storage.

However, the storage capacity of the batteries is limited, and since they store power chemically, they are not a very practical solution for long-term storage, other factors support this such as the degradation, self-discharge and power losses.

As an interesting energy carrier, hydrogen is an energy oriented storage, it represents a suitable solution for long-term and large-scale storage. It offers more flexibility in the storage scale, when needed more hydrogen tanks can be added with less material involvement. The dynamical characteristics of the hydrogen related equipments Electrolyser (EL)/Fuel Cell (FC) make the hydrogen storage characterized as a slow

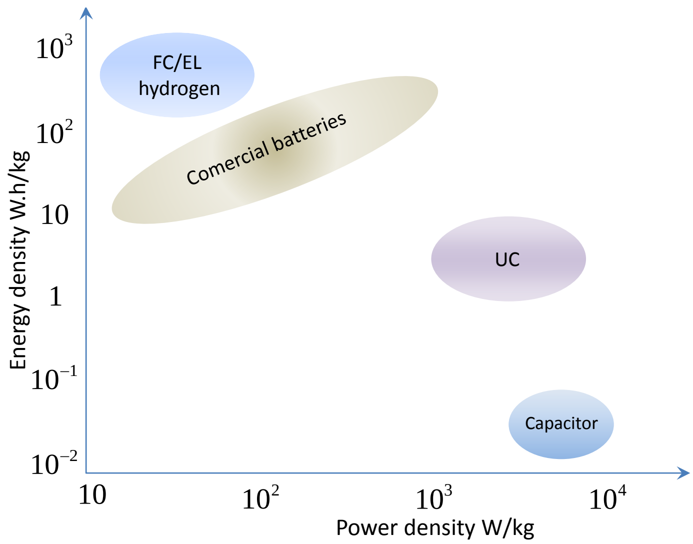

Figure 2 – Ragone plot: power and energy oriented stationary storage technologies

dynamical storage. For high power systems Ultra-Capacitor (UC) can be considered. For system where both energy and power capacities matters such as in the electrical cars hybrid storage such as UC/ battery is considered.

In this work, we are more interested in the hydrogen/ battery hybrid storage. The produced hydrogen represents a unique use flexibility, it can be stored to eventually regenerate electricity, mechanical work or to be used in various chemical applications. As car fuel, hydrogen can be transmitted from the storage tank to the car tank more effectively and faster than charging the embedded batteries. These hydrogen applications are illustrated in Fig. 3, the figure shows how hydrogen can play a major key role in controlling the pollution on many levels. Providing solutions for both major pollution sources: production of electricity and the transportation, hydrogen can lower the dependency on carbonized fuel in both contexts electrical cars [3, 4] and combustion engine powered vehicles [5, 6]. It also can be used as power source in stationary applications. As a raw product, it can be involved in many chemical process. Methanation, for example, is one interesting chemical application where greenhouse gases: (carbon oxides (CO_2, CO)) and hydrogen are used to produce Methane. It can also be mixed with the Methane to produce Hythane (mixture of 20% hydrogen and 80% Methane).

One main step holding the expansion of the hydrogen production through electrolysis, is the cost of the electrolyser and the lifetime of the fuel cell. Combined with multiple renewable energy sources, the EL and the FC represent interesting energy storage

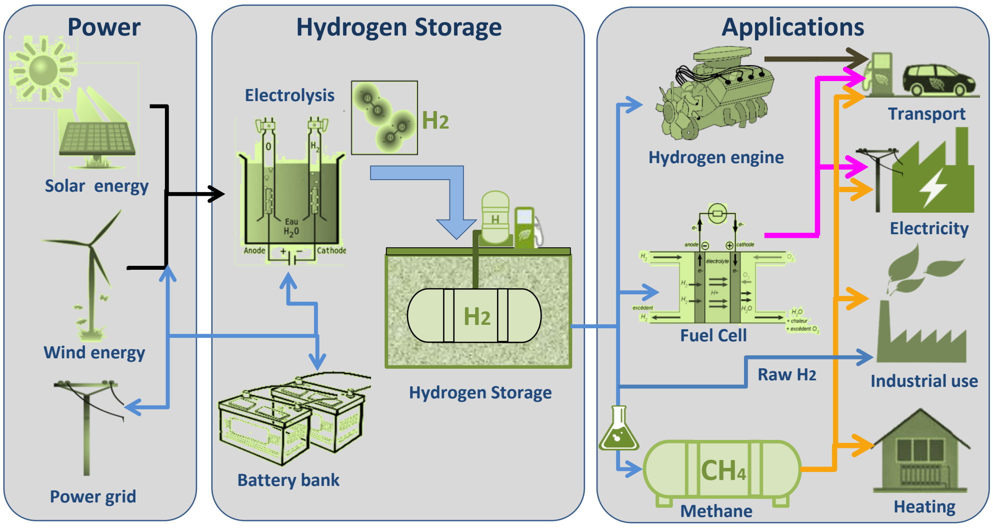

Figure 3 – Green hydrogen applications: variety and flexibility

devices. They couple electricity, as the most common useful energy form, with hydrogen, as a zero-emission flexible energy storage. When produced using electricity issued from renewable sources, green hydrogen can lower the cost of the energy production. From energetic point of view, such combined systems are often defined HRES.

Hybrid Renewable Energy Systems (HRES)

A HRES represents set of energy components that belong to different energetic domains in order to harvest energy from multiple sources, transform it into electricity and then store it. The stored energy is recovered when needed. This kind of HRES allows higher reliability and higher power generation of the conventional single source single storage renewable systems.

From dynamical point of view, some HRES units (such as the wind turbine, electrolyser, fuel cell and utility grid...) have different operating modes. They need to be disconnected and reconnected to the power system according to different operating conditions and protection measures. Having such interconnection between different varieties of sources and storage units, where each or some can be connected and disconnected, engenders a dual discrete-continuous dynamical behaviour. Mathematically, this implies that the system dynamical behaviour, usually described by the State-Space Equations (SSE), evolves continuously with respect to the time and discontinuously according to the Operating Mode (OM) (switching state). Therefore, for each OM a different set of SSE is needed to represent the dynamical behaviour. In control and automatic engineering, this class of systems is identified as Hybrid Dynamical Systems (HDS) or more precisely switching systems. Because of this dual dynamical aspect, such systems are very difficult to be interpreted as fully continuous nor as only discrete.

It worth to note that in this work, we would refer by the word hybrid to both characteristics (continuous-discrete dynamic) and multi-domain energetic process.

Power and operating modes management

Operating Modes Management

We donate by OM the discrete state of the system in which it operates according to a fixed and well-defined set of working components. Different OM can be identified for any system with different number of available components and different control strategies. In case of the HRES, a transition from one OM to another occurs when one or more component is disconnected or reconnected to the global system. This OM transition can be controlled externally or autonomous depending on inner conditions such as the state variables of the system. The fact that different OM are related to different active-inactive component configurations emphasises the need for a Operating Mode Management (OMM) strategy to control the component connections/disconnections. It is obvious that the lower layer of the continuous control that drives the power flow in or out of each component changes for each component configuration i.e OM.

Power and energy management

The power management refers to the lower layer of the power control allowing to satisfy the user predefined operating conditions for each component of the HRES.

It consists of managing the power flow, extracted via the renewable sources and directed it into the different storage units. Since the power management is related to the HRES operating components, for each OM a specific power management strategy can be applied conveniently to the active components. The control laws for each component are usually continuous and based on conditions such as, meeting the load power, the common bus voltage stability, storage capacity, components power limits, power quality, predictions, etc. On the other hand the energy management takes in consideration the amount of the stored/produced energy. Normally, it defines the storage switching OMM according to the stored energy in each unit.

It is worthy to note that in the literature the expression power and energy management is used to denote both concepts: switching OMM and the set of the control law for the each of the active components.

As a consequence for having the different OM with the OMM, HRES modelling becomes more complicated. The model is needed to be very flexible to test many OMM strategies. Showed in Fig. 4, many other model-based tasks relying on the modelling become quite challenging such as the cost-operating study, designing and sizing studies, control, observers, Model-based diagnosis, optimization, training, prognostic and system checking etc...

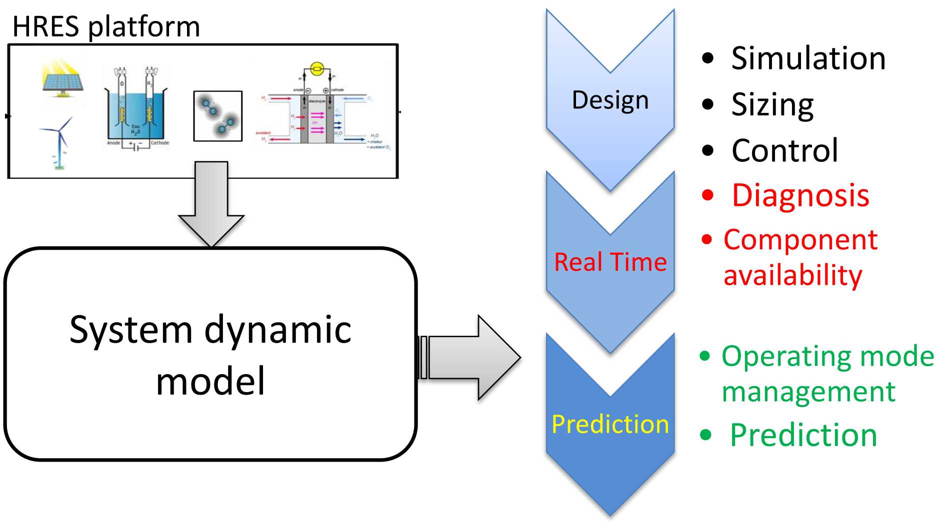

Figure 4 – HRES model-based tasks

The majority of the existing modelling methods in the HDS literature tends to use a multi-model or/and heterogeneous graphical-analytical approach in which empirical and analytical models are used to describe the real system behaviour. While some are very hard to derive, others do not reflect the system structure neither the physical sense of the occurring phenomena. In such methods, an engineer, in order to derive an appropriate model, would need deep knowledge in all the related fields along with all the different operating modes of the hybrid dynamics. This can be very exhausting and time-consuming for large systems specially when accompanied with the multidisciplinary aspect as in the case of the HRES.

Problematic

Dynamic modelling represents the first step toward the proper design of any system. Designing tasks such as sizing, operating condition management, control, diagnosis and cost studies are very crucial but simply achievable through an adequate modelling. Energy and power efficiency of the HRES depend heavily on the implemented OMM. The OMM choice can not be based on only the real-time or short-time estimation of the system optimal configuration. Running simulations using a whole year historical weather data, available global wide (such as the mean solar intensity, daylight time and mean temperature), can be a very essential key to increase the system reliability/availability and avoid the power shortages, the undersizing, oversizing... This shows the vital utility of having virtual prototyping for the HRES that allows performing simulations for long-term periods in relatively short-time of computing. Having that said, estimating the global efficiency based on long-term simulations is sensible and very dependent on the implemented OMM. The utility of the model does not stop on this conception phase, many model-based tasks rest on the easiness and the flexibility of finding and modifying the model. The model-based diagnosis constitutes an example of such tasks. The diagnosis can play a non-negotiable role in the reliability, the safety and the protection of such system. In real-time, it can be used to define the unavailable services and components following to failure detection and isolation. This indicates the dependence of the OMM on the diagnosis results.

The common main problem in all these tasks is the difficulties encountered in the modelling of such systems. The multidisciplinary aspect of the different components (chemical, mechanical, electrical and thermofluidic) and their energy coupling constitute the main deadlocks that makes the modelling effortful since deep physical knowledge in various domains is required. Additionally, the switching behaviour induces different set of non-linear dynamical equations that describe the system, this suggests that to extract the model, the user must investigate all the component possible configurations i.e OM separately. These two issues constitute the general challenges for the whole class of the HDS with multi-physical dynamics. Combined with the need to implement different OMM strategies for long-period simulations, the previous problems can be more serious for the HRES in particular.

Other modelling challenges are more related to the HRES in particular. For instance, the components are characterized by high non-linearities in the behaviour. Having this combined with the cellular structure, the existing non-linearity in each cell makes the model need an enormous computing power. A trade between the explicit structural modelling and the model reduction is needed.

All the challenges encountered in the modelling constitute also obstruction factors in achieving other model-based tasks such as the model-based diagnosis. Beside the modelling-related problems, the model-based diagnosis for HRES faces other complications. First, the existing model-based approach must be compatible with the multi-physical nature of the system along with the changing dynamic due to the switching and flexible with the change of the OMM strategies. The diagnosis approach must be consistent and coherent with the modelling approach. If the model uses graphical representation, the diagnosis need to avoid expressing the algorithm in equation-based approach. When different paradigms are used, deriving the needed representation is more time-consuming and can strip the advantage of having less physical knowledge offered initially by the proposed modelling. Moreover, since the modelling parameters are never obtained with full accuracy, the diagnosis must allow to include the parametric uncertainties to achieve a robust Fault Detection and Isolation (FDI).

From a general perspective, this research work constitutes a general contribution towards a simpler modelling and diagnosis of the multidisciplinary switching systems. HRES where hydrogen is used to store the surplus of the renewable power fits perfectly under this description. A such system gathers different energetic components which are needed to be connected or disconnected according to different operating conditions. These different switching configurations generate different operating modes and depend on the intermittency of the primary sources, the production needs, the storage capacities and the operational availability of the different material resources that constitute the system. The switching behaviour engenders a variable dynamic which is hard to be expressed mathematically without investigating all the operating modes. This modelling difficulty is transmitted to affect all the model-based tasks such as the diagnosis and the operating mode management. To solve this problematic, a new modelling tool, called event-driven hybrid bond graph, is developed. Entirely graphic, the proposed formalism allows a multidisciplinary global modelling for all the operating modes of the hybrid system at once. By separating the continuous dynamic driven by the bond graph, from the discrete states modelled by an integrated automaton, the proposed approach simplifies the management of the operating modes. The model issued using this methodology is also well-adapted to perform a robust diagnosis which is achievable without referring back to the analytical description of the model. The operating mode management, when associated with the on-line diagnosis, allows the implementation of reconfiguration strategies and protection protocols when faults are detected.

Contributions

The general contributions offered by this work can be generalized for all the class of the hybrid dynamical systems characterized with a multi-physical dynamic. They can be related to the HRES modelling, the robust diagnosis, the OMM and the reconfiguration.

Scientific methodological contributions

General

- ✓ Developing new modelling tool named Event Driven Hybrid Bond Graph for multidisciplinary switching systems.
- ✓ Adapting the approach to achieve the OMM separately from the dynamic of the system and based on the operating conditions.
- ✓ Achieving the model-based diagnosis using the graphical Bond Graph without referring to the analytical equations of the model.
- ✓ Extend the graphical diagnosis approach to include the parameter uncertainties in order to generate robust FDI with dynamical and adaptive thresholds.
- ✓ Use the model causality properties to create a map for the available services in case of detected failure.
- ✓ Include the diagnosis results in the OMM to achieve a reconfiguration strategy.

HRES specific

- ✓ Developing the existing theory of the Hybrid Bond Graph in order to cover systems with cellular structure.
- ✓ Developing the LFT for the active bond graph resistance elements RS.

Technical contributions

- ✓ Modelling the HRES using the developed BG theory and assemble the global model using the Event Driven Hybrid Bond Graph.
- ✓ Developing a parameterized simulator including all the common components of typical HRES.
- ✓ Validation of the model using an experimental set-up.
- ✓ Testing the simulator with proposed OMM and reconfiguration over one-day weather data.

In addition, since in the literature the electrolyser robust diagnosis is not addressed, most of the analytical demonstration are given and detailed using the electrolyser as an example for a pedagogical illustration.

Validation

The results were the subjects of 4 international conference presentations, listed here:

- I. Abdallah, A.L Gehin et B. Ould-Bouamama, « Event driven hybrid bond graph for diagnosis », IEEE European Control Conference (ECC) 2016 , Aalborg Denmark, July 01, 2015.
- I. Abdallah, A.L Gehin and B. Ould-Bouamama, « Functional Hybrid Bond Graph for Operating Mode Management », IFAC ICONS, Reims France, June 03, 2016
- I. Abdallah, A.L Gehin and B. Ould-Bouamama, «Hybrid Bond Graph Modelling of Multi-Source System for Green Hydrogen Production», IEEE MED'17 2017, Valletta Malta, July 06, 2017
- I. Abdallah, A.L Gehin and B. Ould-Bouamama "Bond Graph for Online Robust Diagnosis Application: Hydraulic System", IFAC 2017 World Congress, Toulouse, July 13, 2017

Moreover, 3 articles were submitted to international journals. The details of these publications are as follows:

- I. Abdallah, A.L Gehin and B. Ould-Bouamama, "On-line Robust Graphical Diagnoser for Hybrid Dynamical Systems", submitted to Engineering Applications of Artificial Intelligence in January 2017. Accepted in May 2017.
- I. Abdallah, A.L Gehin and B. Ould-Bouamama, « Event Driven Hybrid Bond Graph for Hybrid Renewable Energy Systems. Part I: Modelling and Operating Mode Management", submitted to International Journal of Hydrogen Energy in May 2017. Accepted in October 2017
- I. Abdallah, B. Ould-Bouamama and A.L Gehin, « Event Driven Hybrid Bond Graph for Hybrid Renewable Energy Systems. Part II: Robust diagnosis and Operating Mode Management", submitted to International Journal of Hydrogen Energy in May 2017. In review

The thesis structure

The present PhD thesis is written in 5 chapters. After this current general introduction, the first chapter addresses the state of art of the modelling, the diagnosis and the operating mode management of the HRES. The modelling and the diagnosis methods provided by the literature of the multi-physical and the hybrid systems are also exposed.

The second chapter introduces the Event-Driven Hybrid Bond Graph (EDHBG) tool for the HRES modelling. In this chapter, first the BG is adapted for the HRES modelling. New elements are defined allowing to represent the cellular structure of most of the HRES components. Other elements are modified or generalized allowing to model coupled phenomena. Then the proposed tool is introduced to include the OMM. The second part of this chapter addresses the inclusion of the modelling uncertainties taking into account the HRES specific BG elements.

The third chapter extends the developed approach in order to perform and implement the robust FDI. The chapter starts by explaining the classical approaches used to generate the equation-based diagnosis. Then it is shown how to use the modelling approach proposed in chapter II to perform graphical diagnosis. The proposed diagnosis approach is extended to include the parametric uncertainties allowing a robust fault detection. In the final part of this chapter, the OMM is developed to include the real-time diagnosis results.

In the fourth chapter, the proposed approach is applied on a representative experimental multi-source platform. Normal and faulty behaviours of the system are considered. The on-line diagnosis helps defining the available services and the possible OM. In case of a crucial fault detection, a safety OM is considered. In order to monitor the effectiveness of the proposed approaches, simulations of both scenarios are done under the same weather conditions. At the end of this chapter, the results are discussed and compared. The fifth chapter is preserved for a general conclusion and perspective.

Chapter 1

State of art: modelling, diagnosis and Operating Mode Management (OMM) of HRES

1.1 Hybrid Renewable Energy System (HRES)

1.1.1 Introduction

In order to promote the use of the different renewable energies and increase the power reliability of the renewable energy systems, multi-sources can be combined. Due to the daily and the seasonal intermittency between the different sources, combined long-term short-term storages are recommended. Having all these components together suggests the need to implement an OMM that controls the (de)activation of the different components. The modelling represents an essential task that, beside helping to design the system, allows achieving many other tasks such as designing and choosing the propre OMM and implementing a robust model-based diagnosis. The existing modelling techniques in the literature are not suitable to express the model of such systems with many domains involved and with different OM. Another problem facing the modelling is the vital need for an adequate flexibility towards testing different OMM. In the literature several publications are found concerning the HRES, where few have addressed the described problematic. Since many components are involved in those systems, different variety of HRES is found sharing the same purpose.

1.1.2 HRES components and structure

From a structural point of view, renewable energy systems can be classified into two main classes: isolated and grid connected [7, 8].

- Isolated systems provide an energetic independence with less geographical constraints, they are less fault tolerant and require a reliable local power storage. Such systems need to be wisely designed and sized in order to satisfy a high reliability condition and avoid the power shortages.
- Grid connected systems are more reliable less dependent on the storage but they can be more expensive. The environmental footprints of such systems still depends partially on the electrical sources of the grid.

1.1.2.1 Renewable sources in the HRES

As the most abundant renewable energy forms, solar energy and wind energy are worldwide available. They receive an increasing interest in the research and development.

Photovoltaic solar panels (PV)

The PV is a device that harvests the power provided by the sun irradiations and transforms it into electricity. The PV work relies on generating an electrical current from the electrons mobilised by absorbing the sun radiation. Fig. 1.1 shows the PV general concept, where I_{ph} represents the global current of the mobilised electrons by absorbing the incident photons. Some part of the mobilised current passes through the N-P layer junction, this is often expressed as the diode reverse current I_d. The remaining current I_r constitutes the net generated power without counting the ohmic losses through and between the different layers. Today many Solar Photovoltaic Panel (PV) technologies exist, the majority are silicon-based (others are Gallium Arsenide-based). In the silicon-based class, there is the mono-crystalline and poly-crystalline PV. Mono-crystalline PV are characterized by higher efficiency due to higher silicon purity, they require more processing (Czochralski process) to be produced therefore there are more expensive. Poly-crystalline PV are generally less efficient and manufactured more simply, they are more affordable. Both PV types maintain the same functioning principles and phenomena, their efficiency differences are resulting from the difference in the silicon structure and purity. There is a large mathematical physical theory that describes the phenomena involved in the PV functioning. Fig. 1.2 shows a very popular equivalent electrical model of the PV. This very common one-diode electrical model

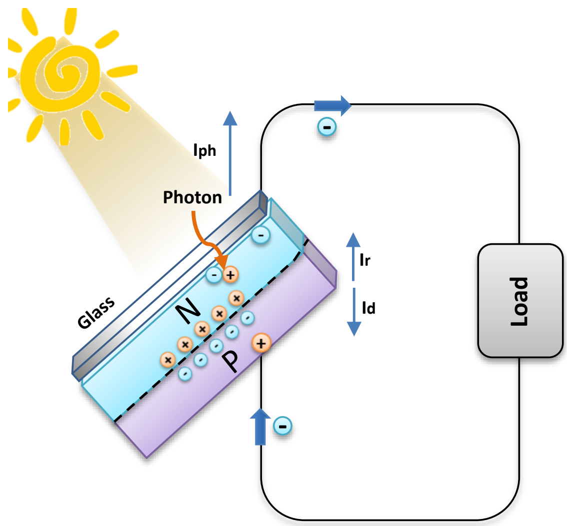

Figure 1.1 – PV functioning general concept

consists on modelling the total current I_{ph} by a current source. The diode d mounted in parallel to the current source I_{ph} represents the diode reverse current losses. R_s and R_{sh} represent respectively the serial and shunt resistances. For more accuracy, some

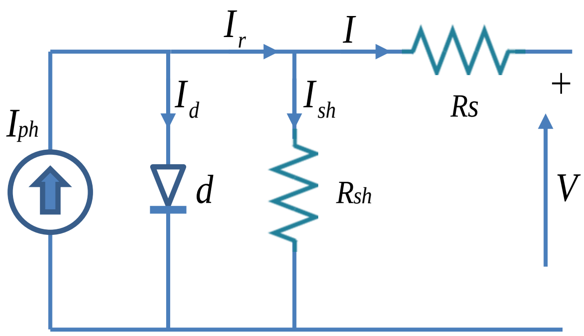

Figure 1.2 – PV cell one-diode electrical model

works have considered a PV model with more than one diode [9], others have studied the serial or the parallel resistance effect on the model accuracy [10]. For instance, Bajpai et al. [8] has reviewed number of published works of many electrical equivalent models for the PV. Depending on the required accuracy and the available computing power, different modelling assumptions can be carried out.

A PV module is assembled using many PV cells mounted in different configurations (serial-parallel). The mathematical equations describing the PV behaviour specially the diode are highly non-linear. In a structured modelling, many cells models must be assembled to construct the global model of the module, having one diode model of each cell requires already a huge computing power. Having the two diode model implies spending too much of the processing power on a small improvement in the model accuracy.

From a control point of view, the extracted power from the PV depends on the ambient operating conditions such as (temperature, incident solar irradiation, etc...). For the same ambient conditions, the extracted power is affected by the operating voltage on the output of PV cell as shown by Fig. 1.3. For each combination of the ambient operating conditions, there exist an optimal voltage U_{MPP} at which the extracted power is optimal, this voltage is called Maximum Power Point (MPP).

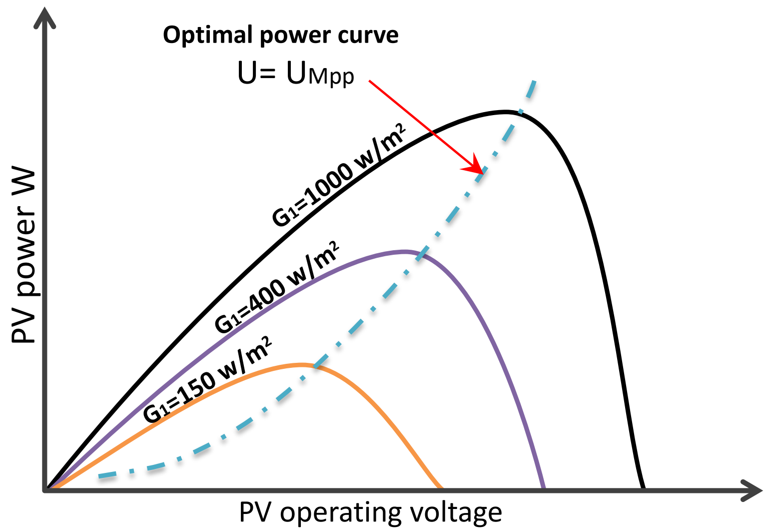

Figure 1.3 – PV optimal power curve

In order to control the operating voltage on the PV model a DC/DC converter is needed. The curve (or 2D surface) that defines the optimal point U_{MPP} according to the irradiation G (and temperature T) is called the optimal voltage curve. It can be obtained experimentally or provided by the manufacture. Having irradiation G and temperature T measurements, the lookup tables can be used to set the PV voltage at the optimal point U_{MPP} using the DC/DC converter.

In [11], Hua et al. introduced the control strategies in order to track the MPP, these algorithms are now called MPP tracking. Different algorithms are proposed, reviewed and compared with different DC/DC converters.

Wind Turbine WT

The WT extracts part of the kinetic energy of wind and turns it into useful mechanical work and then electrical energy. In order to continue blowing, the wind can never be stripped off of all its kinetic energy. Thus, the WT extracted energy is always limited by maximum theoretical limit of 59% (Betz limit). This power extraction efficiency

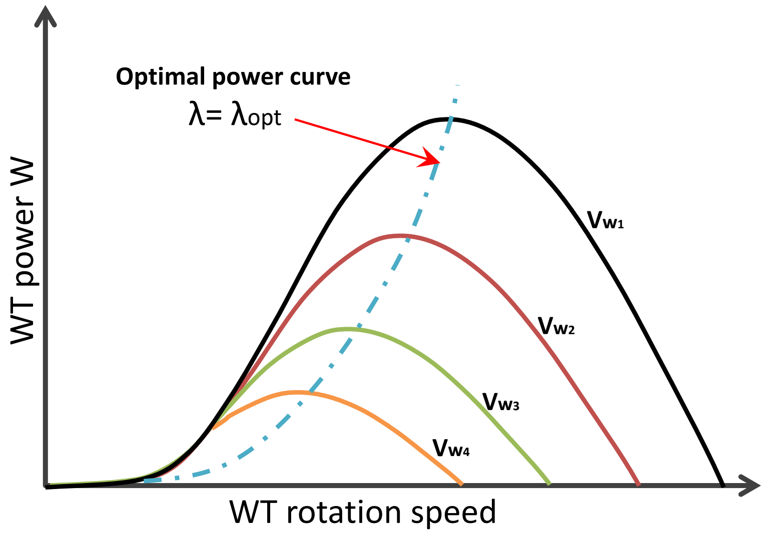

Figure 1.4 – The aerodynamical efficiency of a WT according to the rotation speed on different incident wind speeds

between the wind kinetic energy and the extracted mechanical power is often referred to by the aerodynamical efficiency coefficient denoted as C_p. This latter depends mainly on the aerodynamical properties, the airfoil and the ratio between the incident wind speed v_w and the rotation speed of the WT blades as illustrated by Fig. 1.4. Usually look-up tables are constructed from wind-tunnel experimental tests, nevertheless some authors, such as in [12, 13, 14], have presented analytical empirical Cp formula used into block simulation model.

There is a large variety of Wind Turbine (WT) generators used in the HRES. Mainly, WT are divided based on the control strategies, into two classes: Fixed Speed WT and Variable Speed WT. Fixed speed WT uses control laws that drive the rotating blades at constant speed regardless of the incident wind speed v_{wi}. On one hand, this makes this kind of WT cheaper and less vulnerable to mechanical failures, on the other hand they are characterized with very low efficiency. Variable Speed WT uses control laws that allow controlling the rotating speed of the blades. This kind of WT is more advanced, it allows the WT to extract the maximum power from the incident wind by adapting the rotation speed according to v_{wi}. In [15], Cheng et al. presented and compared variable speed wind turbine generators. In general, two main classes of electrical generators are used in WT, Double Fed Induction Generator (DFIG) and Permanent Magnet Generator (PMG). The WT most used generators are reviewed in [16].

- PMG [17] uses a permanent magnet usually as a rotor as shown in Fig. 1.5, they tend to be used in small power WT. They are more immune to mechanical failures and need less effort in the maintenance.
- DFIG [16] are self induction WT generators where the permanent magnet in the PMG is replaced, as in the asynchronous generators, by electrical coils as illustrated by Fig. 1.6. However, unlike the asynchronous generator, the electrical coils of the rotor are not directly connected to the generator outputs. The output of the generator supplies the rotor with controlled power via converters. These are very common WT generators as they allow very high power and control flexibility.

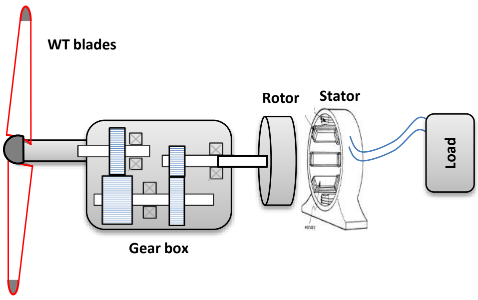

Figure 1.5 – PMG wind turbine schema

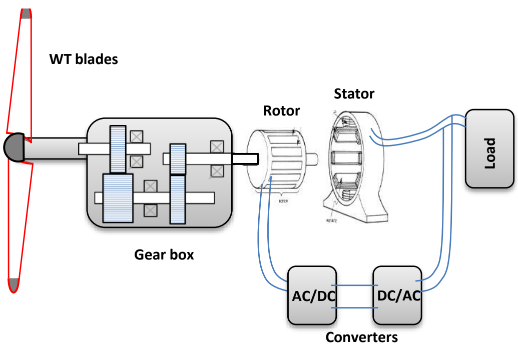

Figure 1.6 – DFIG wind turbine schema

In order to maintain Cp at its maximum, a Maximum Power Point Tracking (MPPT) control algorithm is usually needed. Authors in [18, 19] reviewed nine MPPT for the PMG.

For protection measures, most of the WT have a certain limited operating range, defined according to the incident wind speed between v_{in} and v_{off}. Within its operating range, a WT is usually associated with different OM as illustrated by Fig. 1.7. They are related to many essential limitation factors involved in the WT work. For instance, all the WT needs a minimum wind speed v_{in} to be effectively operational, this limit is called "cut-in" speed. Whenever the wind speed v_w is less than this limit, the WT is in mode I, where it is stopped as the generated power is not enough or does not worth the operational cost of the WT. When the wind speed overpasses the cut in limits $v_w > v_{in}$, the WT operates in mode II. In case of variable speed WT, the control laws will track the optimal rotational speed in order to extract the maximum power. For some high power WT, in order to avoid the mechanical wearing related to the high speed rotation, another OM mode III is triggered when the wind speed reaches v_s ($v_w \succeq v_s > v_{in}$). The mode III changes the control strategy form seeking the WT optimal rotational speed to aim on setting it constant. In order to avoid overpassing the power limits of the WT electrical components, when the wind speed v_w reaches the rated value v_r, the WT starts a power regulation control. Above this limit v_r, the maximum rated power is fixed regardless of the increase in the incident wind speed v_w. Beyond v_{off}, the WT breaking system is set active and the WT is then stopped.

In most of the high power industrial WT, all the four modes are present. However, for small WT, mode III can be sometimes ignored, also but less likely mode IV. Two limits are for sure present in all the WT applications the "cut-in" and the "cut-off" speed.

1.1.2.2 Storage units in the HRES

Most of the renewable sources collect power from the ambient environment, this latter is characterized by cyclic and/or random variations such as the day-sun light and the wind speed etc. The instability in the available power suggests the use of the short-term storage. Because of the seasonal intermittency of the solar and wind renewable energy, a long-term storage is also required. Generally in HRES, there exist many storage technologies. Four solutions are presented:

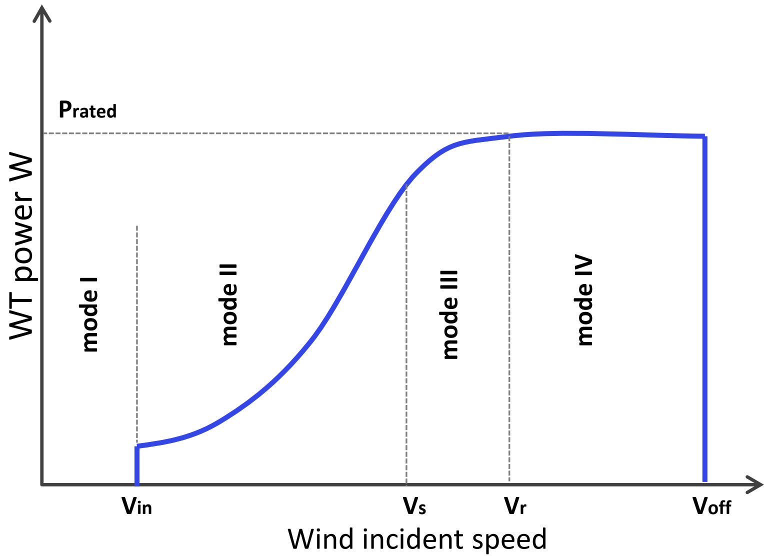

Figure 1.7 – WT different operating modes

Batteries

The batteries are the most used storage technology. They represent of short-term storage device with moderate capacity to mass ratio. Hybrid Electrical Vehicule (HEV) and HRES share the interest in developing battery technologies with high energy capacity, high cyclic charge endurance and low manufacturing costs. Many battery technologies are developed to satisfy these operating conditions and reduce the self-discharge and the ageing. In this context, a progressive improvement in Lithium-based batteries is noticed.

Hydrogen

To store the power in form of hydrogen, three main devices are needed. An EL is supplied by electricity, as a main source, to produce hydrogen from water. The FC in its turn, uses the stored hydrogen to recover and reproduce electricity. Hydrogen tanks are also required.

The EL and the FC present reversibly the same phenomena. For each device, two main technologies are present: alkaline and Proton Exchange Membrane (PEM).
Alkaline EL/ FC uses liquid electrolyte with non noble electrodes. It represents the first introduced electrolysis technology. Despite the fact that it is well-developed and cost effective, this technique does not allow very high current density and high hydrogen purity.
PEM EL/FC uses solid proton exchange electrolyte. It is more suitable for high

current density, high power small size cells allowing more compact systems specially in case of the FC suitable for embedded applications. The PEM provides (resp. requires) a high hydrogen purity (leak-less) and more dynamical operation. However, the PEM is more expensive and have less lifetime spam than the Alkaline technologies. Other techniques such as solid oxide electrolysis are very efficient but still in research phase. Carmo et al. [20] performed a full review and compared all these technologies.

As for the hydrogen storage also, two main technologies are widely used. The first consists in storing hydrogen in a normal container under high pressure. The second is to use the metal hydride. Due to the high specific volume of the hydrogen, the first technique requires lot of energy to be spent on the hydrogen compression. However, the hydrogen containers requires less maintenance. The second technique is more volume effective but more expensive, requires more control (temperature, etc) and has a limited lifetime.

The FC and the EL constitute playgrounds for multi-physical energetic phenomena. These are detailed in Chapter 4.

Ultra-Capacitor

Unlike the Hydrogen storage, UC are characterized with their lower time response. In a multi-storage context, they are used to absorb and provide high power peaks in relatively short-time.

Utility Grid

The Utility Grid (UG) can be used as a backup source and/or a dump storage.

1.1.2.3 HRES coupling options

Having a system with many components of these different options and their combinations to harvest and store the power leads to different coupling configurations and structures. The main classifications found in the literature are described in the list defined below. **Single source HRES** use one type of power source such as PV [21, 22, 23, 24] or WT [25] in different storage contexts (hybrid or single, grid connected, or isolated).

Systems with single source such as PV coupled to battery bank as a single storage are less expensive and categorized as short-term storage systems, they are susceptible of losing part of the stored power and their storage capacity with the time. For a long-term flexible storage unit, solar-hydrogen can be produced via electrolysis in a multiple storage contexts such as (batteries with EL/FC) [6, 23, 24]. To produce solar-hydrogen, an additional cost is needed for hydrogen electrolyser and its storage unit.

A WT may be also used as a single source along with multiple storage system (hydrogen, batteries and ultra-capacitor) [25]. Single sources systems are less defiant against power shortage, failures, specially if they are not grid connected [21]. Having the rated powers, sometimes single sources systems can be more expensive and can harvest less power than multi-sources, this is related to the weather conditions, sources natures and the location. This points out the need for an optimization studies between the (cost-power-components). Such studies provide the perfect set of sources ($n\times$ PV with $m\times$ WT) having the lowest cost to the higher generated power according to the annual weather data.

Multi-source HRES use multiple sources of different natures to harvest renewable energy from the surrounding environment. Having these different sources indicates the possibility of different electrical coupling configurations where the sources can be coupled through a DC or AC bus [26].

DC bus-Coupled Systems: In this configuration, all the different sources are connected together via a DC bus through the convenient power converters if needed as shown in Fig. 1.8a. DC sources and loads can be connected directly or through DC/DC converters. AC loads can be supplied with power from the DC bus through an AC inverter.

The DC-coupling configuration is simple and synchronization-needless for the different sources. On the other side, it leads to less reliability for the AC loads against the inverter failures.

AC bus-Coupled Systems: In this configuration, similarly all the different sources are connected together via an AC bus through the convenient power converters as shown in Fig. 1.8b. In this case, the system is more flexible, AC voltage and frequency can be chosen for a more effective power transmission. On the other hand, the inverters of the sources must be synchronized, the system is more sensitive to the quality of the generated power.

Other configurations are also possible (AC high and low frequency, combined DC and AC bus), these are shown and discussed in [7].

To design a HRES, different set of sources and/or storages are available in the literature [27, 28, 29, 30, 31, 32, 33]. Fig. 1.9 sums up the different HRES structure-based classes. Due to theses different configurations and components that can be used in the HRES, a large variety of the HRES can be found.

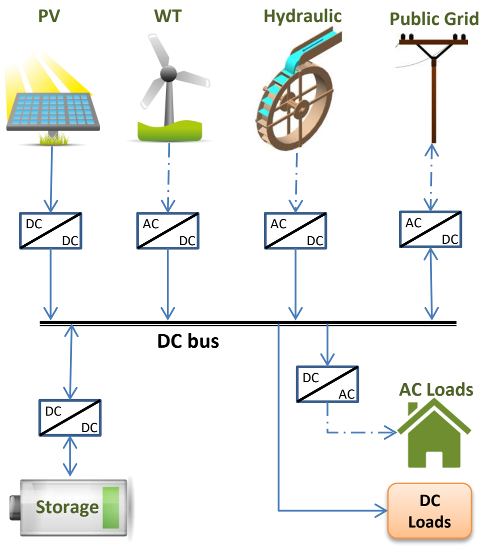

(a) HRES DC coupled

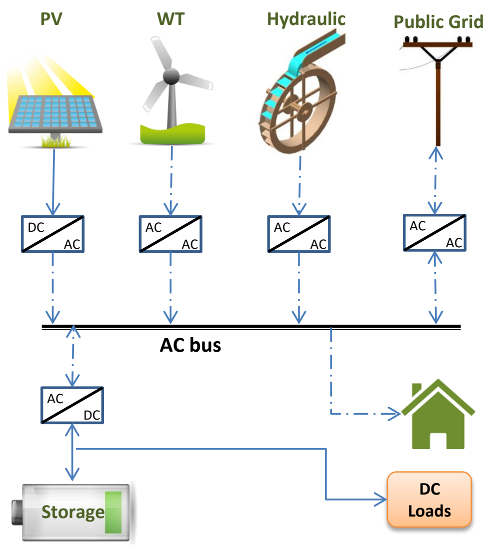

(b) HRES AC coupled

Figure 1.8 – HRES main coupling configurations

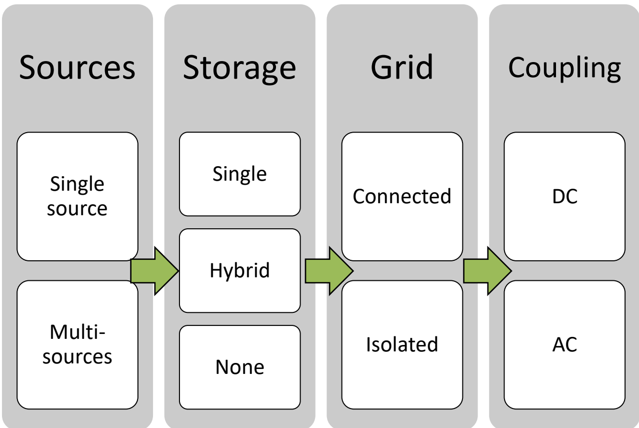

Figure 1.9 – Different HRES structure classes

Tab. 1.2 sums up the HRES studies along with the used components for each one.

Sources			Storage					Bus	
PV	WT	Other	UG	FC	Bat	EL	SC	DC or AC	
✓				✓				DC	Khanh et al. [21]
✓				✓	✓			DC	Bigdeli [34]
✓				✓	✓	✓		review	Yilanci et al. [22]
✓				✓	✓	✓		DC	Lu et al. [23]
✓				✓	✓	✓		DC, both	Zini et al. [24] and Bajpai et al. [8]
✓				✓		✓	✓	DC	Nasri et al. [35]
✓		Diesel		✓	✓			both	Halabi et al. [36]
✓				✓	✓			DC	Jiang [37]
	✓		✓	✓	✓	✓	✓	DC	Zhou et al. [25]
	✓		✓					-	Finn et al. [38]
		Review						review	Nehrir et al. [7]
✓	✓							both	Dursun et al. [39]
✓	✓			✓	✓	✓		DC,DC, DC,AC, DC	González et al. [40], Belmili et al. [41], Torreglosa et al. [42], Fetanat et al. [43], and Ipsakis et al. [44]
✓	✓		✓	✓	✓	✓		both	Panahandeh et al. [45]
✓	✓		✓	✓				review	Logesh et al. [26]
✓	✓		✓		✓			AC, both	Ahmed et al. [46] and Das et al. [17]
✓	✓		✓	✓	✓	✓		DC,DC, AC	Coelho et al. [29], Paska et al. [30], and Wang et al. [31]
✓	✓		✓	✓	✓	✓		-,DC,DC, both,DC	Vivas et al. [47], Garcia et al. [27], [48], Gao et al. [32] and Agbossou et al. [33]
✓	✓	Diesel		✓	✓			DC	Dahmane et al. [12]
✓	✓	Diesel			✓			both	Bernal-Agustín et al. [49]
✓	✓	Bioethanol		✓	✓			DC	Feroldi et al. [50]
✓	✓			✓	✓			DC	Brka et al. [51]

Table 1.2 – HRES Publications

1.1.3 Power management

Due to the operational redundancy in the HRES where several devices can be used to produce and store the power simultaneously, a global control strategy to manage the power for the different components is needed. As the lower layer of the HRES control, the power management consists of the set of the continuous control laws applied on each of the system components (power regulation, Mppt, etc.). The main objectives of such management are:

- Ensure the energy balance, voltage and frequency regulation [52].
  Having a non-steady power generation coupled with variable consumption induces power fluctuations. Almost all the electrical applications need a stable high quality electrical power. This accents the obligation of a voltage regulation in DC bus added to the frequency regulation in AC bus. Using the storage or/and the grid coupled with power electronics to the HRES allows to control the current flow in order to have a steady voltage at DC bus. Colson et al. [52] has reviewed many power management approaches used to stabilize the voltage and the frequency at AC bus. The sources can also be controlled, when possible after dropping the Mppt, to stabilise the power flow.
- Components power capacities
  An appropriate power management must consider the component limitations such maximum of the directed current through the converters or into the battery and the hydrogen units. This is different from the storage capacity which designates the limit of the amount of energy that can be stored. Since, the activation of the concerned storage can be based on its storage capacity, this latter can be related to the OMM while the power limits concerns more the continuous control laws.
- Components healthy operating conditions
  The power control associated to the power management must take into consideration the healthy operating conditions of the different components. Therefore, such power control must:
  - Ensure an optimal operating range for the sensible components such as the EL and the FC.
  - Respect both the sources and storage, components different dynamics [53, 54, 55].

Since the system components are divided into two groups with different missions, renewable sources and storage units, two main axes of power management strategies can be distinguished.

First, let consider a general case where there is a variable load P_{load} and a variable generated power P_{gen} from all the renewable sources, the residual power is defined as the "algebraic" excess of power $P_r = P_{gen} - P_{load}$.

For the renewable sources: it is clear that for a better productivity the sources are preferred to be always working, if ignoring the protection measures, on extracting the maximum available power. Therefore, the majority of the consulted works considers, in default, the power control of the sources is the MPPT algorithms. As a result, the sources generated power P_{gen} is variable and weather dependent. For the general case the power balance comes down to satisfy the excess of power P_r. Nevertheless, some works with multi-sources PV/WT have really considered only one source as the primary source in context of multi-sources HRES, therefore the primary source is working at the MPP, and the other is controlled in order to satisfy the rest of the variable load profile (not tracking the MPP).

For the backup sources or storage units: Very common power management strategies to satisfy the residual load P_r, introduced by Lasseter [56], are the Unit Power Control (UPC) and Feeder-Flow Control (FFC). The UPC, illustrated in Fig. 1.10, consists in draining a constant power P_{cons} from a local storage/source which is usually a limited power source or sensitive for dynamic loads (for example batteries, FC/EL). At the same time a secondary storage/source such as the grid is used to compensate the rest of the variable load profile $P_r - P_{cons}$. This strategy, used in default conditions, allows protecting and extending the lifetime of the sensitive storage components. For the FFC, the secondary storage/source (grid) injects or stores a constant maximum power and the other storage/sources is used to satisfy the variable residual profile as showed in Fig. 1.11. The FFC allows satisfying peak power input or outputs. Khanh et al. [21] used these two power management strategies in a HRES where PV/FC are considered without storage. The available hydrogen was not considered nor the slow dynamic of the FC.

Another power management strategy for HRES, known as peak shaving strategy [57] or frequency based distribution [58], consists on managing the storage components each according to its dynamical behaviour. For example, in a HRES combining a fast dynamical storage and a slow one such as (Batteries+FC/EL), the batteries have a fast dynamic response compared to the FC/EL. Power management could filter the storage consummation P_r as shown in Fig. 1.12, by attributing the fast changes in the demand to the batteries and the slow changes to the FC/EL. Compared to the

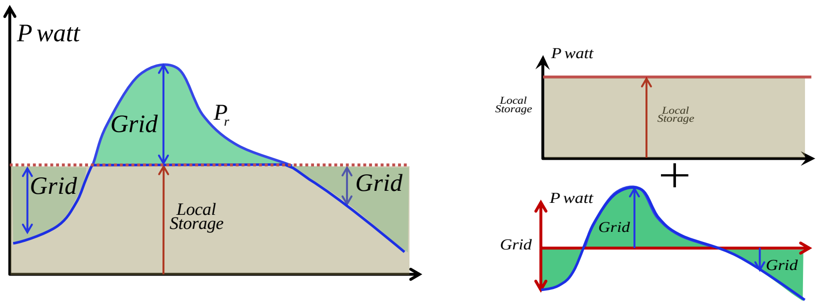

Figure 1.10 – UPC power management

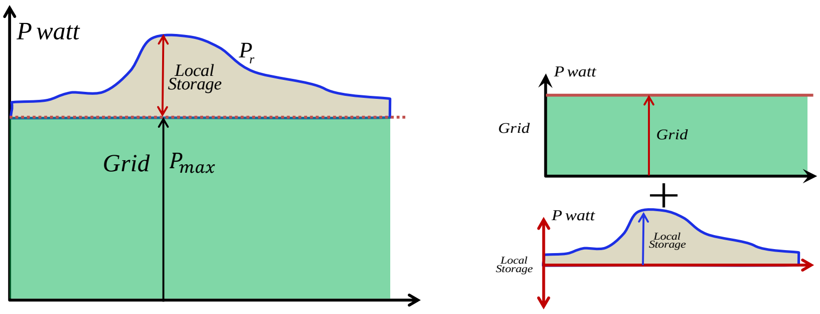

Figure 1.11 – FFC power management

UPC, frequency-based distribution strategy is more tolerant and less protective for the concerned sensitive components. Zhou et al. has combined these power managements (FFC, UPC along with the peak shaving technique) for a WT/batteries/EL/FC/UC in [25]. Using an emulator representing the system, the fast (high frequency) dynamical change of the residual power P_r is handled by an UC, while the slow dynamical changes are dealt with using the batteries and FC/EL unit. When the FC/EL power is constant the batteries satisfy the dynamical rest.

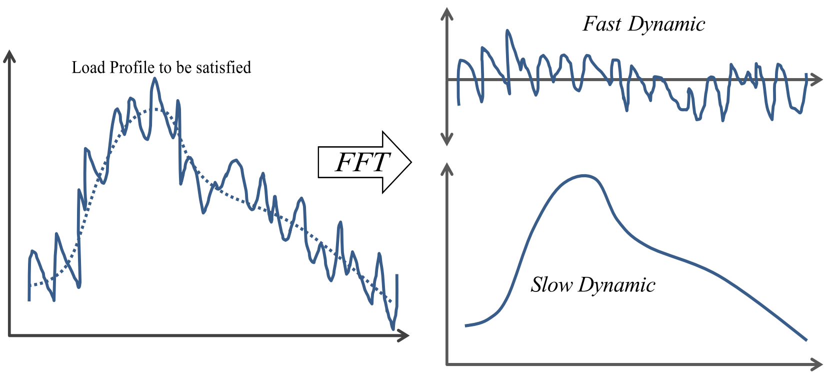

Figure 1.12 – Power management according to components different dynamics

1.2 Modelling of HRES

1.2.1 Modelling of the multi-physical systems

1.2.1.1 General overview

As mentioned before, the HRES gathers different components characterized by their distinct energetic nature. WT encloses mechanical, electromechanical and electrical components coupled together. PV represents an electronic device, while batteries, EL and FC constitute the mediums for electrochemical-thermal and fluidic coupled phenomena. Additionally, the hydrogen tank operates according to the thermodynamical principles. Integrated together to constitute a global model of the system, the different nature of these elements represents an additional constraint for the modelling and, therefore, its derived tasks. In the classical SSE analytical model, all the involved phenomena and dynamics are boiled down to some few differential analytical equations. In order to achieve this, the users are required to have wide multidisciplinary expertises.

As there are many applications that fit under this assortment, many approaches, paradigms and coding languages aim to cover the multi-physical dynamical modelling [59]. Two main axes exist: declarative equation-based modelling and graphical-based model listed in Fig. 1.13

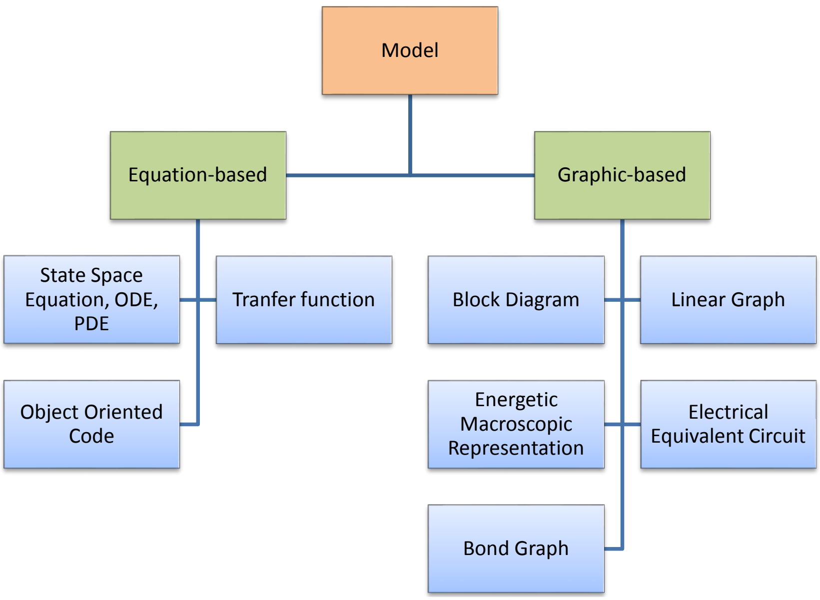

Figure 1.13 – Different multidisciplinary modelling approaches

Declarative equation-based modelling

This stands for low-level description of the system using the Ordinary Differential Equation (ODE), many programming environments are developed to simplify this task specially for multi-physical system. Object-Oriented Modelling languages are examples of such environments in which the model can be decomposed to blocks of code where each represents a subsystem or a component. Modelica, CAMP-G and SIDOPS+ are such examples [60].

The declarative modelling approach is very expressive, it can handle many types of dynamical systems including HDS and multi-physical systems and consequently, the HRES. On the other hand as the dynamical equations of the whole system are needed, this modelling techniques are considered as less user-friendly.

Graphical-based modelling

With the evolving programming environments and languages, it was not too late for the graphical-based modelling paradigms such as Block diagrams Equivelant Electrical Circuit (EEC) [61] Linear Graph (LG) [62] Energetic Macroscopic Representation (EMR) [63] and Bond Graph (BG) to come forth. In this approach, the model is decomposed into graphical components with ports, the global assembly of these blocks constitute both the model structure and its behaviour. In this concept, the user can connect, reuses or modify the different components which provides a more flexibility and offers a highly user-friendly modelling regardless of the component natures. In addition, the graphical models have also the advantage of showing the topology of the represented system.

Block diagrams: The block diagram model describes the equations of the model through graphical blocks. They represent the basic mathematical operations such as gain, derivation and integration etc. This approach comes as the first attempt to create a higher-level modelling, the model still depends on the knowledge of the basic mathematical equations of the system, yet it can describe somehow the assembled structure of the system. As a result, it is very convenient to model both HDS and systems including different components. However, like the declarative approach, it depends heavily on the knowledge of the dynamic of each component of the system and it is not abstracted.
Moreover, this approach is more suited for complex algebraic loops.

EEC: The EEC rests on the existing analogies between the different dynamical fields and the electrical one. By concept, it uses the electrical equivalences to describe the dynamical behaviour of the different components. It facilitates the derivation of the model and provides a unified representation of the different dynamics. Benefiting from the advance in the softwares developed to simulate the electrical systems, the model issued from this approach can be simulated on many platforms or even create physical electrical emulators. However, for complex non-linear systems, it is not trivial to represent thermo-fluidic phenomena by their electrical equivalent due to their energetic coupling.

Linear flow signal graph [62]: In this approach the model is represented by a graph, the nodes symbolise effort or flow references such as voltage or velocity. It works as generalized form of the mesh method and the Kirchhoff law used in electrical circuit to generate the system equations. From the LG, another graph can be extracted called a normal tree, which is derived by simply taking the longest unclosed paths. The eliminated branches from the LG to get the normal tree are called links. Using the normal tree, the equations of the system are obtained by writing the equations expressing the links variables in terms of other graph elements. This is usually called continuity equations (similar to mesh law). The constraint equations are also needed, they represent the energy conservation laws (similar to kirchhof law). The modelling aspect is highly abstract, it is mainly used to extract the dynamical equations of the system. A limitation is difficulties in modelling non-linear systems, coupled phenomena and HDS.

EMR: To build the system model, EMR uses blocks that represent the main occurring energetic phenomena. Each block represents a set of equations which express the energy interactions between the components. These equations are computed using inputs and outputs ports of the blocks The block shapes verbalize the nature of the represented energetic phenomena (dissipative, conservative, storage...) This approach is very suitable for multi-physical non-linear systems. Very useful to apply control, it provides a great flexibility in modelling continuous the HRES. However, modelling the HDS is not addressed.

Bond graph: BG is also a graphical modelling approach, founded long before the most of the previous mentioned approaches by [64]. It is a graphical representation of the dynamical system, it consists of different elements that represent the inner dynamic of the system. Each of these elements represents one basic fundamental phenomenon that exist in the nature (energy dissipation, energy accumulation, energy transfer etc.). By connecting those elements via power exchange bond, a constructed block model is created. In fact, BG represents a fair trade between the LG and the EMR. It is less dependent on the model equations than the EMR, but more simple from the construction point of view. The BG succeeded to get the attention for much research. This allowed to develop the BG theory to studies and achieves many tasks related to the dynamical systems. The BG methodology is still evolving to cover more and more dynamical systems (HDS, coupled domains, chemical [65], biological [66] etc.). Many features were developed even uncertain modelling approach such the Linear Fractional Transformation (LFT). Furthermore, due to its causal and structural properties, the BG serves not only for modelling but also to perform sizing studies, derive the proper control laws and establish the diagnosis algorithms. All of these offer the BG as a powerful tool to be used especially for the multidisciplinary switching systems such as HRES. The BG modelling is presented in details in chapter II.

1.2.1.2 Models in the literature

In all the consulted papers of the HRES, few works have considered the dynamical modelling of a global HRES. Most authors have studied whether real experimental systems or equation-based continuous models that describe only the steady state of each component. Less few have addressed the dynamical model. Nevertheless, some works have used the BG model for only single part independently such as PV as in [67, 68] or the WT in [69] or FC in [70]. Only one work of two parts is found in [71, 72], where the authors considered a full BG modelling of a system of PV, WT and unlimited hydrogen FC as multi-sources with only batteries as a storage. However, the proposed model does not take into account the hybrid dynamical (switching) aspect of the system nor the OMM. In [73], Chan et al. reviewed all the modelling formalisms used in modelling HRES in hybrid electrical vehicle context.

Photovoltaic

Many BG PV models can be found in the literature [74, 67], Andouisi et al. in [74] used a BG model as a tool to derive an analytical average model of the PV-DC/DC system. in [67] Mezghanni et al. used the PV BG model in context of a hydraulic storage system.

Wind Turbine

In [13, 14], authors have presented analytical and block diagram model of the WT. A review on the published WT modelling works is presented in [69], the authors also introduce a BG model of two mass for the WT.

Fuel cell and Electrolyser

Many models for the PEM components are provided in the literature [75, 76, 77, 78]. These models are provided on different modelling scales, from the cell cores to the full PEM FC or EL system. These models are in some empirical, or analytical models. Some represent the statical behaviour of the electrolysis while others includes the dynamical model [79, 80]. As multidisciplinary device, the FC dynamical model is usually given using the EEC, the EMR or the BG [81].

For instance, Bajpai et al. [8] provided many EEC for the FC electrical model showed in Fig .1.14a. Wang et al. [82] also presented an EEC for the electrical and the thermal phenomena. The model is implemented on Matlab and Pspice, the obtained results are compared with the real system measured data. The El modelling is less

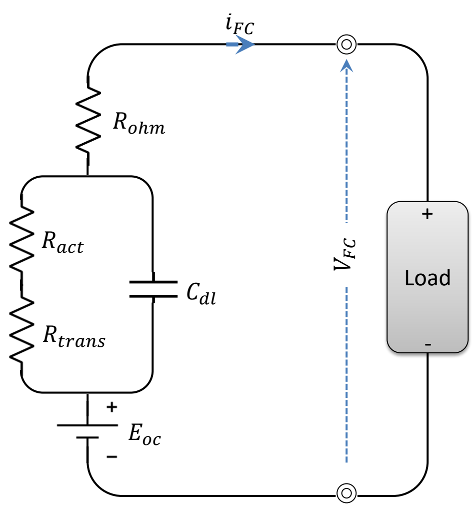

(a) FC EEC mode

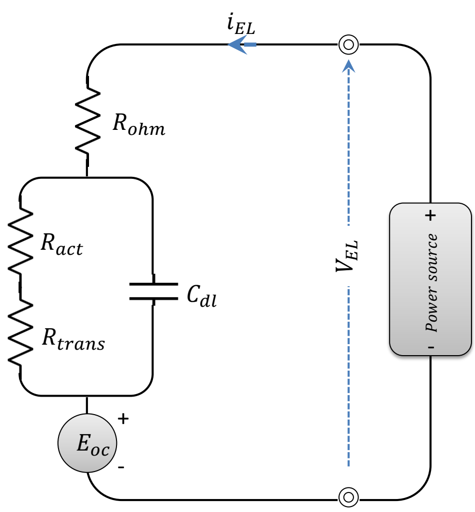

(b) EL EEC model

Figure 1.14 – EEC models for the EL and the FC

addressed in the literature, but it still can be inspired from the FC models. Agbli et al. [63] introduced a EMR model for the PEM EL, while [83] presented an EEC static model and compared the model and the real system behaviours. The model is used to test the system behaviour under different operating conditions. [84] presented a dynamical EEC model of the EL showed in Fig .1.14b with the parameter identification procedure. [85] introduced a full BG dynamical model for the EL and its auxiliary parts.

1.2.1.3 Conclusion

All the previous modelling approaches are able to represent the multi-physical dynamical systems including the HRES. Using the declarative modelling, a great difficulty marks the extraction and synthesis of the dynamical equations of the different sub-domains of the HRES. The ineptitude of the model to be used to achieve other tasks constitutes the main disadvantages of the block diagram, LG and EEC methods. In the literature, the EMR approach has been developed in order to both model and control multidisciplinary Renewable Energy (RE) continuous systems. As consequence, the EMR evolved with the lack for a convenient switch representation. In addition, the EMR still more equations based and less developed than the BG theory. As a well-developed methodology, the BG theory can be considered as a good foundation to model such systems.

1.2.2 Switching, hybrid dynamics and OMM

1.2.2.1 Literature review: Operating Mode Mangement

Most HRES present different OM corresponding to the different subsets of components that are set active or not in order to perform the energy management. An example is the WT that is needed to be stopped in very high wind conditions or the EL that is needed to be switched off in case of very low generated power or full hydrogen storage. Many OMM strategies are provided by the literature. For each configuration, the system limitations, constrains and structure change. The power management strategy must be specified conveniently for each OM. The main objectives of the OMM management are:

- Prevent power shortage:
  When the available power is not sufficient, back up units are activated.
- Respect the component energy capacities:
  When a storage reaches its maximum capacity, it must be disconnected and stopped.
- Ensure the component protection and healthy operating conditions in order to extend the lifetime:
  - When bad operating conditions are detected, the concerned component must be disconnected
  - Reduce the frequent ignitions and stops for the EL and the FC [8].

For the renewable sources: Without considering the protection measures, it is obvious that in order to extract the maximum power, the renewable sources are required to be always operational. This is the case in of the most of the consulted studies. In some cases, authors have considered OM where one or more renewable source are disconnected in a very high surplus power and full storage conditions. As explained before in case of using the WT as a source, it is known that different OM are already defined according to the incident wind speed see Fig. 1.7. At very high and very low wind conditions the WT must be stopped. In the context of HRES, it seems that none of the consulted works has considered these WT OM.

For the storage units: Most of the HRES consider at least battery bank as a part of multiple storage unit (see Tab. 1.2). In a multi-storage system, the OMM is needed as the power management strategy as well. In such systems, the batteries are considered as the primary power storage. Thus, the OMM depends mainly on the battery State of Charge (SoC). The first simplest OMM considers two SoC levels (SoC_{min}, SoC_{max}) associated to the battery bank. The secondary storage units (such as FC/EL) are activated or deactivated, according to the actual (estimated or measured) SoC value of the battery relatively to the defined limits (SoC_{min}, SoC_{max}). Fig. 1.15 shows an example of a battery/FC/EL storage. The figure shows that the OM are defined according to the actual SoC value:

- When $SoC_{min} < SoC < SoC_{max}$, only the battery is connected.
- When $SoC \succeq SoC_{max}$ another storage is activated to reallocate the power and prevent the battery overcharge. In some works the batteries are deactivated.
- When $SoC \preceq SoC_{min}$ another backup storage is activated to recover and supply power. This helps to prevent the power shortages and extends the battery lifetime.

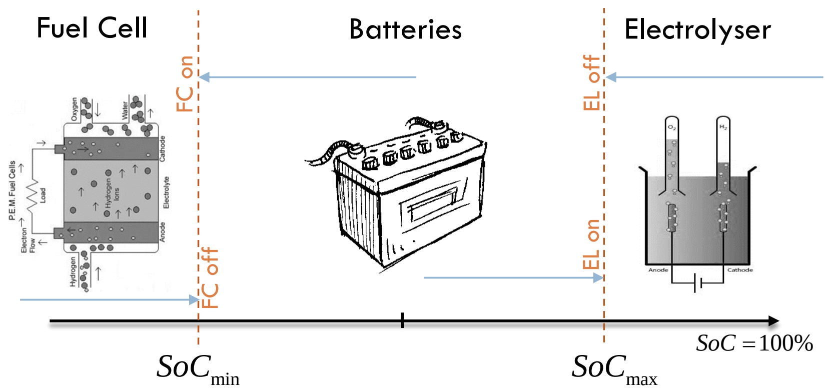

Figure 1.15 – Battery SoC limits defining the OMM

Depending on the number of the storage units, many SoC limits can be defined [86]. To reduce the frequent activation/deactivation of the FC and the EL, a hysteresis can be introduced [47, 86] on the previous OMM.

To manage all these OM, the main developed approaches in the literature rest on linear programming represented as flow chart or state machine.

Linear programming for OMM via flow chart

Flow charts represent soft computing algorithms that set the rules of transitions between the different configurations of active components. An example is illustrated by Fig. 1.16.

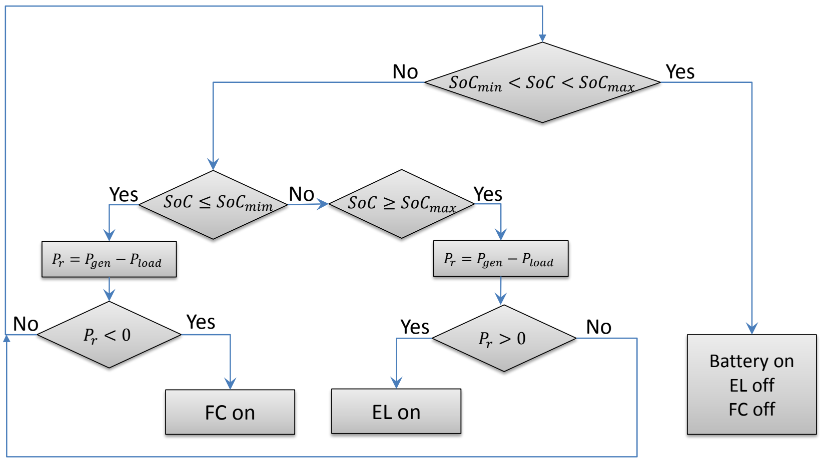

Figure 1.16 – Flow-chart describing the OMM

In this case, the OMM is based on the estimated SoC value of the battery. When the battery is full $SoC > SoC_{max}$, the residual load P_r is checked, if it is positive (i.e a positive excess of produced energy) with full battery, the EL is activated. When the battery SoC is critical $SoC < SoC_{min}$ and P_r is negative then the FC is activated to back up the sources. Otherwise, the battery operates as single storage.

Linear programming for OMM via state-machine:

The state machine represents a simple approach to define the OM and their related transitions. It is introduced in [50, 42], where each discrete state of the automaton is associated to distinct configuration of active components. For instance, Feroldi et al. [50] used the state machine (state-chart) to design the different OM for a PV/WT/batteries/FC/bioethanol HRES. The system was represented by an analytical model on Matlab and serves as virtual platform to test different OMM and power management strategies. In this paper, the authors have considered five different OM illustrated by Fig. 1.17:

- S_1: The WT is active and used as primary source tracking the Mppt. The extracted power is enough for satisfying the load and charging the batteries, the PV is inactive.
- S_2: When the WT is not capable of satisfying the load profile, this mode is accessed. The PV are set active and controlled to meet the load including the batteries.
- S_3: When both the PV and the WT can not fully supply the load, the batteries are set to discharge.
- S_4: This mode is active when the batteries reach their maximum storage capacity. In this case, both sources are disconnected and batteries are used as the main power source.
- S_5: When the batteries reach the lower limit of charge, the FC and all the other backup sources are triggered to recharge the batteries.

The transition conditions ($a \longrightarrow h$) are defined conveniently in [50].

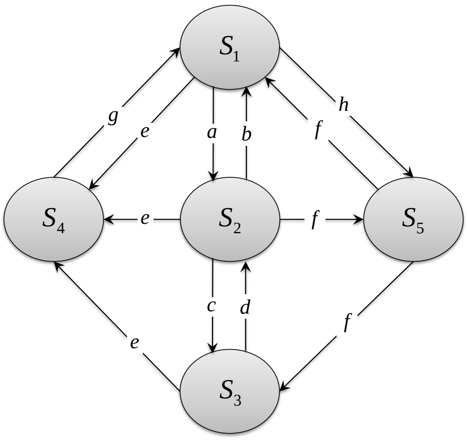

Figure 1.17 – State-machine of the HRES

Intelligent techniques for the OMM

More advanced OMM techniques can be found. Nevertheless, they need much more processing capacities and more detailed data. Three axes can be identified: Artificial intelligence, Fuzzy Logic [27, 48], Model predictive control [87]. As an example, for a PV/WT/Battery/FC system, Brka et al. [51] used predicted SoC battery value in a linear programming OMM. A neural network is used to provide forecasts for the source powers and the load profile. By estimating the excess of the power, a static model of the battery is, then, used to predict the future SoC which is used in the OMM.

Tab. 1.3 sums up the recent publications about the different HRES OMM.

Publication	System	OMM
Ipsakis et al. [86]	PV/WT/battery/EL/FC	SoC-based with Hysteresis
Vivas et al. [47]	PV/WT/EL/FC/UG simulator	SoC-based with Hysteresis
Coelho et al. [29]	PV/WT/EL/FC/UC	Surplus power: Hydrogen
Nasri et al. [35]	PV/UC/FC/EL simulation	Surplus power: Hydrogen then UC then PV are disconnected
Torreglosa et al. [42]	WT/PV/battery/FC/EL	Surplus power: Hydrogen then UC then PV are disconnected Degradations and life-time
Bajpai et al. [8]	PV/battery/FC/EL	Surplus power: Battery then Hydrogen then PV match the demand
Logesh et al. [26]	PV/WT/UG	Surplus power: Mpp PV and controlled WT to meet the load Low power: connect UG
Dursun et al. [39]	PV/WT/battery/FC/EL	SoC-based and Hydrogen pressure
Dahmane et al. [12] and [88]	PV/WT/Battery + Diesel engine	To meet the load: PV then PV+WT then PV+WT+battery then All+Diesel
Halabi et al. [36]	PV/Battery + Diesel engine	HOMER
Bernal-Agustín et al. [49]	General review	TRANSYS

Table 1.3 – HRES different structures and different OMM strategies

Following the obligation to manage the different OM, the HRES are by definition classed as HDS. Their dynamical behaviour evolves in both ways continuous and discrete, this dual aspect can not be separated in most of the classical modelling approaches devoted to model the switching systems.

1.2.2.2 Representation of the HDS: Switching systems

Depending on the nature of the discrete phenomena, HDS can be classified into different sub-categories such as switching systems, jump linear systems, mixed logical dynamical systems.

Switching Systems

Switching systems are HDS that contain switching elements, HRES belong to this class. The switch operates in "dual-state". When it is active, it allows the power to flow through. On the other side, when it is inactive, it cuts off the power exchange. Thus, the inner dynamic changes according to switching state. Controlled switches are controlled by an external signal which does not depend on the state of the system (switch, valve). In autonomous switching system, the switching state depends on inner conditions of the system (diode) [Fig: 1.18].

Generally in the HDS literature, the discrete behaviour is in fact a simplification of a very fast dynamic or phenomenon, this latter is seen as an instant change in the inner dynamics of the concerned system. The simplification is taken by considering a spontaneous transition of the dynamic from one state to another (usually called mode). Mathematically, this implies that the dynamical behaviour, which is often expressed by the SSE, does not always conserve the same ODE or/and the same variables. For systems such as the HRES with different OM, disconnecting one component from the global system suggests necessarily the change of the mathematical models that describe the behaviour of the whole system. This toggling between the different dynamical behaviours must be expressed within the model representation.

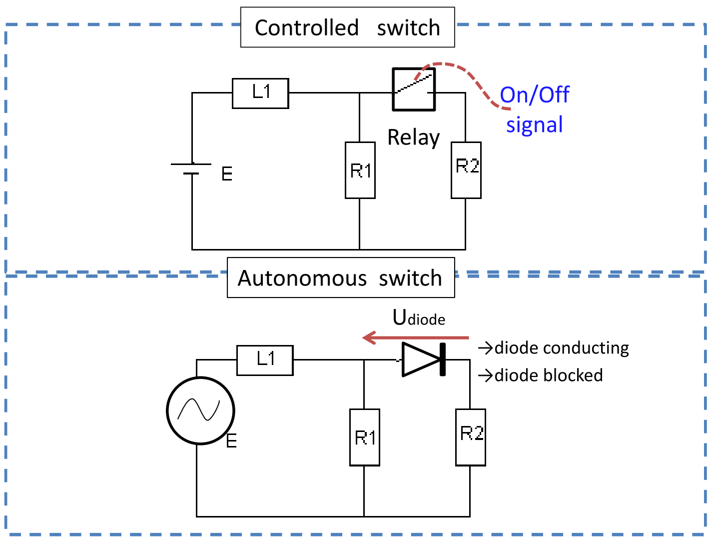

Figure 1.18 – Controlled junction on-off cases.

Modelling Hybrid Dynamical systems

Compared to continuous systems, modelling the HDS is more challenging. Any hybrid dynamical model needs to take into account the parallel evolution of the continuous and the discrete states of the system. Actually, finding the convenient tool to model the HDS is still an active topic in research [89, 90, 91, 92, 93], all the actual modelling methods of switching systems express the discrete behaviour by boolean firing expressions which define the conditions to switch between the different dynamical equations called OM. In each mode, the dynamic evolves continuously with respect to a given set of continuous differential equations [94, 95]. The main existing approaches to represent the behaviour of such systems are: Hybrid Automaton (HA) [96, 94, 95], Mixed Petri Net (MPN), Hybrid Petri Net (HPN) [97, 98, 90, 92], Hybrid Bond Graph (HBG) [99] and Hybrid Hamiltonian port [100]. HA, MPN and Hamiltonian port, are multi-model approaches. They represent each dynamical OM by its own analytic differential equations (SSE). In all these HDS modelling frameworks (except for the HBG), the explicit analytic equations of the system model must be found for each mode. This can be manageable for a few modes, however, when dealing with large complex system such as HRES with many modes, this can be a very hard and time-consuming task specially if a new component is been added.

Hybrid Automaton It is an extension of the classical simple automaton used for modelling discrete systems. As mixed representation, it consists of a graphical-oriented method representing a state-machine to drive the discrete behaviour with its modes and an analytical representation for the continuous dynamics. In each mode the associated dynamic is expressed by the analytic SSE. There is always only one activated mode, this implies the HA must be deterministic. By definition [94, 95, 90, 96, 101], a hybrid Automaton is a collection:

$$HA = (X, f(x), Q, Init, D, E, G) \tag{1.1}$$

Where:

- X — State space vector field
- $x \longrightarrow f(x)$ — x is State space vector; f is Vector field of the dynamic
- Q — Set of the discrete state q
- $(q, x) \in Q \times X$ — State of HA
- $Init \subseteq Q \times X$ — Initial conditions of all the states

- $D : Q \longrightarrow P(x)$ Set of the mode domains
- $E \subseteq Q \times Q$ Transition arc from one mode to another
- $G : E \longrightarrow P(x)$ Set of the guard conditions

Discrete modes are represented by nodes. In each node the corresponding continuous dynamical model is included. A generic example of two OM-HA model is illustrated by [Fig: 1.19.a]. The transition conditions and the domains of each mode/node along with the continuous dynamic evolve with respect to the local equations of each discrete mode. When the current domain condition is no more satisfied, the system switches, with respect to the existing transition arcs and the guard conditions, to the next mode.

This method is widely used to express the HDS models, it is very effective and flexible to be implemented. The differential SSE, if given, can be coded easily. The automaton enveloping and governing the transitions can be implemented more easily on almost any simulation software (using C, Stateflow or ladder Logic Diagram). One major drawback of such representation is the need to express the equations of each mode, not to mention the heterogeneous aspect (Graphical-analytic) of the global modelling. Additionally, by resting on the analytical description of system dynamics the HA can not be considered as a causal modelling tool, the cause-effect relation is not explicit. For the complex systems with many modes and multidisciplinary components, applying this method seems to be very hard as for each dynamical mode the set of the coupled dynamical equations must be stated which could lead to risk of combinatory explosion.

Mixed and Hybrid Perti Net

Mixed Petri Net: Similarly, inherited from the Discrete Event System (DES) literature, it rests on representing the discrete states by nodes interconnected by transition arcs in their turn supervised by guard conditions see [Fig: 1.19.b]. An active Marker usually called token (Marker) marks the current operating mode, each node contains the continuous dynamic in its analytic form which is triggered when the node is set active. The entire MPN generates the global model of the HDS. More incisively, the global MPN can be defined as a collection:

$$MPN = (X, F(x), P, T, C) \tag{1.2}$$

Where:

- X State space vector field

- x State space vector
- $x \longrightarrow f(x)$ Vector field of the dynamic
- P Set of places of the discrete state p
- $(p, x) \in P \times X$ State of MPN
- T Transition set

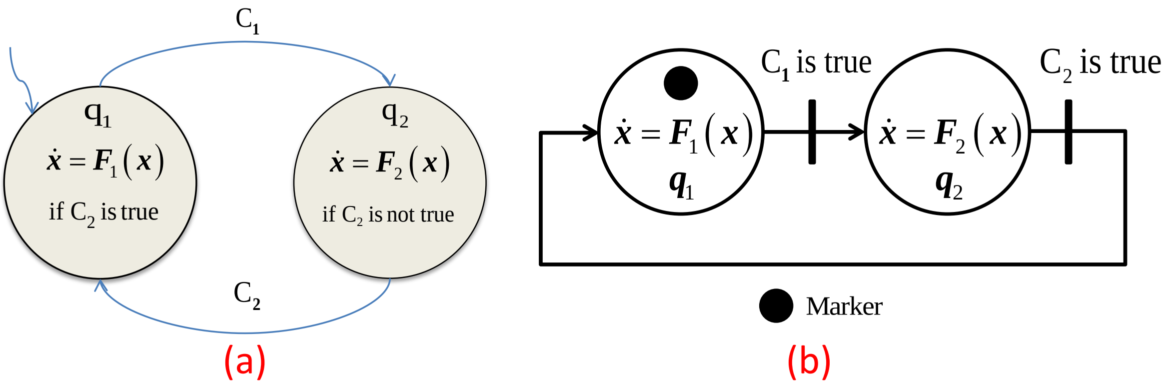

Figure 1.19 – Dual state HDS models: a) Hybrid Automaton, b) Mixed Petri Net

Same as for the HA, there is an absolute need to express the equation for each mode separately, same for the heterogeneous aspect (graphical-analytic) of the global model. With many OM, this method is not practical.

Hybrid Petri Net HPN is another approach that uses an extended from the discrete modelling of the Petri net method. It consists in representing each continuous state variable of the system by a continuous node and the discrete ones by a normal discrete node [102]. This induces many nodes, by default the continuous state evolves unidirectionally. Bi-directional states need additional nodes to be represented.

Hybrid Hamiltonian port It is a pure analytic representation, for the multidisciplinary energetic hybrid systems. It is a very similar approach to the bond graph which also lies on the power exchange concept. Although the modelling looses the graphical structured criteria which makes the diagnosis, model update quite difficult compared to the other methods.

Furthermore, similar methods are also proposed such as the Hybrid Grafcet, Statechart [103],[104].

Hybrid Bond Graph BG modelling is detailed in chapter II. By introducing the ideal switch dynamical representation into the continuous BG theory, this latter is extended to cover the HDS modelling. All the BG characteristics, properties, applications are then transmitted to the HDS. As all the previous approaches rest on the analytical equations of the dynamics, the strength of the HBG is that it matches perfectly with both objectives. It maintains its graphical abstract approach suited for an energetic structured modelling and provides at the same time a global model for the all the OM eliminating the need for an explicit modelling all the OM.

Unlike the HA and the MPN, the HBG represents only the full dynamics modes of the HDS. It does not show the behaviour of the discrete state and its transitions. This can be solved by integrating into HBG, the HA approach of handling the discrete states and their transitions. Therefore, in order to achieve this, a simple automaton can be added to the HBG. The obtained tool is, then, named Event-Driven Hybrid Bong Graph (EDHBG). It guarantees a fully graphical representation for HDS multidisciplinary applications HRES included. The EDHBG is fully detailed and explained in chapter II and represents the main original contribution of this work.

1.3 FDI for HRES

1.3.1 Objectives and motivations

As power harvesting units, the renewable energy sources operate under lot of cyclic stresses in wearing and hostile corrosive environment conditions. Similarly, electro-chemical storage units such as EL are also subjected to a highly non-steady alternating powers where highly active chemical reactions take place. By concept, HRES are vulnerable to lot of various components failures. [Fig. 1.20] illustrates a list of common faults occurring in a typical HRES composed from PV, WT, FC EL, etc.

For hydrogen related HRES, the FDI task can be more crucial. The equipment sensitivity against bad operating conditions, the maintenance costs of the EL and FC along with the hydrogen-oxygen-electricity related risks, are some of many factors that highlight the diagnosis as a significant critical task for such process. In fact due to the component redundancy in a HRES, it is possible to avoid a high risk situation or the power shortage issued by minor faults. For example, severe consequences of a WT bearing malfunctioning can be avoided, if the fault is identified and the WT is stopped. In a multi-source context, the power will still be available by the PV, the batteries or

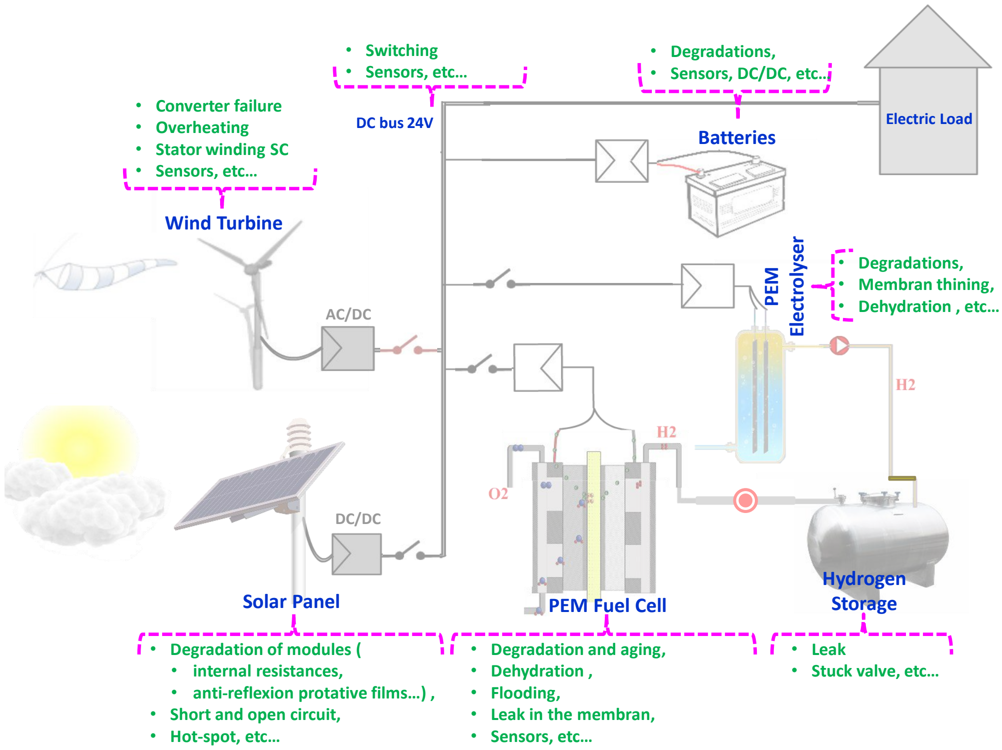

Figure 1.20 – Common faults and undesirable phenomena in HRES

the FC.

As mentioned before, a proper FDI can be related to the OMM strategies. With an on-line FDI, detecting the occurring fault can help in both protecting the system components and/or ensuring the continuity of the service when possible. Thus, an OMM that takes into consideration the FDI results can achieve a system reconfiguration [105]. Such reconfiguration must put in priority:

- The safety measures (of the users),
- the system protection (of the components),
- the continuity of the service.

1.3.2 Diagnosis of HRES: Method review

In order to monitor the safety and the availability of the provided services by the different components and OM of the system, an online FDI is needed. The FDI algorithms, as the name suggests, consist mainly of two steps. The first, called the detection, consists in investigating the consistency between the actual data (provided by the sensors) and the reference behaviour described by the model. When it occurs, the inconsistency (between the measured data and the model behaviour) generates an alarm. It is worth to mention that due to measurement noises and the parametric uncertainties, this FDI approach can suffer from robustness issues.

After the detection alarm, the second step consists in finding the faulty component using a logic procedure such as the Fault Signature Matrix Fault Signature Matrix (FSM). When speaking about the Fault Detection, Isolation and Diagnosis (FDID), a third step is added which concerns the Diagnosis i.e interpretation of the type and the cause behind the detected fault. Depending on whether the model is used or not and the kind of the modelling approach used for the detection, the FDI approaches can be assorted, as shown by Fig. 1.21 under two main axes:

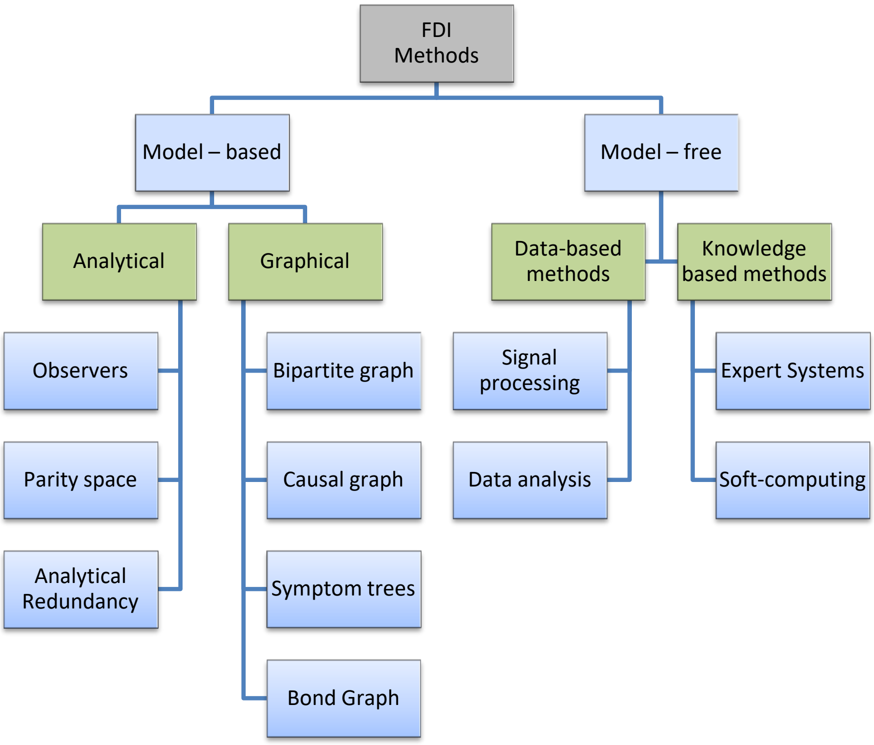

Figure 1.21 – FDI different approaches

- Model-free approach
  The model-free approach rests on exploiting the experimental data or the experience i.e to build an expected behaviour of the system. A great advantage of such approach is the independence from having the model, therefore the multi-physical complex dynamics is not the main issue. This approach has two separate techniques: Data-based FDI and Knowledge-based FDI.

Due to the great progress in the artificial intelligence and the machining learning, Data-based FDI is getting a great attention in the research field [106]. Some disadvantages of such approaches is the need for historical data collection and expertise in both normal and faulty behaviours. Having some possible destructive faults with expensive materials makes the training data sets very costly to build.

However, the dual continuous-discrete aspect of the HDS results in a more complex diagnosis process than the ordinary systems. When the dynamical behaviour of the system depends on the active components according to the OM, the training data sets must consider each possible OM, admitting that n switches generates 2^n theoretically possible OM. This leads back to the same geometric expansion problem faced in the modelling approaches adding to it the training time with the considerable processing power needed complicates the on-line implementation. In the context of the HRES, this approach faces an additional difficulty if the dynamical system and its modes depends heavily on the random state of the weather as in the HRES case.

Knowledge-based FDI depends heavily on the skilful experience. This approach shows weakness in case of complex systems, where faults can be unwillingly neglected or others unprecedented entirely (new faults) which marks the need to maintain the diagnosis algorithm updated.

- Model-based approach
  Model-Based Diagnosis (MBD) approach consists in using the knowledge wrapped in the model in order to perform and implement the diagnosis algorithm. It has two different outlooks: analytical and graphical. From the graphical technique, some sets of rules are applied based on the causal and structural properties embedded in the graph. This approach provides an intuitive diagnosis approach based on techniques such as bipartite graph [107], causal graph [108], Symptom trees [109] or the Signed Direct Graph (SDG). Bipartite graph and causal graph use as a node set of equations and variables. SDG use a directed graph representation to capture causal relations relating the system variables. In their structure, they are similar to the digraphs with the difference that the system variable nodes carry qualitative values "0", "+" and "-" obtained with respect to the variable of the reference. For the detection, a robustness issue can occur when using fixed thresholds. However, all these techniques gets more difficult and long with complex coupled dynamics.

It is convenient to note that these qualitative principles may be effective in allocating the fault cause. Nevertheless, the results of such diagnosis can not be used in order to estimate the faulty parameter. This implies the unsuitability for estimating the severity of the damage nor to be used to achieve the prognostic.

On the other side, the quantitative or analytical MBD [110, 111, 112] is more interesting specially for the HRES. The existing methods in the literature [93] use the model dynamic as a consistency reference to detect and identify any unexpected or unusual behaviour of the real system.

The BG provides the solution by representing both the dynamical behaviour (quantitative) of the system and its causal properties (qualitative) as detailed in the next parts.

Fig. 1.22 illustrates the general architecture of the MBD. By comparing the real system behaviour with the model behaviour, residual signals are generated. Assorted as a vector, when it shifts from the neighbourhood of zero, this indicates a non-consistency between the reference behaviour issued from the model and the output of the real system. The figure shows the different steps related to the FDI supervision and the OMM, with some general FDI notions defined as:

- Detectability: It is related to the capability of the approach to alert, through the monitored signals, a specific fault. When some critical faults can are not detectable, more sensors are needed.
- Isolation: It represents the ability to identify the cause behind the detection. So, some faults can be detected but have the similar signature, this is refereed to by the non-isolability.
- Availability: It stands for the possibility to use the different components. It can be related to two different factors, the operational and fault-related availability of the concerned components. The operational availability is associated to the operational limits (capacity, power limit). These limits are needed to be included to set the availability of the component. Also, the FDI results must be involved. Normally, when a fault is detected and associated to a component (isolated), the component is marked as unavailable.

Quantitative model-based diagnosis: Observers vs Analytical redundancy To generates the fault indicators called residuals, two procedures can be used: observers or the Analytical Redundancy Relation (ARR) [113] as shown by Fig. 1.23.

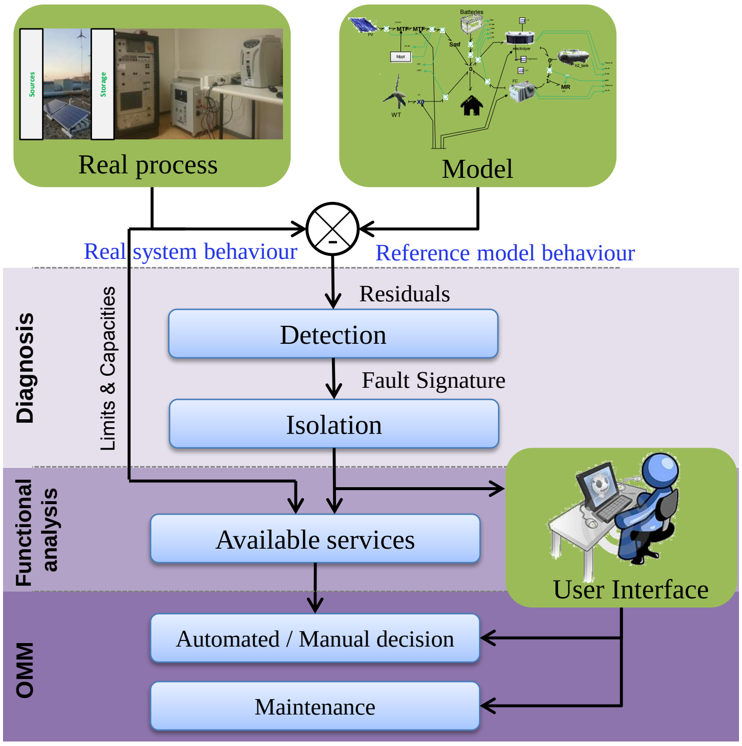

Figure 1.22 – OMM and model-based supervision steps and architecture

Observer based FDI In normal faultless case, by comparing the observer output (estimated by the observer) with the system measured real output, the obtained residual, must be equal to zero. In case of faulty situation, the system will differ from the observer model. If the fault is detectable, a difference between the outputs will be noticed and an alarm is generated. At least one of the residuals will take a non-zero value alerting the detectable fault.

Since it uses observers, this method needs always to converge rapidly. Kalman filter is widely used for noised systems [112]. For continuous systems, the observer method can be effective and more suited for the diagnosis of the actuators and sensor faults with low isolability performance. It suffers from the difficulty in locating the fault source within the model and then related to the responsible component. In case of the HDS, this method is difficult to be implemented. The changing mode and the discrete behaviour require lot of work to insure the stability and the fast convergence of the observer in each mode specially when dealing with non-linear systems. This can pose serious difficulties in complex systems with lot of operating modes.

ARR based FDI The ARR are algebraic differential equations describing the model and containing only known variables (control input, output variables, modelling

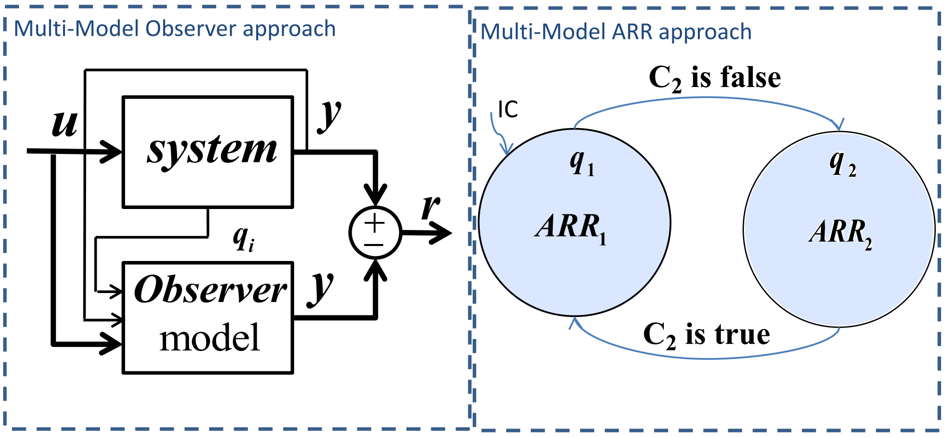

Figure 1.23 – FDI of the HDS

parameters), the numerical evaluation of these relations based on the measured data of the real system represents the fault indicators [114, 112, 115, 116, 111].

In case of the HDS, the ARR must cover all the OM. For this, there exist two solutions: by finding the ARR for each mode and then using a simple automate as shown in [Fig: 1.23] in similar way to the HA modelling or by generalizing the ARR to cover all the HDS OM modes using boolean variables to represent the discrete states. This generalized ARR are called the Global Analytical Redundancy Relation (GARR) [117, 91, 115, 118] .

Unlike observers, the ARR, once found, are easy to implement to achieve the FDI. Theoretically, they do not need a time to converge (derivative causality). Nevertheless, the derivation of the system outputs implies the need of low noise signals and some signal processing and filtering. The ARR can be helpful not just in detecting the fault but also in locating the defective part of the system, this isolation process can be achieved using structured residuals and Fault Signature Matrix FSM logic. Extracting the ARR is achievable using the BG model, this is discussed and developed in chapter III.

In the HRES literature, the FDI approaches focused on the diagnosis of independent power units. Al-Sheikh et al. [119] have listed and explained the occurring faults in each of the PV, WT and FC. The work also reviewed the different diagnosis approaches used in each case. Tab.1.4 sums up the recent publications concerning the diagnosis of HRES components with the adopted approach.

Component	Approach	Publication
WT	Data based: Machine learning, Classification	Brandão et al. [120]
WT	Model-based: BG redundancy	Badoud et al. [121]
WT	Review	Lu et al. [122]
PV	Model-based: Observes	Chao et al. [123]
PV	Data based: Neural network	Wu et al. [124]
FC	Model-based: parity-space redundancy	Aitouche et al. [125]
FC	Model-based: Observers	Steiner et al. [126]
EL	Model-based: Observers	Lebbal et al. [127]
Converter	– –	Daniel et al. [128]
PV+FC	Model-based: Observers	Zhang et al. [129]
PV+WT+FC	Review	Al-Sheikh et al. [119]

Table 1.4 – FDI publications concerning HRES components

1.4 Conclusions

The multi-sources HRES with their different components and configurations present an interesting solution towards clean reliable power production. These kinds of systems impose the use of hybrid power storage. Batteries constitute normal potential basis of the most of the storage units, they allow a relative fast and dynamic response to store and supply power. The batteries represent a convenient solution for a short-time small scale power storage. Hydrogen plays an essential role as any energy carrier. When used as power storage, hydrogen can be stored for long-time and in huge quantities. This can be introduced as a parallel solution for a long-term storage increasing the overall seasonal reliability of an HRES. Due to its various developing applications, stored hydrogen can be used in multiple energetic contexts.

The literature of the HRES allows insisting on the significance of the proper power management and the OMM. In order to perform a simulation, sizing analysis and others tasks a model is needed. This model must take into account the multidisciplinary hybrid aspects. It must be able to represent the different OM and offer the possibility to perform a model-based diagnosis. The state of art shows that such global modelling method is not developed yet.

HBG is a very adapted modelling tool to represent the multidisciplinary switching systems. It allows deriving the ARR responding to the diagnosis objectives.

With associating a state-machine (an automaton) that drives the modes through the controlled junctions, we obtain a new tool called EDHBG. This latter is the developed subject of the next chapter which represents the main innovative interest of the presented research.

Chapter 2

Event Driven Hybrid Bond Graph For HRES Modelling

2.1 Bond Graph for HRES modelling

BG modelling is based in representing the power exchange between the different components that constitute the system. This power is represented by a half arrow labelling the two power variables (effort e and flow f) independently from the physical nature of the modelled part of the system. The advantage of the BG is its causal concept that allows not just the modelling but also the control analysis, sizing, diagnosis etc. BG Theory and its applications can be consulted in the literature [64, 130].

In this work, the BG theory is developed to obtain the EDHBG proposed for the OMM of the HDS and in particular the HRES.

Definition 2.1.1 (Bond Graph)**.** *A BG is an oriented graph $BG = (\mathcal{E}, \mathcal{A}_{BG}, \mathcal{J})$ where $\mathcal{E}$ and $\mathcal{J}$ are node sets representing respectively set of physical elements and junctions. $\mathcal{A}_{BG}$ is the set of edges showing the mutual influence between the nodes describing, in the BG, the power exchange.*

1. $\mathcal{E}$ is the set of elements representing fundamental energetic processes, $\mathcal{E} = \{Se\} \cup \{Sf\} \cup \{R\} \cup \{I\} \cup \{C\} \cup \{TF\} \cup \{GY\} \cup \{De\} \cup \{Df\}$. Usually each element representation consists of two parts, the element nature, defined in Tab.2.1, and its related modelling parameters and dynamic laws.

   From behavioural point of view, each element is associated with some dynamical properties that translate the relations governing both of the power variables: the

BG element	Definition
Se, Sf	Effort source, flow source
De, Df	Effort and flow detectors
R	Resistor element
I	Inertia element
C	Capacitive element
TF, GY	Transformer, Gyrator
0-junction	Common effort junction
1-junction	Common flow junction

Table 2.1 – Common basic BG elements

effort e and the flow f.

$S_e : u$ is a single-port element called an effort source. It supplies the interacting element-junction structure of the model with an effort-based power through a single power bond. u is the value of the constant effort which represents the modelling parameter of the element. The corresponding equations are, for the effort $e := u$, the flow is not constrained i.e $Se : u$ can produce (resp. receives) any flow. As a power source, the half-arrow (bond) connected to $Se : u$ has a forward orientation as an output. Such element can represent many energetic phenomena depending on the concerned physical domain. For instance, it designates an ideal DC voltage source electrically, a constant pressure provided by a pump in the hydraulic domain or a constant temperature delivered by a thermal source in the thermal domain.

$Sf : i$ represents, analogously, a constant flow source. It supplies the BG structure with a constant i flow power. Such element can represent many energetic phenomena depending on the concerned physical domain. For instance, it designates an ideal DC current source electrically, a constant volume flow in the hydraulic domain or a constant entropy or heat flux in the thermal domain, etc.

$R : r$ represents the passive power dissipation in the system. This resistive element $R : r$ behaves generally according to the general law $\Phi_R(e, f) = 0$, where e represents the effort, f is the flow and $\Phi(.)$ (linear or not) expresses a general form of the relation between these elements (e, f) and the resistance parameters r. In electrical domain, this equation comes down back to express the linear resistance law that ties both of the resistance potential difference (voltage) e with its passing-through current f. Hydraulically, in a hydraulic conduct the pressure drop $e = \Delta P$ due to the viscous friction phenomenon modelled by r

is proportional to the square of the mass flow f passing through. In this case, the corresponding relation can be written as $e = r.\Phi(f)$ where the parameter r represents the hydraulic resistance and $\Phi(f) = f^2$ is the constitutive equation. Thermodynamically, the general law of the heat dissipation through an isolated medium suggests that the difference of temperatures (i.e effort e) between the two sides of the isolation is proportional to heat flux passing through the isolation f. This can be expressed by the same equation with r representing the thermal resistivity ($\Phi(f) = f$).

$I : L$ represents a passive inertia energy storage element. $I : L$ behaves, linearly, according to the dynamical law $\Phi_I(L, f, \int e(t)dt) = 0$ (see Fig. 2.1). In the mechanical domain, this element represents an inertia power storage element such as mass, where e represents the effort, f the position deviation rate (velocity) and L denotes the mass value. In such case the behaviour equations will be expressing Newton dynamic law. Electrically, I represents the electrical inductance.

$C : c$ represents a passive potential energy storage element. The capacitive $C : c$ behaves, linearly, according to the dynamical law $\Phi_C(c, e, \int f(t)dt) = 0$, where c is denoting the modelling parameter. In the mechanical domain, this element represents an explicit or implicit stiffness power storage phenomenon, where e represents the effort, f the position deviation rate (velocity) and c denotes the inverse of the stiffness. In such case, the behaviour equations will be expressing hook law. Electrically, C represents the placement of an explicit or implicit electrical capacitor. Also, C represents the placement of an explicit or implicit heat or hydraulic power sink.

$De : u_m$ is associated with the effort u_m measurement functions. With a zero flow, $De : u_m$ does not affect the BG model. It serves as a monitoring and/or control function allowing to indicate the positions of the effort sensors and their corresponding simulated output within the model.

$Df : i_m$, similar to $De : u_m$, serves as a flow i_m sensors. It indicates the positions of the flow sensors and their corresponding simulated output.

$TF : n$ and $GY : k$ are dual-port elements used to represent energy transformations from one domain to another. They are characterized by the power conservation between their two bonds.

2. $\mathcal{A}_{BG}$ is the set of two-ends oriented bonds, graphically represented by half-arrows,

verbalizing the power exchange between the distinct elements and the junctions $\mathcal{E} \cup \mathcal{J}$. The bonds are associated with two conjugated variables: the effort e (above the bond) and the flow f (below the bond). Effort is the intensive variable (e.g. pressure, force, voltage) and flow is the derivative of quantitative extensive variable (e.g. volume flow, velocity, current). The power exchanges (energy variation) are determined through the so-called relation $P = e \times f$. The positive direction of the power flow is represented by the half-arrow on the bond (see Fig. 2.1).

3. $\mathcal{J}$ is the set of multi-port junctions represented as nodes that connects elements of $\mathcal{E}$. It contains two types of junctions: a 0-junction and 1-junction. The first acts as a generalised equivalent form of the kirchhoff law, where all the connected bonds (and their connected elements) share the same effort value and the sum of the flows around the junction is zero. As for the 1-junction, it shares the same flow to all its connected bonds and the sum of the efforts around the junction is zero.

$\mathcal{A}_{BG} \cup \mathcal{J}$ constitutes the BG internal structure that describes the energy flows and the component placements and configurations. In its turn, $\mathcal{E}$ models the physical components and phenomena according to their different nature, parameters and characteristics. Using this idea, many analyses can be performed by keeping the same internal structure and modifying the element capacities or sizes through their parameters. Graphically, this plug and play feature reveals the great value of the BG as a powerful design and sizing tool for the different dynamical systems such as HRES. Furthermore, this structure enables the user to gather different bonds, elements and junctions to constitute sub-models or groups representing an upper-level of modelling architecture of the system physical structure. This enables an evolutive structure where sub-models can be assembled and connected to an already existing model. For large complex system, this higher level of the BG modelling is sometime referred to by the word BG. These are valuable characteristics, specially for system such HRES. They allow constructive assembled models, where many can be modified, resized, used separately or as sub-models in more complex systems. This leads to the possibility to build a useful model library.

Fig. 2.1 shows a BG model of an electrical circuit, where:

- $L :_{L1}$ represents the inductance storage capacity.

- $Df : i$ represents a current sensor measuring the flow.
- $Se : E$ represents the effort (voltage) power source.
- $R : R1$ and $R : R2$ represent the parallel resistances.

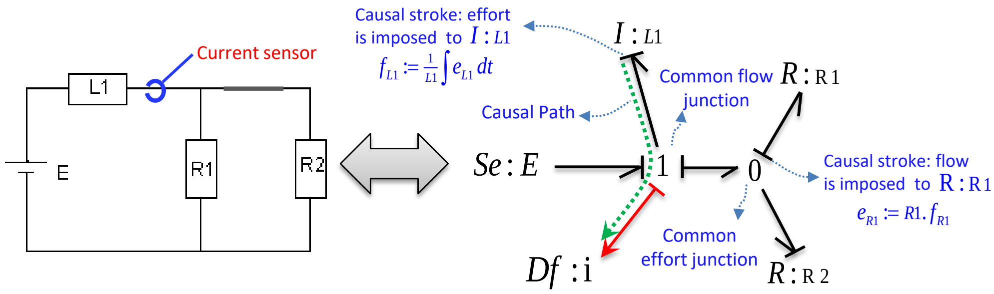

Figure 2.1 – An example of a BG model

2.1.1 Causal properties of the BG

Another very helpful feature of the BG is the cause-effect relationship called the causality. By convention, it is denoted by a cross-stroke which is placed near (resp. far from) the BG element for which the effort (resp. flow) is the input (see Fig. 2.1). For instance, the Kinetic energy storage element $I : L1$ is given in Fig. 2.2.d in both derivative and integral causalities. The equivalent block diagrams are also shown for each case.

Definition 2.1.2 (Causal path). *A causal path is a path of successive bonds following the same causality stroke direction [131]. Since a gyrator flips the effort and the flow physical senses, in case of the presence of a gyrator GY on the path, the stroke direction flips to the opposite side when the causal path passes thought the gyrator.*

A causal path that connects one or more elements to an output represented in the BG by an effort or flow detector De or Df, indicates elements affecting the concerned output (the dependencies between each output and the different BG elements). Usually the causal paths are used to study the observability, controllability and the diagnosability of the system using the bond graph model [132].

Fig. 2.2.b shows an example of causal path relating the output of $Df : i$ to the BG element $I : L_1$. This indicates that the output effort of $Df : i$, i.e the current, is imposed by the output of the block $I : L_1$ (1 junction has a common flow imposed by the bond that has a distant causality stroke).

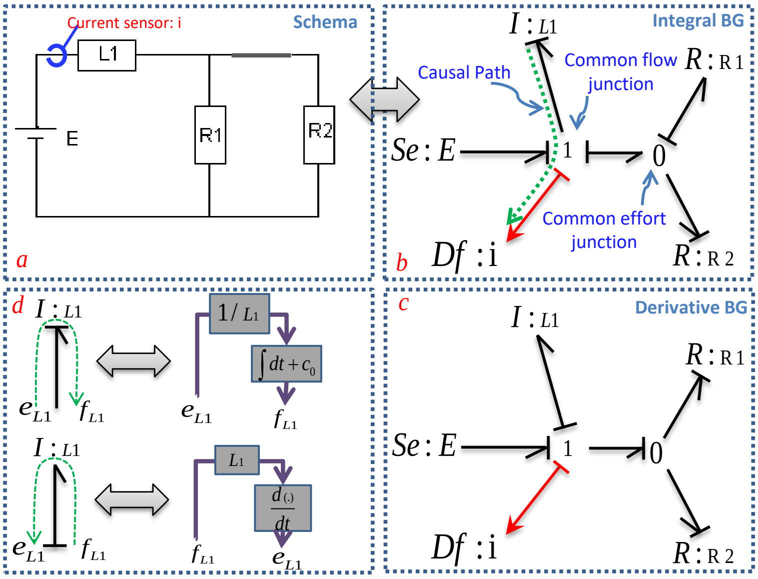

Figure 2.2 – Models of electrical circuit (a) and the corresponding causal integral BG (b), derivative BG (c) with the simulation block diagram (d)

A BG is a causal model, this means it shows the cause-effect relations and the computation traces of the unknown variables from known ones. Each element such as C, I and R has two possible causality configurations, they are marked by the stroke placed at the end of each bond. Dynamical elements (C, I) are characterized by the derivative or integral causality. Having this dual causalities, two BG for the same system can be found.

Integral BG: in which the dynamical elements are in integral preferred causality (see element I : L1 in [Fig. 2.2.b]). The dynamical equation of the system, in this case, is given by Eq. 2.1.

Derivative BG: in which the dynamical elements are in derivative preferred causality (see element I : L1 in [Fig. 2.2.c]). The dynamical equation of the system, in this case, is given by Eq. 2.2.

$$i(t) = \frac{1}{L1} \int_{t_0}^{t} e(t)\, dt + i_0 \tag{2.1}$$

$$e(t) = L1 \frac{di}{dt} \tag{2.2}$$

Notice that since both equations Eq. 2.1 and Eq. 2.2 are equivalent and represent the same dynamical behaviour, both BG are equivalent. One difference between the two representations is the need for the initial conditions i_0 to compute Eq. 2.1. Actually, the physics is acausal and is modelled by acausal BG which represents the physical level of the modelling. The causal BG represents the algorithmic level of the modelling and it is devoted for the simulation and the control analysis. For this reason the integral causality is preferred for the simulation and the derivative for the FDI where initial conditions are unknown in the real process.

Using the BG model, the system dynamical behaviour can be simulated using simulation tools such as 20sim® [133] and symbols® [134]. The SSE can also be extracted by tracking the causality paths to write unknown variables in terms of known ones (control inputs and measured outputs).

Remark 2.1.1 (Pseudo-BG)**.** *A pseudo-BG is BG where some power bonds do not carry a real power physical quantity dimension. In such cases, the effort-flow product* ***can not*** *be expressed as power. Example: Consider a thermal system where the effort is the temperature $e = T$, and the flow is considered as the entropy flux $f = \Delta\dot{S}$. In this case, we obtain an ordinary BG where the effort-flow product is the power: $e \times f = T\Delta\dot{S}$. Practically sometimes, it is more convenient to represent the flow as a heat flux $f = \dot{Q}$ where $\dot{Q} = T\Delta\dot{S}$. In this case, the previous product does not represent any physical meaning and the power is represented by the flow itself, therefore such BG is called a pseudo-BG. Generally, it is more used in process engineering.*

2.1.2 BG for HRES

A)- Modulated elements

All the previous elements are passive and predefined. Variable sources, transformers, resistance, capacitive and inertia elements are represented, respectively by MSe, MSf, MTF, MGY, MR, MC, MI. Maintaining the same number of the BG ports, these modulated elements are characterized, each, by an extra input signal port allowing to feed the corresponding variable from an external variable signal ("M" stands for modulated).

In order to extend the BG modelling approach to cover the renewable energy systems, extra BG elements are needed to be defined:

B)- BG elements for multi-cellular systems

Definition 2.1.3 (Multi-cellular systems)**.** *Multi-cellular systems are class of systems that possess a cellular structure. They are generally constructed of $m = n_s \times n_p$*

cells, where n_s cells are mounted in series power configuration i.e sharing the same flow (current in electrical domain), and n_p cell arrays mounted in parallel power configuration i.e sharing the same effort (voltage in electrical domain).

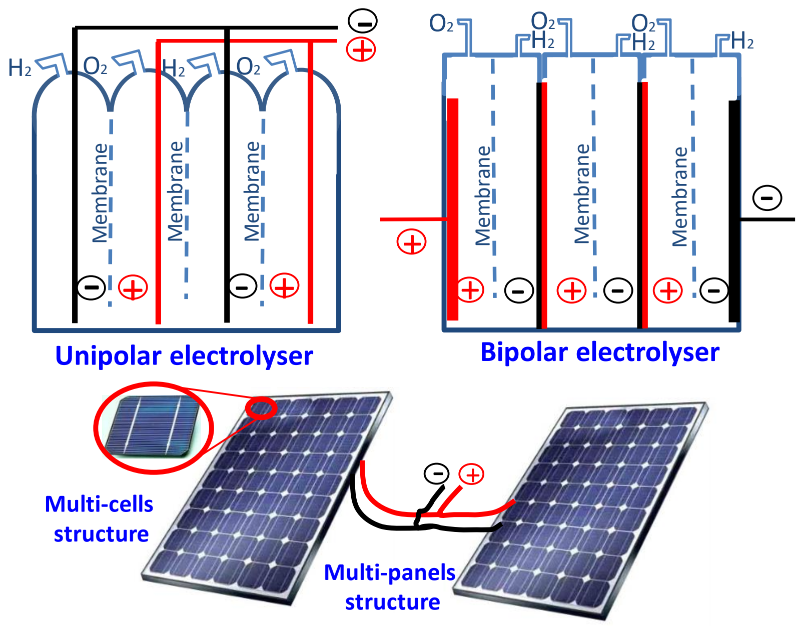

Figure 2.3 – Multi-cellular systems

This concept is very common within the renewable energy systems. A solar panel farm is constructed of many panel arrays mounted in parallel and series. Each panel itself is made of number of cells mounted generally in series allowing a higher voltage output. Electrolysers and fuel cells identically are constructed using stack of cells, array of electrolysis cells are mounted in bipolar or unipolar configuration [135] as shows Fig. 2.3.

The dynamic of these cells is usually highly non-linear and complex, modelling all the cells at the same time needs an enormous processing capacity. By assuming all cells are identical and working in homogeneous operating conditions (i.e temperature, irradiation etc.), it is convenient to model one cell of a multi-cellular system and amplify the power according to the cell configuration and number. To integrate this approach to the BG model, BG power amplifiers are defined:

BG amplifiers

Definition 2.1.4 (BG amplifier elements)**.** *A power amplifier is a dual-port BG element. Between the input and the output bond, the power is not conserved, output power =*

$n_i \times$ input power, where $n_i > 1 \in \mathbb{N}$ denotes the amplification factor. Sme is an n_s times effort amplifier. Smf, similarly, is a n_p times flow amplifier, see Fig. 2.4.

The causality behaviour is the same as for power transformer TF. Through the amplifier the input and the output conserve the same power type (effort or flow).

Sme is used to amplify and imitate n_s serial cells sharing a common flow. Smf is used to amplify and imitate n_p parallel cells sharing a common effort.

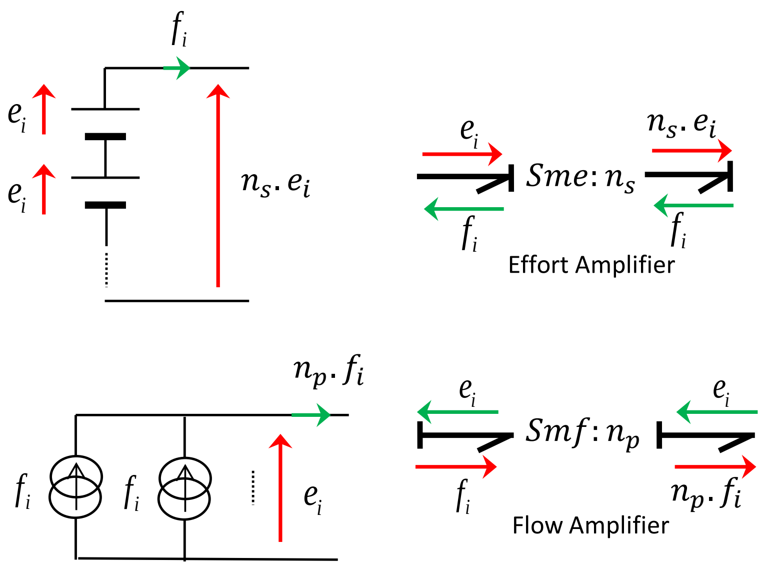

Figure 2.4 – Effort and flow power amplifiers

Unlike the other BG elements, an amplifier does not represent a real physical component. Therefore, the relative position of the sensors and the other elements with respect to the amplifiers can be confusing. To simplify the BG detector placements relatively to the new defined amplifiers, properties 2.1.1and 2.1.2 must be considered.

Property 2.1.1. *In the BG model, the detector elements, De or Df can be implemented before or after the amplifiers. When measuring the effort or the flow of a single cell (such as one-cell voltage in series assembly, one-cell current in parallel assembly), then the correct place to implement the BG detector is before the amplification. If the measured variable concerns the whole cell assembly then the detector must be placed after the amplifier. In some cases, where an intensive power variable such as the temperature is measured then the detector $De : T$ place can be chosen arbitrary before or after the amplifier (in the temperature case, flow amplifier Smf is used).*

Property 2.1.2. *If the parameter of the element, such as a capacitor C : cal, is obtained for a single cell then its correct place is before the amplification. Else-wise, if the parameter of the BG element is obtained for the global set of the cells then its representative element must be placed after the amplification. If moved from one side to the another, the element must be replaced by its equivalent.*

Due to the different coupled phenomena that exist in multi-physical systems such as HRES, the BG theory includes some number of coupled elements allowing to model some complex coupled dynamics. Here, we are most interested in the dual-port active resistance element RS defined as follows.

C)- RS multi-port active resistance

Definition 2.1.5 (RS multiport active resistance R). *[136] Unlike the single-port ordinary resistance R, the coupled resistance RS is a dual-port BG element Fig. 2.5. From one side connected to an energetic domain (e.g electrical, mechanical, hydraulic...), it behaves as the ordinary resistance element $R : r$. In its resistive causality, it receives the effort e_r and responses back with the corresponding flow (if linear $f_r = e_r/r$). From the other side which is related to the thermal domain, it behaves as power source injecting the dissipated power from the first domain into the thermal sub-model. The power is injected via the thermal bond in form of flow or effort according to the causality of the thermal bond.*

Fig. 2.5 illustrates the generalized form of the resistance RS. Showed in its conductance causality, the associated relation between the non-thermal effort e_1 and flow f_1 is: $e_1 = \Phi(f_1, e_2)$, where $\Phi(f_1, e_2)$ can be linear or non-linear and may depend on the thermal effort e_2 i.e the temperature.

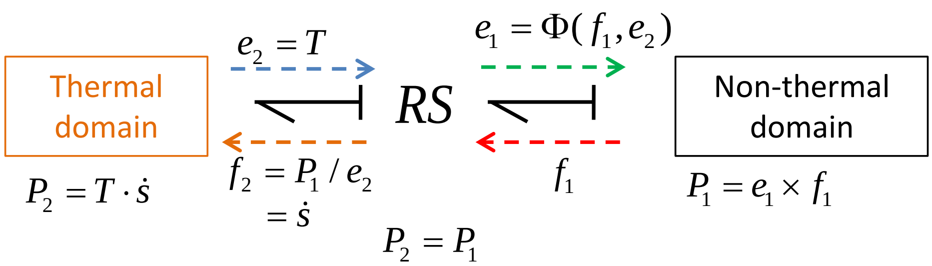

Figure 2.5 – Dual-port resistance element

On the thermal side, RS injects the consumed power on the first bond $P_1 = e_1.f_1$ as a flow $f_2 = P_1/e_2$ (an entropy flow in the ordinary BG and heat in the case of pseudo-BG as explained in Remark 2.1.1). The type of the injected power through the second bond (flow or effort) is defined by the second bond causality. In this case e_2 (usually temperature in thermal domain) is considered as an input, therefore the coupled resistance RS injects the power as a flow f_2 where $f_2 = P_1/e_2$.

Property 2.1.3. *Following the thermodynamic laws, the thermal bond is always imposing the temperature of the thermal domain on the resistance RS. In its turn, the resistance responds back with the corresponding entropy flow in case of the real-BG, or in the heat flow in case of the pseudo-BG.*

2.1.3 Hybrid Bond Graph (HBG)

HBG is an extended version of the BG theory that includes the switching elements. Many researches are conducted in order to introduce the ideal switch behaviour into the BG [137, 138, 139, 99].

An ideal switch acts as a power switch. When it is off, it cuts off the power link between parts that it connects. In the electrical domain, it could be representing a manual switch, a relay, a transistor or an ideal diode. In hydraulic domain, it could be an electro-valve.

From modelling point of view, two types of switches can be distinguished. The first one, called controlled switch (e.g. electrical switch, valve), is controlled by an external signal (as control input) . The second one, named autonomous switch, depends on inner conditions of the system such as the value of the state variables (case of ideal diode).

Generally, there exist three main ways to represent the controlled or the autonomous switch in the BG model:

- Dual-state modulated resistance toggling between a very high or very low resistance [138]. This representation is simple but the resistance presents a permanent dissipation that can not be avoided.
- Transformer with two states associated to the transformation parameter $n \in \{0, 1\}$ [139]. Using this method the causality needs to be conserved.
- The controlled junctions [99]

Definition 2.1.6 (Controlled Junctions)**.** *There exist two types of dynamical controlled junctions (X1 and X0) associated, each, with a boolean control signal. When receiving the ON signal, X1 and X0 behave respectively as an ordinary 1 or 0 junction. In X1*

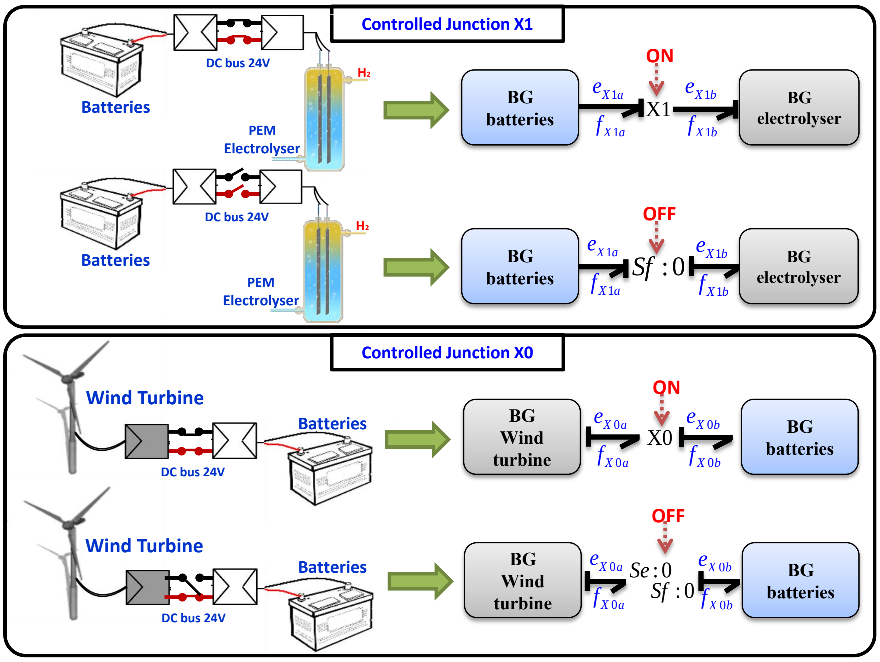

Figure 2.6 – Controlled junctions

case, the flow value (resp. effort value in 0-junction) associated with all connected bonds are equal and the sum of the effort values (resp. flow values in 0-junction) is equal to 0. When an OFF signal is sent to a X1-controlled junction, X1 forces a value of zero flow to all its connected bonds (as if they were connected to zero flow source) (see [Fig. 2.6]). This expresses that there is no energy transfer across the junction and the current is being cut. In its turn, an OFF X0 junction imposes a zero flow on the bond with the flow-out causality (near causality stroke) and a zero effort otherwise [99].

[Fig. 2.6] illustrates the notion controlled junctions. The ON/OFF switching of an ordinary power component (for ex. an electrolyzer) can be simulated by a current-cut X1 junction. The corresponding equations of X1 relative to each case (ON/OFF) illustrated in [Fig. 2.6] are expressed by Eq. 2.3.

$$u := ON \Rightarrow \begin{cases} e_{X_{1b}} := e_{X_{1a}} \\ f_{X_{1a}} := f_{X_{1b}} \end{cases} \text{ where } e_{X_{1a}} \text{ and } f_{X_{1b}} \text{ are computed in the sub-systems}$$

$$u := OFF \Rightarrow \begin{cases} f_{X_{1a}} := 0 \\ f_{X_{1b}} := 0 \end{cases} \; e_{X_{1a}} \text{ and } e_{X_{1b}} \text{ are computed in the sub-systems} \tag{2.3}$$

A WT (such as Primus Air40), if disconnected from the batteries, needs to be in short-circuit to activate its electromagnetic breaking system. Thus, an X0 junction is used as shows [Fig. 2.6] and the corresponding equations of X0 are showed in Eq .2.4.

$$v := ON \Rightarrow \begin{cases} e_{X_{0a}} := e_{X_{0b}} \\ f_{X_{0b}} := f_{X_{0a}} \end{cases} \text{ where } e_{X_{0b}} \text{ and } f_{X_{0a}} \text{ are computed in the sub-systems}$$

$$v := OFF \Rightarrow \begin{cases} e_{X_{0a}} := 0 \\ f_{X_{0b}} := 0 \end{cases} \; e_{X_{0b}} \text{ and } f_{X_{0a}} \text{ are computed in the sub-systems} \tag{2.4}$$

Until today, the controlled junction represents the most used approach to model such switching. However, in some cases when the switching is associated with a change in the model causality, the controlled junction cannot be used and can be replaced by the dual-state modulated resistance.

2.2 BG Linear Fractional Transformation (LFT)

2.2.1 Uncertainties within the HRES

In practice, it is very difficult to find an accurate model to describe the system dynamical behaviour. The uncertainties on some model parameters, if not considered, can cause a serious robustness problem. Tasks such as control and model-based diagnosis depend heavily on the accuracy and the uncertainties within the model. The answer to how much the model differs from the real process depends on the amount of the uncertainties present in the modelling and the measurements. For HRES, most of the component parameters are obtained using statistical fitting estimations with certain degrees of uncertainty (case of the EL FC and PV). In the presence of the uncertainties, the control and the MBD can be affected and suffers from robustness issues. In order to obtain a robust control or diagnosis of the Dynamical System (DS), the existing uncertainties are considered into the model. The LFT aims to represent and integrate the parameters uncertainties in the model. To be included, the uncertainties of the considered parameters are assumed composed each of two parts: a nominal value and a multiplicative or an additive uncertainty.

In the electrolyser for example, consider the membrane electrical resistance r_{ohm}

with an exact unknown uncertainty $\delta e_{r_{ohm}}$. Then, r_{ohm} can be expressed as :

$$r_{ohm} = r_{n_{ohm}}(1 + \delta e_{r_{ohm}}) \tag{2.5}$$

where:

- $\delta e_{r_{ohm}}$ is the relative uncertainty bounded by minimum and maximum values respectively $\delta r_{ohm_{min}}$ and $\delta r_{ohm_{max}}$; $\in I = [\delta r_{ohm_{min}}, \delta r_{ohm_{max}}]$
- $r_{n_{ohm}}$ is the nominal value of r_{ohm}

Practically, for an industrial process, $r_{_{ohm}}$ is unknown. Only $\delta r_{ohm_{min}}$, $\delta r_{ohm_{max}}$ and $r_{n_{ohm}}$ are given. I is often given symmetric and zero-centred such as $r_{_{ohm}} \pm 5\% \times r_{n_{ohm}}$.

The LFT approach is used to include these uncertainties within the analytical model represented by its SSE. The BG methodology is extended to cover the uncertain systems by introducing the LFT-BG.

2.2.2 LFT modelling

The LFT model is one way to include the multiplicative parameters uncertainties. [Fig. 2.7] shows the general form of LFT model. The parameters uncertainties are represented in a diagonal matrix Δ, while M represents the nominal dynamical part of the model.

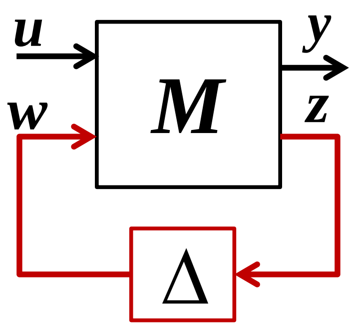

Figure 2.7 – LFT modelling

$$\begin{aligned} M : \dot{x} &= f(x) + B_1 u + B_2 w \\ y &= C_1 x \qquad\qquad ; w = \Delta . z \\ z &= C_2 x \end{aligned} \tag{2.6}$$

Eq.(2.6) shows the LFT general SSE representation, where:

- x denotes the state vector
- y represents the system output vector
- u is the input vector
- z denotes the system dynamics affected by the concerned uncertainties
- $f(x)$, B_1 and B_2 represent the system dynamical behaviour

By multiplying z and Δ, the resulting product w is re-injected to the model [140]. This analytical approach of the LFT needs lot of mathematical reformulations, such as matrix diagonalization and inversions.

Extended from the analytical representation to the BG theory, the LFT-BG allows displaying explicitly all the uncertainties on the BG model and uncertain dynamical model is then easily deduced.

2.2.3 LFT HBG

The method to include model uncertainties directly into the BG or HBG is detailed in [141, 142]. The obtained BG is then called LFT-BG (resp. LFT-HBG to cover the hybrid systems). To illustrate this, consider a BG resistance r_{ohm} as an uncertain parameter.

In the HRES models, the resistances are most likely to be non-linear but affine. Therefore, we consider the general case of the resistance where $e_r = r_{ohm}.\Phi(f_r)$. The resistance parameter is given by r_{ohm} and $\Phi(f_r)$ represents a function of f_r. In case of the causality where the flow is imposed (f_r is the input of the nominal resistance and e_r is the output), using the nominal resistance we have $e_{n_r} := r_{n_{ohm}}.\Phi(f_r)$.

In the LFT HBG, the desired output is shown in Eq.(2.7)

$$e_r := r_{_{ohm}}.\Phi(f_r) \tag{2.7}$$

Where $r_{_{ohm}}$ represents the exact resistance which includes the uncertainty and e_r represents the associated effort.

Replacing $r_{_{ohm}}$ by Eq.(2.5), Eq.(2.7) can be re-written as Eq.(2.8)

$$\begin{aligned} e_r &:= r_{n_{ohm}}(1 + \delta e_{r_{ohm}}).\Phi(f_r) \\ &:= \underbrace{r_{n_{ohm}}.\Phi(f_r)}_{e_n} + \underbrace{\delta r_{n_{ohm}}.\left[r_{n_{ohm}}.\Phi(f_r)\right]}_{e_{unc}} \end{aligned} \tag{2.8}$$

where e_n is the nominal value of the effort and e_{unc} is its associated uncertainty. Notice that when $\delta e_{r_{ohm}}$ is equal to zero, then we obtain only the nominal value e_n.

To include the uncertainties within the model, we consider first the Block Diagram (BD) illustrated by [Fig. 2.8]. In the resistive causality, the nominal resistance block $r_{n_{ohm}} \cdot \Phi(.)$ represents the nominal behaviour of the dissipation phenomenon. The uncertainty is introduced by the gain block $\delta_{r_{ohm}}$ that receives as an input the nominal effort e_n (output of the nominal block). By adding the output of the uncertainty block e_{unc} with the output of nominal block e_n, the total effort e_r, which includes the uncertainty, is obtained same as in Eq.(2.8).

To achieve this using the BG representation, the original BG (respectively HBG), refereed to by nominal BG, is simply modified to include the uncertainty by applying the LFT as shown in [Fig. 2.9]. The figure illustrates the integration of the uncertainty on the resistance element in both causalities (resistive and conductance).

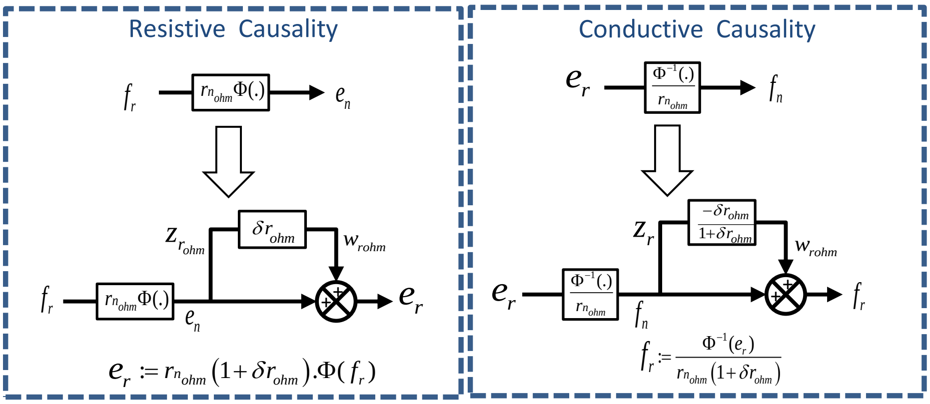

Figure 2.8 – Block diagram representation of the resistance LFT

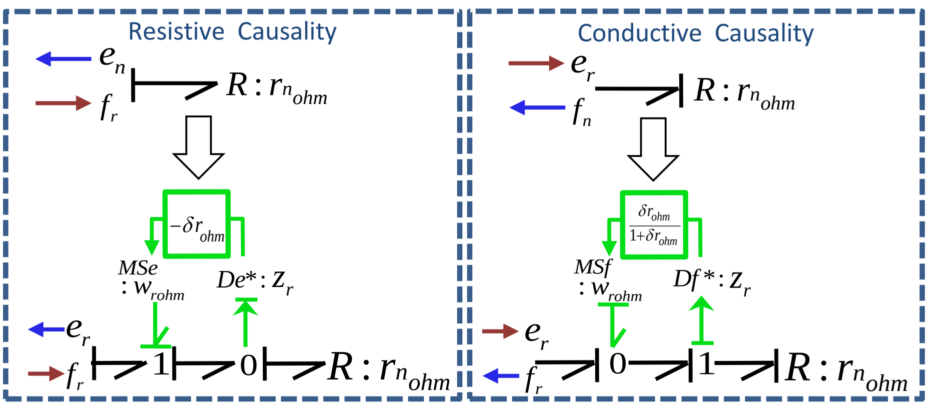

Figure 2.9 – Injecting uncertainty on R BG element

In the resistive causality case, e_n can be measured using a virtual effort sensor $De^* : zr$ on the bond of the nominal resistance as shown in the figure. For a chosen δr_{ohm}, the product $e_{unc} = \delta r_{ohm} \times e_n$ is injected to the nominal bond using effort source $MSe : w_{rohm}$ connected to 1 junction (effort adder which conserves the input flow). The obtained BG representation is then equivalent to Eq.(2.8) .

In case of imposed effort (conductive causality), the nominal flow f_n is given by Eq. 2.9.

$$f_n := \frac{\Phi^{-1}(e_r)}{r_{ohm}} \tag{2.9}$$

The desired final output flow is the total flow f_r can be expressed by Eq.(2.10) by considering Eq.(2.5) and Eq.(2.9).

$$\begin{aligned} f_r &:= \frac{\Phi^{-1}(e_r)}{r_{n_{ohm}}(1+\delta_r)} \\ &= \frac{f_{n_r}}{(1+\delta_r)} = \frac{f_{n_r}(1+\delta_r-\delta_r)}{(1+\delta_r)} \\ &= f_n + f_n \cdot \underbrace{\frac{-\delta_r}{1+\delta}}_{\delta'_r} = f_n + \underbrace{f_n \cdot \delta'_r}_{f_{unc}} \end{aligned} \tag{2.10}$$

To compute f_r using the BD, f_n can be obtained using the nominal resistance as shown in [Fig. 2.8] (resistive causality). By multiplying the nominal flow f_n (representing the nominal output) by the conductive uncertainty $\delta' r$, the uncertain flow f_{unc} is obtained. The total flow f_r expressed in Eq.(2.10) is, then, evaluated by adding both the obtained uncertainty flow f_{unc} and the nominal flow f_{n_r} as shown by [Fig. 2.8].

Finally, in the BG model $f_n \cdot \frac{-\delta_r}{1+\delta_r}$ must be added to the nominal flow. A virtual flow detector $Df^* : z_r$ on the nominal resistance collects f_n. A flow source MS_f injects the product $f_n \cdot \frac{-\delta_r}{1+\delta_r}$ to the nominal flow through a 0 junction as shows [Fig. 2.9]. Other methods to integrate model uncertainties in a BG also exist such as incremental BG used in [91, 117].

Similarly, on the nominal model for all the single port BG elements, the multiplicative uncertainties can be introduced using the LFT form.

As mentioned in (section 2.1.2, page 60), the HRES are characterized by the coupled resistance with the thermal domain. The LFT transformation needs to cover the active resistance BG element RS.

First consider, in the nominal case, the RS equation of the non-thermal domain is linear and expressed by Eq. 2.11.

$$e_{1n} = r.f_{1r} \tag{2.11}$$

where:

- e_{1n} is the nominal non-thermal effort (e.g voltage in the electrical domain),
- r is the resistance parameter associated to the RS,
- f_{1r} is the non-thermal flow (e.g current in the electrical domain).

The desired effort affected by the uncertainty e_1 can be obtained from Eq. 2.11 by substituting r with $r_n.(1+\delta_r)$ as given by Eq. 2.12.

$$e_1 = r_n.(1+\delta_r).f_{1r} = \underbrace{r_n.f_{1r}}_{e_{1n}} + \underbrace{\delta_r.[r_n.f_{1r}]}_{e_{1unc}} \tag{2.12}$$

where:

- e_1 is the total non-thermal effort (e.g voltage in the electrical domain),
- r_n is the nominal resistance parameter associated to the RS,
- δ_r is the relative uncertainty on r_n,
- e_{1n} is the nominal non-thermal effort (e.g voltage in the electrical domain),
- e_{1unc} is the uncertain effort.

In the thermal domain, the expression nominal heat flux f_{2n} generated by RS, that corresponds to the pseudo-BG, is given by Eq. 2.13.

$$f_{2n} = e_{1n}.f_{1n} = r.f_{1n}^2 \tag{2.13}$$

where:

- e_{1n} is the nominal non-thermal effort (e.g voltage in the electrical domain),
- r is the resistance parameter associated to the RS,
- f_{1n} is the nominal non-thermal flow (e.g current in the electrical domain).

The desired heat flux affected by the uncertainty f_2 can be obtained by substituting r with $r_n.(1+\delta_r)$ as given by Eq. 2.14.

$$f_2 = r_n.(1+\delta_r).f_{1n}^2 = \underbrace{r_n.f_{1n}^2}_{f_{2n}} + \underbrace{\delta_r.[r_n.f_{1n}^2]}_{f_{2unc}=\delta_r.f_{2n}} \tag{2.14}$$

where:

- f_2 is the total thermal flow i.e affected by the uncertainty,
- r_n is the nominal resistance parameter associated to the RS,
- δ_r is the relative uncertainty on r_n,
- f_{1n} is the nominal thermal flow,
- f_{2unc} is the uncertain thermal flow.

Fig. 2.10 shows a proposed BG-LFT for the RS element by Djeziri [143]. The proposed LFT guaranties obtaining the desired heat flux affected by the uncertainty f_2. However, in this proposed transformation, only the thermal domain is affected by the uncertainty.

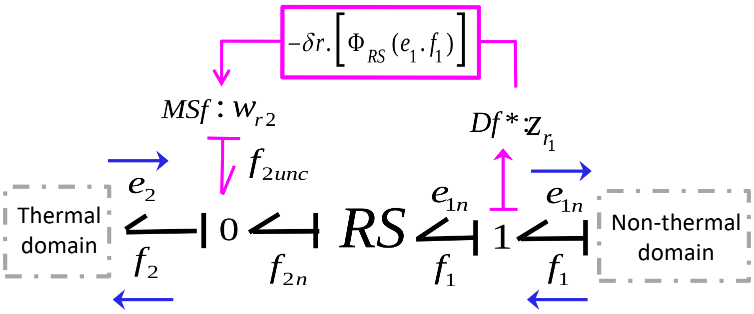

Figure 2.10 – A proposed LFT for a RS [143]

Since the uncertainties affect **both** the non-thermal (electrical, chemical...) and the thermal domains, the LFT is needed to be applied on each bond associated to the RS. This is achieved using the same uncertainty value with the corresponding LFT with respect to causality of each bond. [Fig. 2.11] shows the new proposed LFT form of the RS in resistive causality at the non-thermal domain and in conductive causality at the thermal domain.

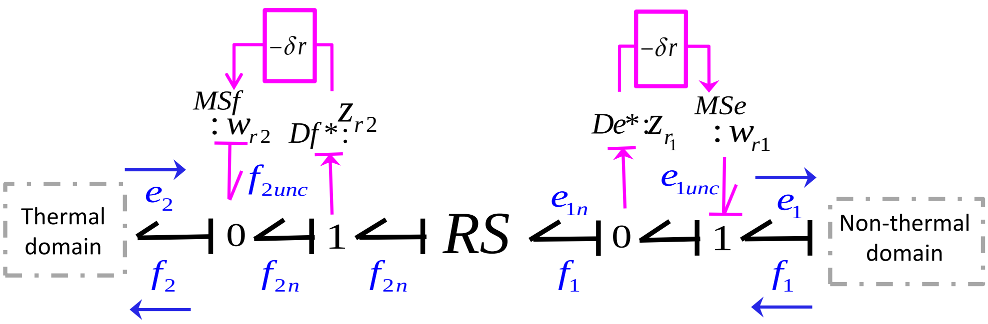

Figure 2.11 – Injecting uncertainty on coupled R element

On the non-thermal side (right side), the ordinary LFT is applied according to the causality, similar to a regular R element. In the resistive causality shown by [Fig. 2.11], this will allow obtaining the total effort that includes the uncertainties $e_1 = e_{1n} + e_{1unc}$ as explained by Eq. 2.12. On the thermal side, where the RS is usually in conductive causality (i.e the temperature e_2 is imposed by the medium which receives the heat flux f_2 generated by RS), the generated heat flux that includes the influence of the uncertainty f_2 is obtained by adding, through a 0-junction, to the nominal flow f_{2n} the uncertain flow f_{2unc}, as explained in Eq. 2.14. This latter (f_{2unc}) is computed by collecting the nominal flow f_{2n} via $Df^* : z_{r2}$ and multiplying it by the resistive uncertainty δ_r. As a result, both sides of the RS are affected with the same uncertainty.

When the non-thermal side is in conductive causality (i.e the effort e_1 is the input and f_{1n} is computed), the conductive uncertainty $\delta_r' = \frac{-\delta_r}{1+\delta_r}$ must be used for the both sides of the RS.

An advantage of the LFT BG is the ability to get the LFT form simply by minor modifications of the nominal BG which is more complicated when dealing with equation-based models.

2.3 Example

In order to illustrate the use of the new defined BG elements, [Fig. 2.12] shows BG model of a PEM bipolar (i.e in series) multi-cell electrolyser. This example is presented here for illustrative purposes. In Chapter IV section 4.2.3.3, the EL model is described and explained in details.

[Fig. 2.12] shows that the model is constructed using a single cell BG model. Amplifiers associated to cells bipolar configuration (serial electrical, parallel gas outputs) are used to simulate the multi-cell behaviour. In the cell core, the electrolysis can be seen as a coupled reaction between the electro-chemical and the thermal domains. The EL core model is composed of two main junctions:

- 1-junction that express the electrolysis electrical phenomena
- 0-junction to express the thermal dynamic

Coupled resistances, such as $RS : Rohm$ which represents the PEM resistance, are used. These coupled resistances injects the generated heat into the thermal 0-junction. An effort amplifier Sme amplifies the voltage of the electrical port to simulate the multi-cell behaviour and the flow amplifier Smf amplifies the heat and the gas respectively on the thermal and gas ports. A controlled X1-junction is used to represent the on-off switch of the electrical power. The electrolyser is supplied with AC source represented by $Se : Ac$.

The average model of an AC/DC power converter is represented by $TF : ac\_dc$ and the shunt resistance $R : Rsh_e$. The variable resistance $MR : r\_act$ is used to set the current. On the thermal side, Smf amplifies the generated heat according to the cell number. A temperature sensor $Water\_temp$ is added. $C : cal$ represents the thermal capacity of the global assembly of the cells and the water. $R : rth$ represents the thermal conductivity between the electrolysis and the outside medium temperature denoted by $MSe : Tout$ receiving the signal of the output temperature Out_temp.

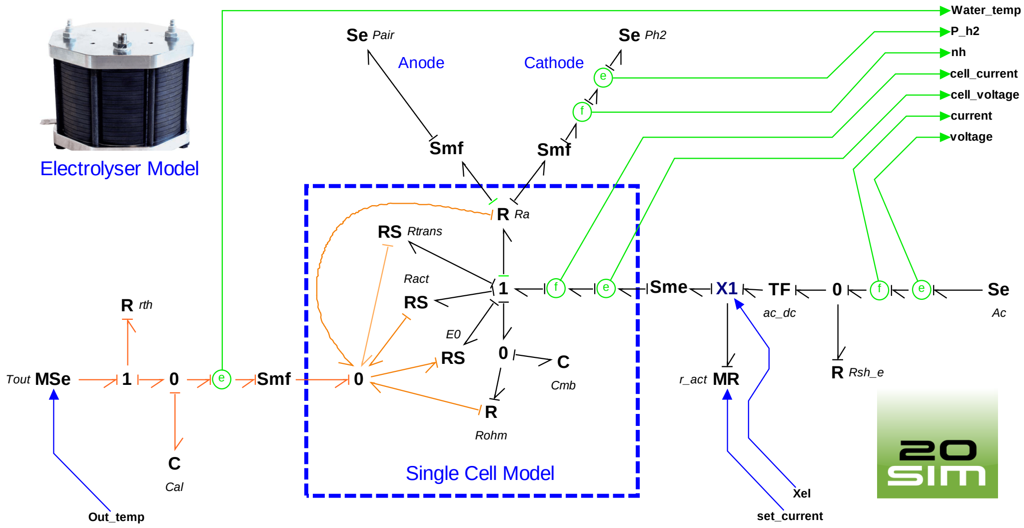

Figure 2.12 – Electrolyser HBG model

By this section, the BG has been adapted to cover the HRES. The covered aspects include components characterised with multicellular structures, switching components, and uncertain parameters. However, the switching state of the controlled junction are still not well-defined. The next section addresses the management of the switching state for all the controlled junctions, this allows to simplify the OMM and separated the system discrete switching behaviour from the dynamical continuous states handled by the BG. This provides a simpler and flexible OMM and a pure graphical modelling and OMM.

2.4 Event driven Hybrid Bond Graph (EDHBG) For HRES

2.4.1 Operating Mode Management (OMM)

An OM is defined by the set of objectives needed to be fulfilled, in their turn these are associated to a set of components that are putted in the service or not. Each element of the system can be designated by a boolean variable that describes its state (active or inactive). By regrouping all the these switching states together, the switching vector β_i is obtained. β_i derives the switching state of the whole system.

Since for each OM, a specific configuration of active and deactivated components is defined, a general definition of an automaton (state-machine) is introduced, where in each OM, the state is the boolean vector.

The automaton operates separately from the dynamic computation. The OMM can be easily defined regardless of the dynamical model. In the HRES context, by defining the automaton guard conditions and the distinct OM, the OMM can be based on both of the user objectives and operational availability of the components as shown [Fig. 2.13].

The user objectives can be based on:

- The required power to be stored or consumed.
- The produced power given by **the output of the system** and related to other qualities of the system such as **the input power** (solar radiations and wind speed).
- **The predictions** such as low incident power forecast.

In their turn, operation availability conditions can be based on:

- The **component operational states** and capacities such as full hydrogen tank, overcharged batteries or max power limit of the different electrical components.
- The **component health** and **diagnosis states** such as fault detection or significant degradation and wearing detection...

Any discrete state machine approach can be used to manage these distinct OM. The choice of the automaton as state machine is justified as it is the easiest way to achieve this propose. As a graphical approach, it is very suitable with the HBG framework. The automaton can be represented by state machine coded in C, although many simulation

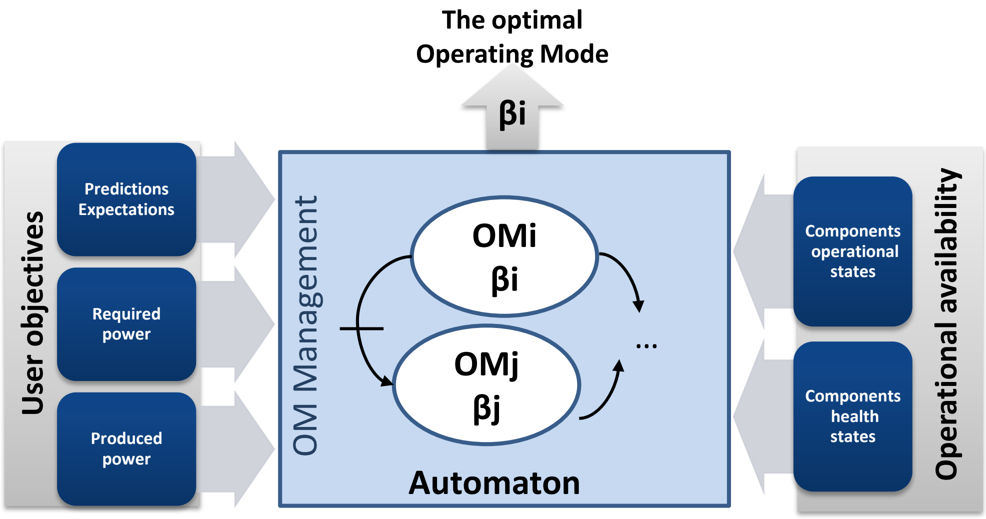

Figure 2.13 – The OMM objectives

software allow a graphical implementation such as Stateflow Matlab etc. The automaton signals can also be obtained from a real PLC or relays controlling the real HRES switches. This allows synchronizing the model OM with the real system, representing an interesting feature to be used in the FDI.

2.4.2 Definition and modelling

To cover the general case, consider a switching system with n controlled switches and m the autonomous switches. Let $\beta_{ci} = [sw_{i1}, sw_{i2}, ...sw_{in}]$ (resp. $\beta_{ai} = [sw_{i1}, sw_{i2}, ...sw_{im}]$) be the vector representing, at a given time i, the state of the n (resp. m) junctions. sw_{ij} represents the state of the j_{th} junction. Let $\mathcal{S}_c$ (resp.$\mathcal{S}_a$) be the set of 2^n (resp. 2^m) possible vectors β_{ci} (resp. β_{ai}). Let $\mathcal{B}$ be a set of bond graphs BG_i. β_{ai} depends on inner conditions or on the values of the state variables of the system. β_{ci} depends only on external conditions (such as the values of the control inputs). Let define $\mathcal{S} = \mathcal{S}_c \times \mathcal{S}_a$ and $\beta_i = [\beta_{ci}; \beta_{ai}]$.

The HBG can then be defined as follow:

Definition 2.4.1 (HBG)**.** *A Hybrid Bond Graph is a bijective map:*

$$\begin{aligned} HBG : \mathcal{S} &\longrightarrow \mathcal{B} \\ \beta_i &\longmapsto BG_i \end{aligned} \tag{2.15}$$

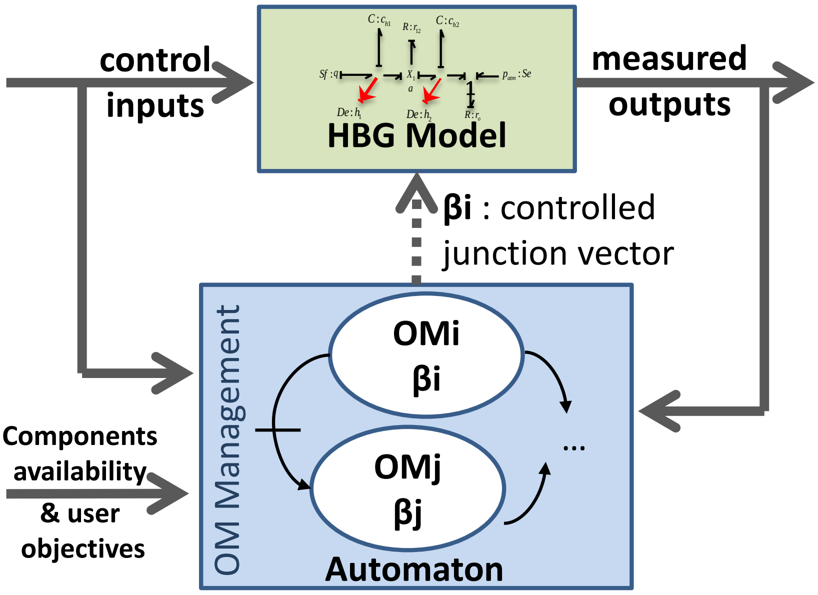

Figure 2.14 – Event Driven Hybrid Bond Graph

Here, the HBG is seen as a set in which p continuous bond graphs are wrapped corresponding to p configurations, where $p = card(\mathcal{S}_c) + card(\mathcal{S}_a)$. These configurations are resulting from the switching behaviour. [Fig. 2.6] gives an example of the two BG generated from a controlled junction. They correspond to a same HBG. [Fig. 2.14] shows the coupling between the HBG and the automaton to generate the HDS global model. The transition from one OM_j to another one OM_i is controlled by an automaton and is based on a predefined condition named guard condition. Events such as modification of the value of a state variable of the system, modification of the user objectives, detected faults or time periods can be taken into account in the specification of the guard conditions. These conditions allow to evaluate the possibility to stay in the current mode or to switch to another one [144]. According to the selected OM, the appropriate subgraph $BG_j \subseteq HBG$ is selected. More formally, the Event Driven Hybrid Bond Graph is defined as follows.

Definition 2.4.2 (EDHBG)**.** *An Event Driven Hybrid Bond Graph is an automaton*

$$\begin{aligned} HA &= (HBG(.), Q, Init, D, E, G) \\ &= (HBG(.), H_s) \end{aligned}$$

Where:

- $HBG(.)$ *Global hybrid bond graph including all the OM.*

- Q *Set of the discrete states q*
- $Init \subseteq Q \times X$ *Initial conditions of all the states*
- $D : Q \longrightarrow P(x)$ *Set of the mode domains*
- $E \subseteq Q \times Q$ *Transition arc from one mode to another*
- $G : E \longrightarrow P(x)$ *Set of the guard conditions*
- $H_s = (Q, Init, D, E, G)$ *Simple state automaton that controls the states of the controlled junctions.*

The HBG is used to represent the set of the distinct system configurations, while the simple automaton $H_s = (Q, Init, D, E, G)$ handles the discrete states, the initial conditions, the mode domains, the transition arcs and the guard conditions [95]. The signals of β_i are dispatched for each corresponding controlled junction in the HBG allowing the user to define its own OM.

LFT EDHBG

By considering the parameters uncertainties in the HBG of an EDHBG as described in Section 2.2.3, we obtain the LFT of the EDHBG.

2.5 Conclusion

The previous sections show that HDS modelling using the classical approaches such as the hybrid automata is simple when dealing with simple dynamics with small number of modes. For large complex systems with many modes, there is an absolute need to represent all the modes by their SSE. On the other hand, the BG assembling aspect of modelling, in which each element is associated to a real physical component in the real system allows the user to have less physical knowledge in all concerned domain. Therefore, HBG consists a good framework in order to represent the HRES. Compared to the HA, the Petri Net (PN) (HPN,MPN), the HBG, by itself, does not explicit the transitions between the different OM.

This issue is solved by adding a simple automaton to the HBG, the HBG is then called EDHBG. The EDHBG along with the introduced elements allows the modelling to cover the vast majority of the HRES that includes cellular structured components, coupled dynamics, switching elements and parameter uncertainties. It also allows a simple OMM independently from the dynamical state. In which, the HBG represents all the continuous dynamics, while a simple automaton evaluates the discrete states and the associated conditions to switch between the different OM. This separation allows the user to perform an easy OMM of the HDS by defining the different operating modes and their transitions. Moreover, as a powerful modelling formalism, the EDHBG can be also valuable to perform an on-line diagnosis.

Chapter 3

Diagnosis and Operating Mode Management

3.1 Introduction

As discussed in Chap I, BG (resp.HBG) offers the advantages of simplifying the modelling for the HDS and the multi-physical systems, the HRES included. In the context of the multi-physical HDS modelling, the advantages of the HBG approach are not limited to its unified modelling approach. The plug and play and the constructive modelling aspects, where each BG element represents a physical component or phenomenon in the real system along with the causal properties constitute a great deal for the FDI and the faulty component isolation procedure. Furthermore, achieving the MBD rests on finding the proper model of the HRES. The existing modelling issues and difficulties provoked by the multi-physical and hybrid aspect extend to affect also the MBD. All the classical modelling methods, such as the HA , MPN, HPN , Hybrid Grafcet, Statechart where, the explicit analytic equations of the system model must be found and written for each mode aside, are not suitable for such task. When using these modelling approaches with many OM, the MBD as any other model-based tasks can be challenging and mode-depending.

HBG offers a MBD quantitative fault diagnosis and isolation for dynamical system including the HRES [111, 112, 110]. ARR-based diagnosis are easy to extract and establish a consistency check test. Derived from the HBG, the GARR describe the global hybrid dynamic for all OM at once. However unlike the observers, once they are found they do not need special analysis for each OM. When evaluated in real-time, these extracted GARR expressions are used to check the HRES consistency within the predefined dynamical behaviour of the model. Thus, in normal healthy situation, the real time evaluated residuals, are expected to be equal to zero, else-wise a fault is detected.

Implicitly enclosing all the dynamical OM, the HBG as a global model allows, classically, to derive these GARR for all the OM at once. One issue with such method is the mixed aspect of its approach. A graphical modelling framework HBG, that was introduced to simplify the modelling task, is used to extract analytical algebraic expressions for the diagnosis.

3.2 FDI and Diagnosis via BG

3.2.1 Fault detection and Isolation

After the extraction of ARR from the BG, the real time evaluation of their residuals allows to detect the faulty situation. With their complex multi-physical dynamics, the fault detection in HRES is not enough. System faults can represent a serious safety and protection issues if not related to its cause. In general, fault isolation stands for relating the operating anomalies to their root causes in the system. This allows trigging an automated failure decision or safety precautions according to the identified faulty component. In critical cases, the isolation helps to take the appropriate decision. The ARR can be helpful in isolating the defective part of the system. Classically, this isolation procedure is done using the algebraic expression of the *ARR* to derive what called the FSM. A FSM is a binary matrix that relates the numerical evaluation of each ARR (residual) to its affecting parameters or variables. These last ones, in their turn, are related to the system component accountable of its modification [145]. This is done based on the explicit algebraic expressions of the ARR.

Example: FDI using ARR

Let C_1, C_2 and C_3 be three components. Let c_{11} and c_{12} two variables or parameters whose values are related to the physical law applied by the component C_1. Let c_{21} (resp. c_{31}) be the variable or parameter associated to the physical law applied by C_2 (resp. C_3). The k^{th} ARR equation is given by $r_k = f_k(c_{i1}, ..c_{ij})$ obtained from the algebraic relations between the system parameters c_{ij}, the measured output and the input of the real system. Let $r_1 = f_1(c_{11})$, $r_2 = f_2(c_{21}, c_{31})$, $r_3 = f_3(c_{11}, c_{12}, c_{21}, c_{31})$ be the three ARR evaluations. We denote $\mathcal{C} = \{c_{11}, c_{12}, c_{21}, c_{31}\}$ and $\mathcal{R} = \{r_1, r_2, r_3\}$.

The fault signature associated to the parameter c_p is expressed by the binary vector $FS(c_p) = [S_{1p}, S_{2p}, S_{3p}]^T$, where S_{kp} are defined as follows:

$$\begin{aligned} &\mathcal{R} \times \mathcal{C} \to \{0,1\} \\ &(r_k, c_p) \mapsto \begin{cases} S_{kp} = 1 & \text{if } r_k \text{ depends on } c_p \\ S_{kp} = 0 & \text{otherwise} \end{cases} \end{aligned} \tag{3.1}$$

For more convenience, fault signatures are grouped in a FSM as shown by Tab.3.1. In non faulty situation, the coherence normalised vector obtained from the residual values, $v = [r_1, r_2, r_3]^T$, is equal to $v = [0, 0, 0]^T$.

	c_{11}	c_{12}	c_{21}	c_{31}
$r_1 = f_1(c_{11})$	1	0	0	0
$r_2 = f_2(c_{21}, c_{31})$	0	0	1	1
$r_3 = f_3(c_{11}, c_{12}, c_{21}, c_{31})$	1	1	1	1

Table 3.1 – FSM example

Assuming one fault at the time, if this vector is equal to $v = [1, 0, 1]^T$, this indicates that r_1 and r_3 both alerting a fault detection. This signature indicates that c_{11} is detected as abnormal and the associated component C_1 is suspected to be in bad operating conditions. If $v = [0, 1, 1]^T$, then a fault is detected and C_2 and C_3 are two possible sources of the malfunctioning. With several components sharing the same signature, the fault is not isolated. In this case, more sensors must be considered to improve the isolation [146].

Compared with the other FDI techniques, adopting the ARR helps to avoid the convergence and the stability issue. For continuous systems, the ARR expressions can be obtained from the analytical model in its ODE form. Previously used as a graphical unified modelling tool, the BG with its causal energetic properties, serves also as a systematic way to easily derive the ARR expressions [114, 112, 115, 116, 111].

3.2.2 ARR derivation from the BG model

The numerical evaluation of the ARR, using the real measured output of the process along with the prior knowledge on the system dynamics and variables, allows to establish a consistency check that can be implemented in real-time. Using the model dynamic laws as a reference, any unexpected change in the real system behaviour can be detected. This is called the fault detection. With the model represented in SSE form, the ARR can be obtained analytically [147]. However, for complex systems such as HRES these latter can be very difficult to express. As the BG covers implicitly the dynamical laws of the system, there exist another classical systematic approach to derive these ARR from the BG model without refereeing directly to the SSE analytical model. The dualizing method of the BG (resp. HBG) model [115] consists in replacing the detectors in the model with sources of information of the same type: the detector of flow (respectively effort) (Df, De) is transformed into source of flow signal (respectively effort)(SSf, SSe) [Fig. 3.1]. The dynamic elements C, I are needed to be in a derivative preferred

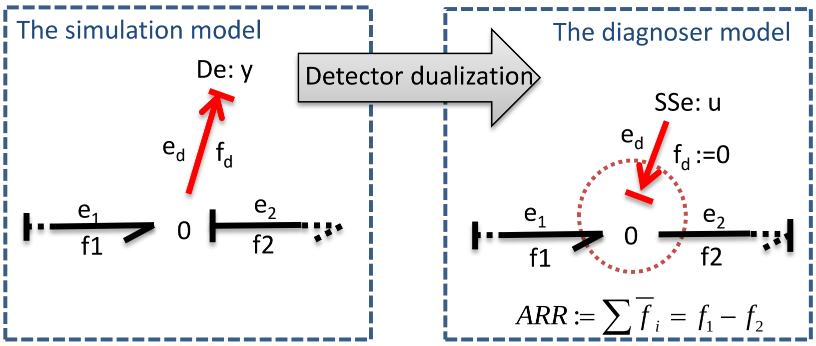

Figure 3.1 – BG detectors dualized

causality in order to avoid the unknown initial conditions of the real process continuous state. Finally, the ARR expression is obtained by writing the sum of the none-constant power components (e or f) on each of the dualized junctions. The unknown variables are eliminated using covering causal path leading to known variables (sensors outputs and control inputs). For each junction linked to at least one sensor, an ARR is deduced [117, 91, 115, 118]. After obtaining the analytical expression of the ARR, the FSM can be found by matching each residual to its related components.

As an example, consider the HBG model of the electroyser in [Fig. 2.12].

It is also fully detailed and developed in Chapter IV.

Notice that, as a simulation model, the HBG is in its integral causality. At the thermal junction the dualizing is done by inverting the effort sensors (originally temperature sensor *water_temp* in [Fig. 3.2]) to a source of signal $SSe : T_w$. [Fig. 3.3] shows the dualization procedure of BG thermal sub-model.

Remark 3.2.1 (Dualizing with respect to the Amplifiers). *As shown in [Fig. 2.12],* *the sensor is on the left side of the flow amplifier Smf, but since Smf transmits the same effort (temperature), the dualizing can be done on the right side (on the thermal 0 junction) (see [Fig. 3.3]). As explained in Property 2.1.1 and Property 2.1.2, physically this is justified since the temperature is an intensive measurement, it maintains the same value for whole stack as for a single cell.*

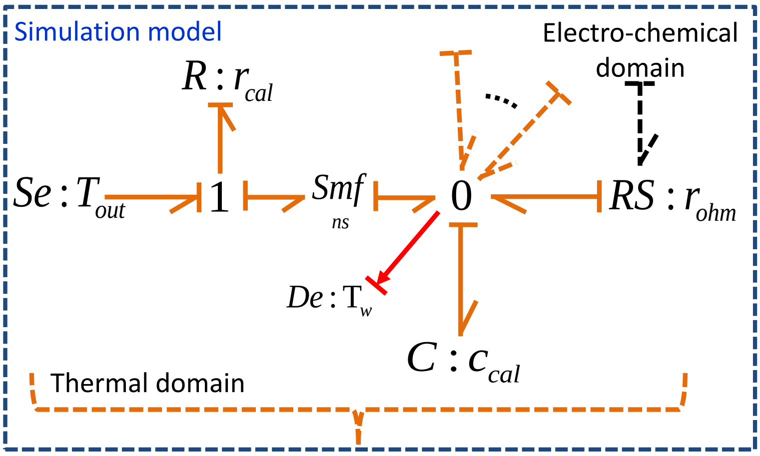

Figure 3.2 – The thermal junction of the Electrolyser HBG before the dualisation

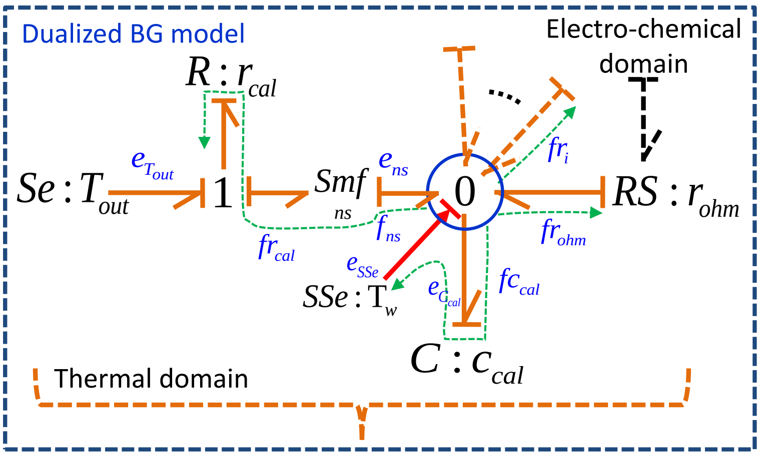

Figure 3.3 – Dualized thermal junction of the Electrolyser HBG

The thermal ARR associated to the residual $Resd_T$ is obtained by written the expression of the sum of the flows on the dualized 0-junction showed in Eq. 3.2.

$$Resd_T = -f_{c_{cal}} + f_{r_{ohm}} + f_{n_s} + f_{r_i} + .. \tag{3.2}$$

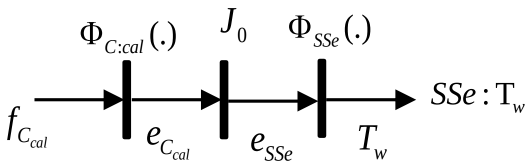

Figure 3.4 – Causal graph of $f_{c_{cal}}$

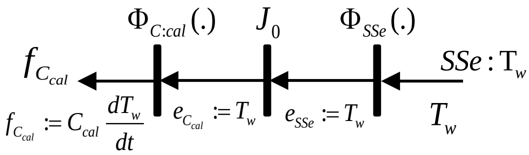

Figure 3.5 – Inversion of the causal graph to express $f_{c_{cal}}$

Indeed, an ARR and the associated residual consists of only known variables, thus the unknown flow variables must be eliminated using the covering causal path from the unknown variables to the known ones. In Eq. 3.2, to express each flow in terms of known variables, the causal paths are used to derive causal graphs. For instance, in [Fig. 3.3] the causal path departing from the flow $f_{c_{cal}}$ allows us to derive the causal graph depicted in [Fig. 3.4]. These causal graphs show the elimination path, where $\Phi_{be}(.)$, J_0 and J_1 represent, receptively, the constitutive equations of the BG elements be, 0-junction and 1-junction. By inverting this causal graph, as shown in [Fig. 3.5], the expression of $f_{c_{cal}}$ is obtained and expressed in terms of only known variables in Eq. 3.3.

$$f_{c_{cal}} = C_{cal}.\frac{dT_w}{dt} \tag{3.3}$$

Similarly, we can find f_{n_s} in Eq. 3.4 and the expressions of the other flows.

$$f_{n_s} = \frac{f_{r_{cal}}}{ns} = \frac{1}{ns}.\frac{(T_{out} - T_w)}{r_{cal}} \tag{3.4}$$

3.2.3 FDI for Hybrid System

In case of hybrid systems with several OM, the derivation of the subsets of the explicit ARR associated to each OM aside is not required. When expressing unknown variables in terms of known variables, if the concerned causal path crosses a controlled junction Xi, then the state of the junction $ax_i \in [0, 1]$ is multiplied by the power component (e or f). The FSM may then contain boolean variables related to the different OM.

From the EL simulation HBG, consider the switching sub-system in [Fig. 3.6]. In

HBG, at the left side of the amplifier $Sme : ns$, $Df : i_{cell}$ and $De : v_{cell}$ represent respectively the current and the voltage sensors of a single cell of the electrolyser. On the right side, the power circuit that supplies the electrolyser with power is shown. It consists of an AC source $Se : AC$ which supplies a AC/DC converter represented by its average model, ($TF : ac\_dc$ with a shunt resistance $R : R_{shunt\_e}$). The output of the converter is connected to the controlled junction $X1$ with its state $ax_1 \in \{0, 1\}$ representing a current on/off switch. A modulated resistance $MR : r_{active}$, mounted in series, is used to control the input current. The described power unit supplies all the serial ns cells of the electrolyser. A $Sme : ns$ is used to amplify ns times the voltage of the single cell model on the left to correspond to the model of power unit on the right.

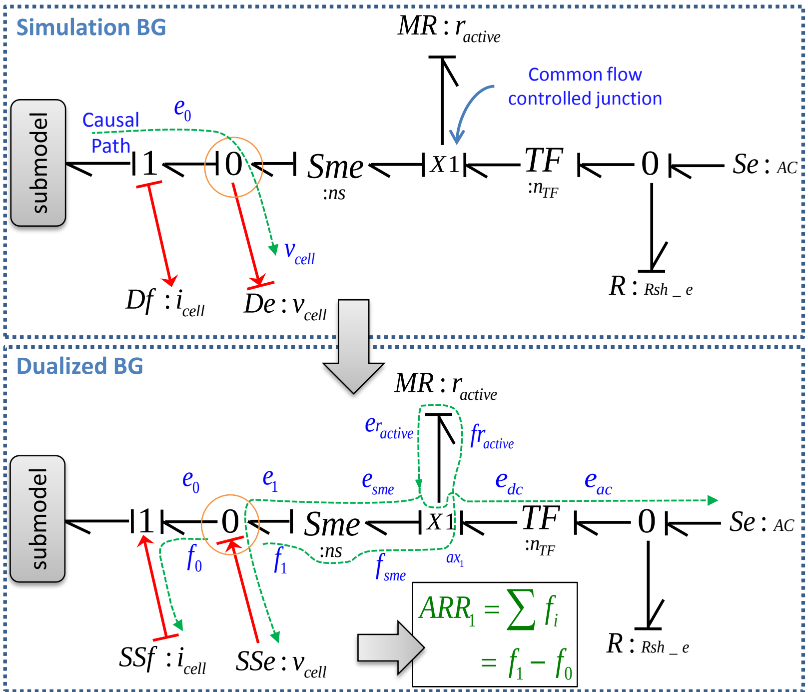

Figure 3.6 – HDS FDI

The figure also illustrates the dualized HBG. The detectors $Df : i_{cell}$ and $De : v_{cell}$ in the simulation model are dualized respectively by source of flow signal $SSf : i_{cell}$ and $SSe : v_{cell}$ (Any existing dynamical element I or C must be in preferred derivative causality). The ARR candidate expressions are obtained by expressing the conservative law of the dualized junctions (i.e previously connected to a sensor). In [Fig. 3.6] two ARR can be found. For the case of the 0-junction, the corresponding ARR_1 is given by Eq. 3.5.

$$ARR_1 = \sum f_i = f_1 - f_0 \tag{3.5}$$

The flow f_0 is eliminated using the causal graph and its inversion shown in [Fig. 3.7] and [Fig. 3.8]. These two causal graphs are derived from the causal path shown on the dualized BG. They show that f_0 is equal to the signal of the current sensor imposed by $SSf : i_{cell}$ (i.e known measured variable).

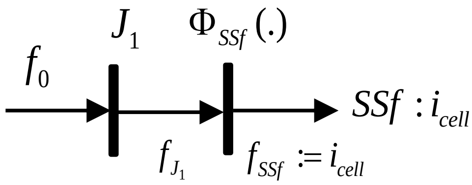

Figure 3.7 – Causal graph of f_0

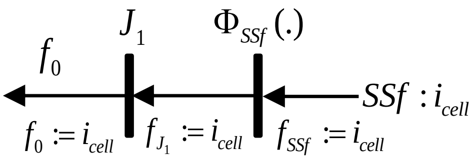

Figure 3.8 – Inverted causal graph to express f_0

f_1 is substituted using the covering causal paths shown on the dualized BG in [Fig. 3.6]. The corresponding direct causal graph is illustrated in [Fig. 3.9]. Using the inverted causal graph, shown in [Fig. 3.10], f_1 can be written as given by Eq. 3.6.

$$f_1 = \frac{f_{sme}}{ns} = \frac{ax_1}{ns}.\frac{e_{dc} - ns.v_{cell}}{r_{active}} = ax_1.\frac{\frac{n_{TF}}{ns}.AC - v_{cell}}{r_{active}} \tag{3.6}$$

Notice that when the causal path passes through the controlled junction $X1$, the switching state variable of the junction aX_1 is multiplied by the flow output. This is why, in [Fig. 3.10], $f_{sme} = ax_1.fr_{active}$.

Finally, [Fig. 3.11] shows the derivation of the corresponding ARR from the known variables. When the junction X1 is on ($ax_1 = 1$), the FDI algorithm checks, based on the known parameters and the measured variables, if the real-time evaluation of $(\frac{\frac{e_{dc}}{ns} - v_{cell}}{r_{active}} - i_{cell})$ is equal to zero. When the junction is in off state ($ax_1 = 0$), then the condition becomes that the measured i_{cell} must be zero.

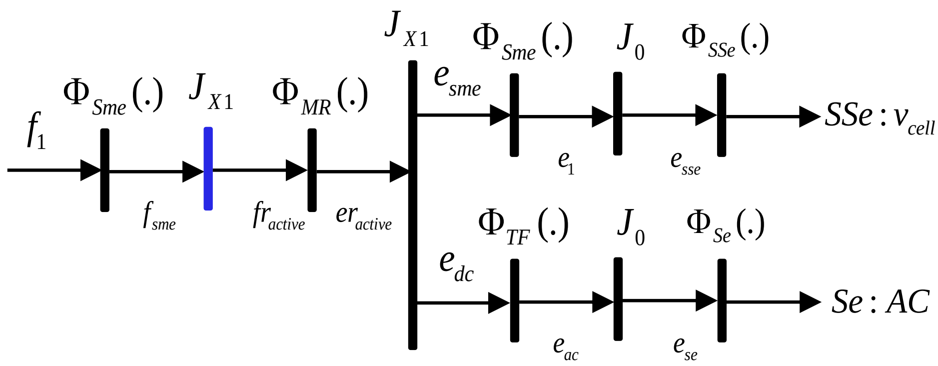

Figure 3.9 – Causal graph of f_1

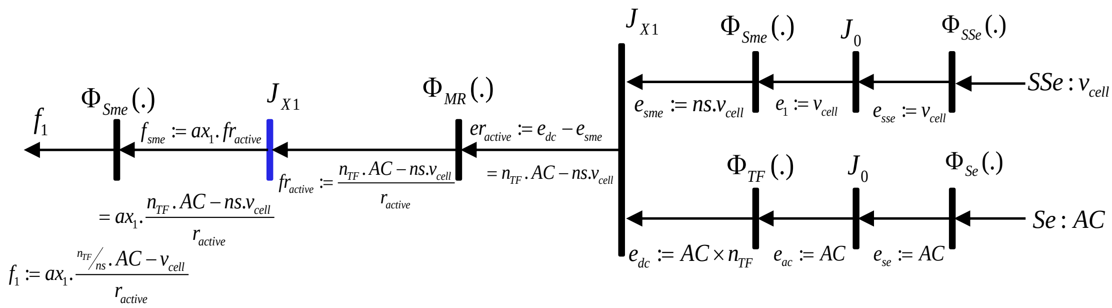

Figure 3.10 – Inverted causal graph to express f_1

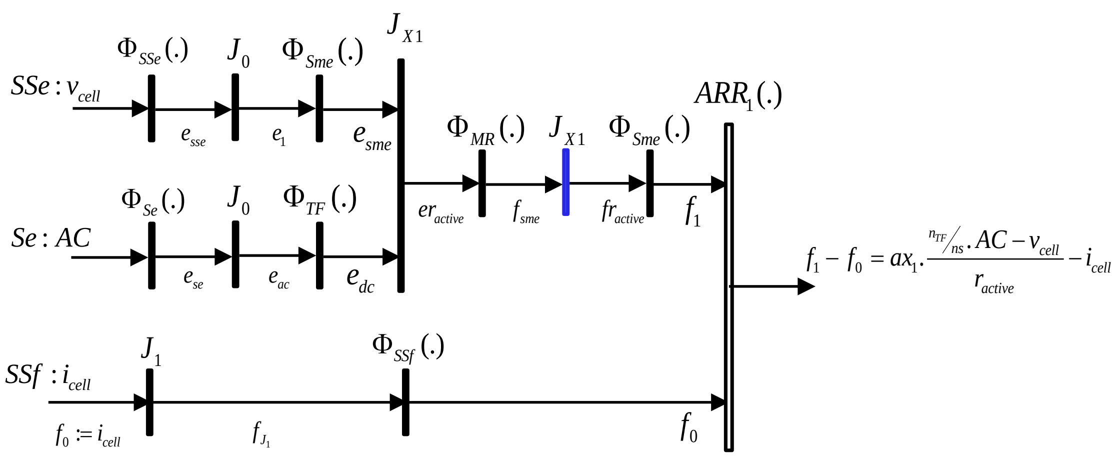

Figure 3.11 – Inverted causal graph to express ARR_1

3.2.4 Bond Graph Diagnoser for an on-line graphical FDI

Even if the previous classical approach to extract the ARR from the BG is effective and appropriate, it stills a long procedure that needs mathematical reformulations, causality tracking and rewriting the analytic expressions of the BG elements. Using the idea that the BG by itself represents a graphical modelling framework similar to the analytical dynamical representation such as the SSE, the ARR are implicitly embedded within its structure. Consequently, with a BG compatible software associated with the measured variables, it must be sufficient to implement an on-line consistency diagnosis based on the system dynamic laws.

Indeed, here we propose to use the implicit description of the dynamical behaviour wrapped in the BG to directly evaluate the residuals. For this, we define the notion of the Bond Graph Diagnoser (BGD).

Definition 3.2.1 (BG Diagnoser)**.** *The BGD is obtained from an ordinary BG simulation model. The procedure consists of:*

- *Dualizing the detectors Df and De respectively into modulated sources of flow MSf and modulated sources of effort MSe. These sources are named the dualizing sources and they represent sources of information.*
- *Adding on each dualizing bond, that connects the dualizing effort source (resp. dualizing flow source) to the rest of the BG, a BG flow detector Df (resp. effort detector De).*
- *Checking the causality and assigning a derivative preferred causality for the dynamical elements C and I.*

Each dualizing source receives as an input the signal measured by the real sensor of the process that corresponds to its previous dualized detector in the simulation BG model. The signals monitored by the added detectors on the dualized bonds directly offer the residual evaluations.

Proof. Consider two cases:

- A BG simulation model, where a flow BG detector $Df : y_f$ is connected to a 1-junction as shown in the left side of [Fig. 3.12].
- A BG simulation model, where an effort BG detector $De : y_e$ is connected to a 0-junction as shown in the left side of [Fig. 3.13].

In both cases E_1 and E_2 represent BG elements such as (R, I, C) and $\Sigma 1$ represents a BG sub-model. In the case of 1-junction as in [Fig. 3.12], the right side of the figure represents the use of the BG graphical diagnoser. The sensor $Df : y_f$, in the simulation BG model is replaced by the dualizing source $MSf : ssf$. This latter delivers, to the BG diganoser, the signal ssf of the corresponding measured output in the real

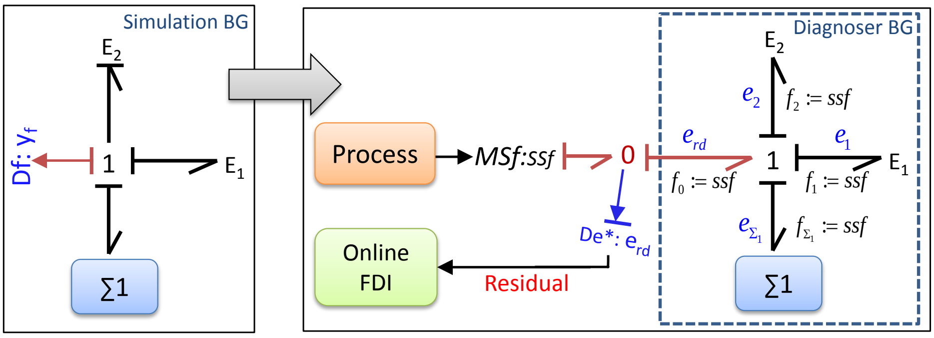

Figure 3.12 – Graphical BG diagnoser through dualized 1 junction

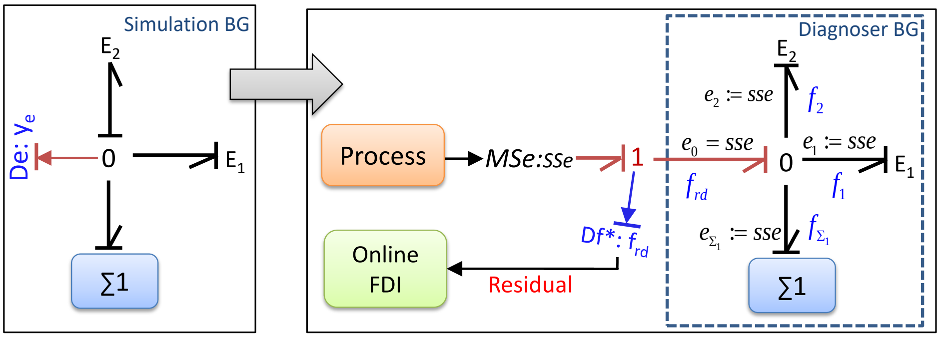

Figure 3.13 – Graphical BG diagnoser through dualized 0 junction

system. In its derivative preferential causality, the obtained BG is a BG diagnoser and represents the supervision platform to evaluate the residual. On the dualized bond of $MSf : ssf$, a virtual effort detector $De^* : e_{rd}$ (i.e does not represent any physical element) is mounted. As mentioned before, the ARR candidate for such junction ARR_1 is expressed by its power conservation law given by Eq. 3.7.

$$ARR_1 = e_1 + e_2 + e_{\Sigma 1} \tag{3.7}$$

where $e_i = \Phi_{E_i}(.)$ and $\Phi_{E_i}(.)$ represents the constitutive equation of E_i which depends only on known variables. According to the junction equations Eq. 3.8, $De^* : e_{rd}$ collects the algebraic sum of the flows of the dualized 1-junction. In other terms, e_{rd} represents the numerical evaluation of ARR_1.

$$\begin{aligned} e_{rd} &= e_1 + e_2 + e_{\Sigma 1} \\ &= evaluationof(ARR_1) \end{aligned} \tag{3.8}$$

where e_{rd} is the output of $De^* : e_{rd}$.

In normal faultless behaviour, $e_{rd} = e_1 + e_2 + e_{\Sigma 1}$ must be equal to zero, if not this indicates a violation of the conservation law and thus a fault is detected.

With the same reasoning applied on the case of the 0-junction in [Fig. 3.13], we obtain Eq. 3.9.

$$\begin{aligned} ARR_0 &= f_1 + f_2 + f_{\Sigma 1} \\ &= f_{rd} \end{aligned} \tag{3.9}$$

□

In other terms, the BG model will be working under the same operating state of the real system (input, output). Verifying the algebraic sum on the dualized junctions stands for checking if the predefined parameters, energy conservation and the dynamical laws of the model are been followed by the real system.

On any BG compatible software, by modifying the simulation model, the BGD can be obtained and used to perform the online FDI. [Fig. 3.14] shows the BGD of the electrolyser on 20sim. The BGD is obtained by copying and modifying the original simulation BG showed in [Fig. 2.12].

The main advantage of this technique is to directly evaluate the residuals without requiring an explicit calculation of the ARR whatever is the current OM. A hybrid BGD allows obtaining the ARR evaluation (residuals values) for the selected OM through the controlled junction state vector β_i.

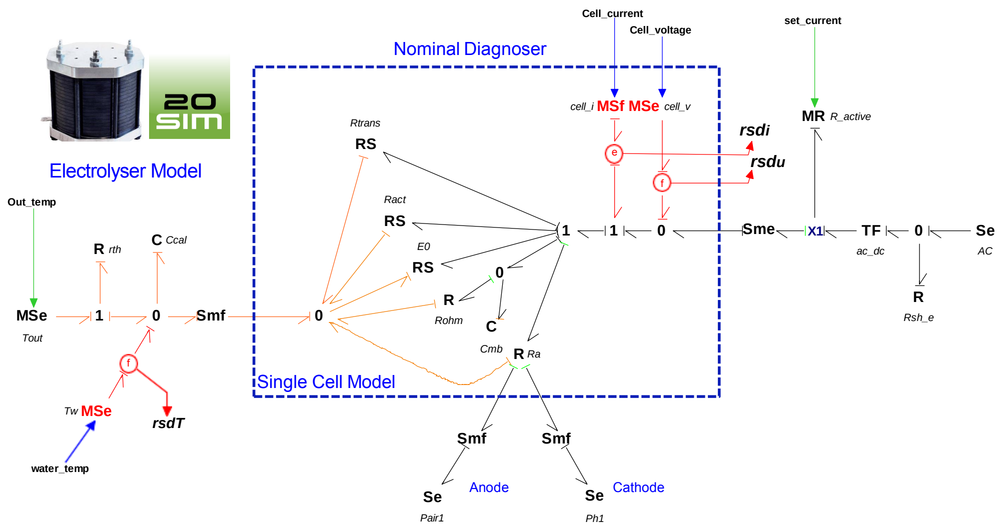

Figure 3.14 – Electrolyser BGD

Similar to the classical analytical ARR-FDI technique, a FSM is needed to locate the faulty component. Classically, FSM is obtained from the ARR expressions. In case of graphical BGD, the FSM can be extracted from the BGD itself using the causal paths.

[Fig. 3.15] represents the causal paths of the electrolyser Hybrid Bond Graph Diagnoser (HBGD). The residual output rsd_T is connected through a causal path to the BG element $C : c_{cal}$. Two other causal paths relate also rsd_T to $R : r_{cal}$ and ($R_{r_{ohm}}$, $RS_{r_{trans}}$, C_{mb}, $RS_{r_{activ}}$, $RS_{r_{E0}}$, R_a). This shows the dependencies between rsd_T and these mentioned parameters. In the first column of the FSM [Tab. 3.2], these dependencies are marked by the one values indicating the elements affecting rsd_T and by zeros otherwise. The second and the third columns are also filled according to the dependencies of rsd_i and rsd_u following the causal paths represented on [Fig. 3.15] by dashed curves.

For rsd_u, notice that the causal path of $MR : r_{active}$ is passing through the controlled junction X1, therefore the state of the junction is included where $ax_1 \in \{0, 1\}$.

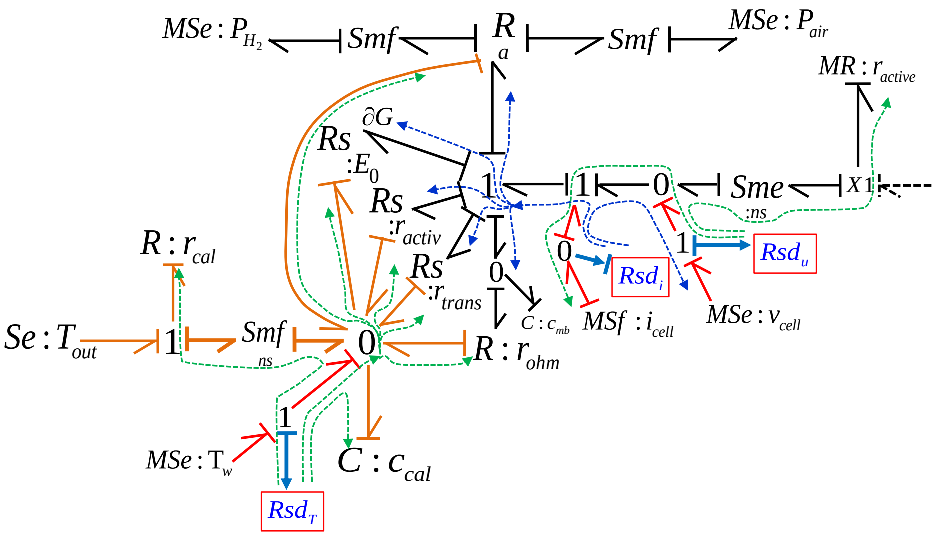

Figure 3.15 – Electrolyser HBGD causal paths to extract the FSM

To avoid false alarms caused by noises, modelling uncertainties and disturbances... statical thresholds are usually used to bound the residual signals. A detection takes place when the residual value overpasses these thresholds.

BG element	rsd_T	rsd_i	rsd_u
no fault	0	0	0
$R_{r_{cal}}$, $C_{c_{cal}}$	1	0	0
$R_{r_{ohm}}$, $Rs_{r_{trans}}$, C_{mb} $Rs_{r_{activ}}$, $Rs_{r_{E0}}$, R_a	1	1	0
$Df : v_{cell}$	0	1	0
$Df : i_{cell}$	0	0	1
$MR : r_{active}$	0	0	ax_1

Table 3.2 – FSM of the EL

3.3 Robust Diagnostic

3.3.1 Overview on the LFT for the FDI

Including parametric uncertainties, the HBG in its LFT form allows extracting the $GARR$ denoted as $GARR(y, u, \beta, \delta)$ where y, u, β and δ represent respectively the system output, input, switching states, and the uncertainties. In general because of the use of the multiplicative uncertainties, $GARR(y, u, \beta, \delta)$ can be decomposed to the sum of two separate parts:

- Nominal one denoted as $gr_n(y, u, \beta)$
- Uncertain part as $gr_\delta(y, u, \beta, \delta)$

Ideally as mentioned before, a fault detection occurs when at least one GARR shifts from zero see Eq. 3.10:

$$GARR_i(y, u, \beta, \delta_e) = gr_{ni}(y, u, \beta) - gr_{\delta i}(y, u, \beta, \delta_e) \neq 0 \tag{3.10}$$

where:

- $GARR_i(y, u, \beta, \delta_e)$ is the real unknown value of residual
- $\delta_e = [\delta_{1_e}, ...\delta_{k_e}, ...\delta_{n_e}]$ is the real unknown exact uncertainty vector. δ_{k_e} is the uncertainty of a parameter c_k and it is bounded $\delta_{k_e} \in I_k = [\delta_{min_k}, \delta_{max_k}]$. Thus, the uncertainty vector is bounded $\delta_e \in I = I_1 \times I_2.. \times I_k...$

In other terms when a faulty situation occurs we have:

$$gr_{ni}(y, u, \beta) - gr_{\delta i}(y, u, \beta, \delta_e) \neq 0 \Leftrightarrow \begin{cases} gr_{ni}(y, u, \beta) > gr_{\delta i}(y, u, \beta, \delta_e) \\ \quad or \\ gr_{ni}(y, u, \beta) < gr_{\delta i}(y, u, \beta, \delta_e) \end{cases} \tag{3.11}$$

Because of the presence of the uncertain part of the ARR $gr_{\delta i}(y, u, \beta, \delta_e)$, the consistency test represented by Eq.(3.11) can not be directly applied. Indeed, the exact uncertainties δ_e are unknown and variable, they are bounded by minimal and maximal thresholds. This suggests bounding the uncertain part of the GARR $gr_{\delta i}(y, u, \beta, \delta_e)$, between two known functions as proposed by Eq.(3.12).

$$\sup_{\delta \in I} gr_{\delta i}(y, u, \beta, \delta) > gr_{\delta i}(y, u, \beta, \delta_e) > \inf_{\delta \in I} gr_{\delta i}(y, u, \beta, \delta) \tag{3.12}$$

Containing only known variables $gr_{n_i}(y, u, \beta)$ can be evaluated. $gr_{\delta i}(y, u, \beta, \delta_e)$ in Eq.(3.11) can be replaced by its boundary functions from Eq.(3.12). In this case the detection condition is then satisfied by considering the fault occurs when:

$$\begin{cases} gr_{ni}(.) > \sup\limits_{\delta \in I} gr_{\delta i}(., \delta) \\ \qquad or \\ gr_{ni}(.) < \inf\limits_{\delta \in I} gr_{\delta i}(., \delta) \end{cases} \Rightarrow \begin{cases} gr_{ni}(.) > \sup\limits_{\delta \in I} gr_{\delta i}(., \delta) > gr_{\delta i}(., \delta_e) \\ \qquad or \\ gr_{ni}(.) < \inf\limits_{\delta \in I} gr_{\delta i}(., \delta) < gr_{\delta i}(., \delta_e) \end{cases} \tag{3.13}$$

$\sup\limits_{\delta \in I} gr_{\delta i}(y, u, \beta, \delta)$ and $\inf\limits_{\delta \in I} gr_{\delta i}(y, u, \beta, \delta)$ constitute the detection dynamical thresholds.

However, not satisfying these conditions is non-conclusive. If a small fault occurs within the uncertainty limits, the fault will be unobservable. In fact, a large uncertainty on the parameters induces a wider non-conclusive margin between $\sup\limits_{\delta \in I} gr_{\delta i}(., \delta)$ (resp. $\inf\limits_{\delta \in I} gr_{\delta i}(., \delta)$) and $gr_{\delta i}(y, u, \beta, \delta_e)$. The evolution of the unknown $gr_{\delta i}(y, u, \beta, \delta_e)$ represents the hidden uncertain dynamic in the system. We define respectively the upper uncertainty distance and the lower uncertainty distance given by d_{sup} and d_{inf}

Definition 3.3.1 (Uncertainty distance). *d_{sup} is the distance between $gr_\delta(\delta_e, .)$ and the $\sup\limits_{\delta \in I} gr_\delta(\delta_e, .)$, it is expressed in Eq. 3.14.*
d_{inf} represents the distance between $gr_\delta(\delta_e, .)$ and the $\inf\limits_{\delta \in I} gr_\delta(\delta_e, .)$, it is expressed in Eq. 3.15

$$d_{sup} = \sup_{\delta \in I} gr_\delta(., \delta) - gr_\delta(\delta_e, .) \tag{3.14}$$

$$d_{inf} = gr_\delta(\delta_e, .) - \inf_{\delta \in I} gr_\delta(., \delta) \tag{3.15}$$

The uncertainty distance characterizes how large is the uncertain zone. Due to the multiplicative uncertainty, gr_δ can usually be expressed as $g_\delta = \sum_{k=1}^{n} \delta_k \cdot z_k(y, u, \beta)$

where $z_k(y,u,\beta)$ is a differential equation representing part of the dynamic that depends on the uncertainty δ_k.
Noticing that $\sum_{k=1}^{n} \delta_k \cdot z_k(y,u,\beta)$ is monotone with respect to δ on I. Consequently $\sup_{\delta \in I} gr_{\delta i}(\delta)$ and $\inf_{\delta \in I} gr_{\delta i}(\delta)$ can be easily chosen as $\sum_{k=1}^{n} \delta_{k\ max} \cdot |z_k(y,u,\beta)|$ and $\sum_{k=1}^{n} \delta_{k\ min} \cdot |z_k(y,u,\beta)|$ respectively.

Proof. To justify the choice of $\sup_{\delta \in I} gr_{\delta i}(\delta)$ and $\inf_{\delta \in I} gr_{\delta i}(\delta)$, we demonstrate that the uncertainty distance is always positive $d_{sup} = \sup_{\delta \in I} gr_{\delta i}(\delta) - gr_{\delta i}(\delta) > 0$.

$$d_{sup} = \sup_{\delta \in I} gr_{\delta i}(\delta) - gr_{\delta i}(\delta) = \sum_{k=1}^{n} \delta_{k\ max} \cdot |z_k(y,u,\beta)| - \sum_{k=1}^{n} \delta_k \cdot z_k(y,u,\beta) \tag{3.16}$$

Having that $|z_k(.)| = \begin{cases} z_k(.) & \text{when} \quad z_k(.) > 0 \\ -z_k(.) & \text{when} \quad z_k(.) < 0 \end{cases}$, Eq. 3.16 can be written as sum of two parts shown in Eq. 3.17.

$$d_{sup} = (\overbrace{\sum (\delta_{i\ max} - \delta_i) \cdot z_i(y,u,\beta)}^{for \quad z_i(y,u,\beta)>0} + \underbrace{\sum (\delta_{j\ max} + \delta_j) \cdot [-z_j(y,u,\beta)]}_{for \quad z_j(y,u,\beta)<0}) > 0 \tag{3.17}$$

Finally, in Eq. 3.17 the first part is always positive. In the second part, $\delta_j \in I_j = [\delta_{j\ min}; \delta_{j\ max}]$ where $-1 < \delta_{j\ min} < 0$ and $0 < \delta_{j\ max} < 1$, this implies that δ_j can take positive or negative value. Therefore, proving Eq. 3.17 is always positive comes down to demonstrate Eq.3.18 is always positive.

$$\delta_{j\ max} + \delta_j >?0 \tag{3.18}$$

By assuming I_j is symmetric(general case) centered at zero i.e $\delta_{j\ max} = -\delta_{j\ min}$ then Eq. 3.18 can be rewritten as in Eq. 3.19

$$\delta_{j\ max} + \delta_j = \delta_j - \delta_{j\ min} > 0 \tag{3.19}$$

As results, Eq. 3.17 has its both parts always positive.

Remark 3.3.1. *When I_j is given as asymmetric $I_j = [\delta_{j_{min}} \delta_{j_{max}}]$, a symmetric interval I_{sj} can be created which is includes I_j where:*
$I_{sj} = [-max(-\delta_{j_{min}} \delta_{j_{max}}), +max(-\delta_{j_{min}} \delta_{j_{max}})]$.

□

These two boundary functions are called the residual thresholds. The nominal GARR $gr_{ni}(.)$, in the normal (or non detectable faulty) situation, must always evolve between these thresholds see [Fig. 3.16]. The detection conditions Eq.(3.13) are not satisfied. To detect the fault, output and input of the system along with the discrete state are injected into the evaluation of $gr_{ni}(y, u, \beta)$. On the other hand $\sup_{\delta \in I} gr_{\delta i}(\delta)$ and $\inf_{\delta \in I} gr_{\delta i}(\delta)$ are used to evaluate the thresholds. When a fault overcomes the uncertainties in the model, $gr_{ni}(y, u, \beta)$ overpasses the thresholds as shown by [Fig. 3.16].

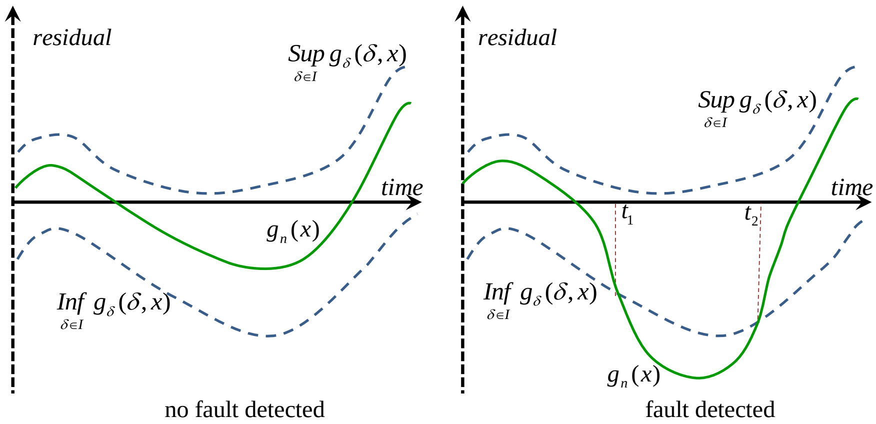

Figure 3.16 – Robust diagnosis in normal and faulty situations

These robust GARR expressions including the threshold expressions can be obtained directly from the uncertain analytic model or following the causal path procedure applied on the LFT-HBG diagnoser where the detectors are dualized [142]. Despite that LFT HBG method improves and eases the extraction of the robust GARR, the user still need to investigate the causal paths, the power conservation and the physical laws associated to the BG elements to extract these expressions in the desired algebraic form, not to forget the extraction of the threshold expressions from the ARR expressions.

To overcome this drawback, we propose to modify the HBGD previously presented in order to directly include the uncertainties. The residuals can then be generated directly for all the OM, with the dynamical thresholds. Again, this approach allows the disposal of the need of any analytical expressions of the model nor of the GARR.

3.3.2 Graphical LFT HBG diagnoser

If applied directly on the LFT HBG model, the procedure of the BGD described in section 3.2.4 provides the residual evaluations as a mixture of both nominal and uncertain part $\bar{r}d_i = gr_{ni} - gr_{\delta i}$. First, to ensure $gr_{\delta i}$ maintains its desired form $gr_{\delta i} = \sum_{k=1}^{n} \delta_k \cdot z_k(y, u, \beta)$, the LFT BG must be constructed following the general rules defined in [141] and briefly explained in Chapter 2.

For a robust diagnosis, having $\bar{r}d_i$ numerical value is not enough. The thresholds derived from $gr_{\delta i}$ are needed separately from the nominal part gr_{ni}. With only nominal parameters, a nominal BGD can be used separately to evaluate gr_{ni}. By considering a coupled nominal BGD with the LFT-BGD as shown in [Fig.3.17], both numerical evaluations of $rd_i = gr_{ni}(.)$ and $\bar{r}d_i = gr_{ni}(.) - gr_{\delta i}(.)$ are obtained. By monitoring $rd_i - \bar{r}d_i$, the numerical value of $gr_{\delta i}(.)$ is obtained separately.

Since in an ordinary LFT-BG, $gr_{\delta i}(.) = \sum_{k=1}^{n} \delta_k \cdot z_k(y, u, \beta)$ where $z_k(y, u, \beta)$ is the output of the virtual detector $Df^* = Z_r$ used to inject the uncertainty in the BG, the real time evaluation of $gr_{\delta i}(.)$ does not provide directly the thresholds expressed in Eq. 3.20

$$\begin{bmatrix} Thr_1 \\ Thr_2 \end{bmatrix} = \begin{bmatrix} \sum_{k=1}^{n} \delta_{max} \left| z_k(y, u, \beta) \right| \\ \sum_{k=1}^{n} \delta_{min} \left| z_k(y, u, \beta) \right| \end{bmatrix} \tag{3.20}$$

Assuming I is symmetric, $\delta \in [-\delta_{max}, +\delta_{max}]$. Then Thr_1 and Thr_2 are symmetric and can be rewritten as shown in Eq. 3.21

$$Thr = \pm \sum_{k=1}^{n} \delta_{max} \left| z_k(y, u, \beta) \right| \tag{3.21}$$

In the LFT-BGD, δ can be chosen as δ_{max}. On the virtual detector, when considering the absolute value of output, the final output supplies $Df^* = |Z_r|$ as shown in [Fig.3.18]. Applying this technique on all the uncertainties in the LFT-HBGD, guarantees obtaining $gr_{\delta i} = \sum_{k=1}^{n} \delta_{max} \left| z_k(y, u, \beta) \right| = \sup(gr_{\delta i})$.
As a result, $rd_i = gr_{ni}$ is evaluated by the nominal BGD and represents the nominal residual. At the same time, $rd_i - \bar{r}d_i = \sup_{\delta}(gr_{\delta i})$ which is the differences between both outputs of the nominal and modified LFT-BGD, represents the thresholds.

For example reconsider the HBG model of the EL showed in [Fig. 2.12]. Considering the uncertain parameter $R : r_{ohm}$, [Fig.3.18] shows the associated LFT-BGD of the electrolyser. Coupled with the nominal HBGD [Fig. 3.14], the global robust diagnoser is illustrated in [Fig.3.17]. Fed by the systems inputs and measured outputs, the Robust

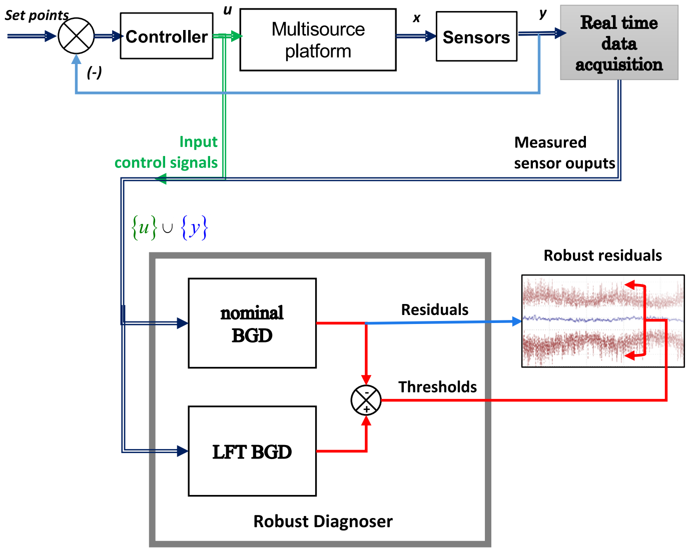

Figure 3.17 – Nominal and LFT BGD coupling

HBGD generates the residuals and the thresholds. A full example is introduced in chapter 4.

Same as before, the robust diagnoser generates the residuals and the thresholds that corresponds to the OM selected through the controlled junction state vector β_i.

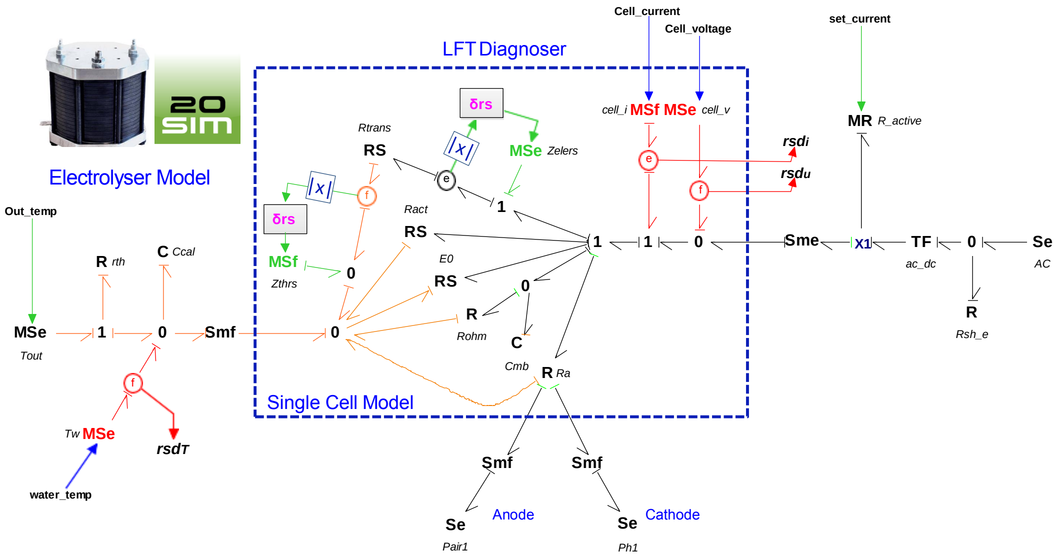

Figure 3.18 – Electrolyser LFT BGD

3.4 Operating Mode Management

3.4.1 Introduction

From a functional viewpoint, the elements of $\mathcal{E}$ of the Bond Graph $BG(\mathcal{E}, \mathcal{A}, \mathcal{J})$ correspond to elementary services provided by the system components (sensors, sources, storage units, power electronics ...). Junctions $\mathcal{J}$ are connection elements used to associate elementary services according to different possible configurations (parallel, serial ...) while respecting energy conservation laws. The bonds $\mathcal{A}$ express the relations between variables that the service consumes and produces. In fact, a HBG model describes one or more high level services, for example a system mission. This latter is achieved using elementary services provided by the system components.

Consider a HRES composed of PV, WT and FC as sources and batteries, grid and EL-H_2 tank as storage components, all connected to a DC bus. Such example is represented by the word BG in [Fig. 3.19]. In the figure, the electrical components (battery, PV, WT, FC and EL) are connected to the common DC bus. From another side, under the same pressure, the FC and the EL share the same output-input valve of H_2 tank. Assuming each element has the possibility to be connected and disconnected from the DC bus. An example of a mission is to store the surplus of the produced power. The needed components to achieve this mission are the power sources (PV, WT) and one or more storage units (battery or EL-H_2 tank). Another mission example is to use the stored hydrogen as backup in case of power shortage risks. The used components in such case are the H_2 tank, the FC, battery and the sources (see [Fig. 3.20]).

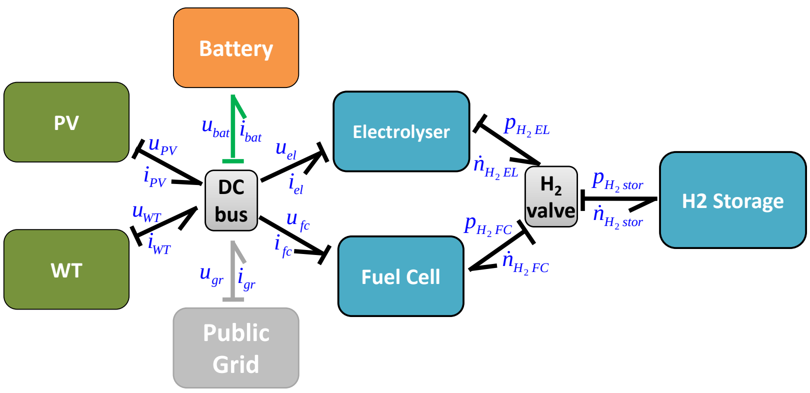

Figure 3.19 – Word BG of a HRES

3.4.2 Components Operational Availability

Fault-tolerant and redundant systems integrate multiple possibilities to provide the same mission, see [148]. Each possibility, named version, rests on a distinct subset of lower level services and produce obviously the same global service. The different versions to achieve a same mission differ by their accuracy, running time and energy consumption. From modelling point of view, these different versions rest on a subset of BG belonging to the same HBG, itself being a subset of a high level HBG. Versions are ordered according to a preference relation defined by the designer. This is the aim of the OM management system to select, at each time, the most preferred versions, to provide the current missions, taking into account the user objectives and the operational availabilities of the components. For example, in HRES, two distinct versions are associated to the power storage mission. Version v_1 consists of using the battery as a single storage unit. Version v_2 uses both the battery with the EL (see [Fig. 3.20]).

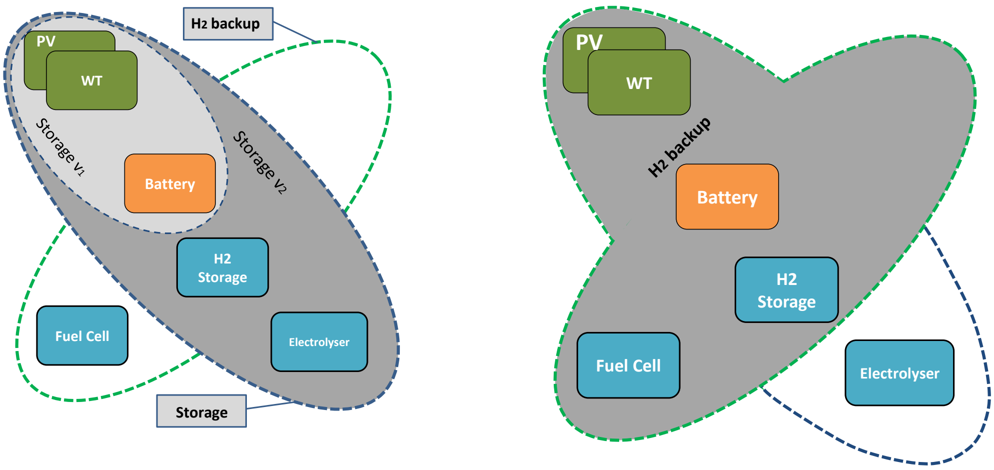

Figure 3.20 – HRES different missions and versions

In fact, a single OM can be associated to one or more missions. For example, let define a mode associated with an objective to store the surplus of the produced power. Beside the power storage mission with the two versions v_1 and v_2, other missions can be associated to the same OM, for example the WT protection against high wind conditions. This allows activating or breaking the WT according to the weather condition. This hierarchical structure between OM, missions, versions, and BG elements is shown in [Fig. 3.21].

With the proposed EDHBG diagnoser, evaluating the component health and diagnosis state called the operational availabilities, this hierarchical structure allows

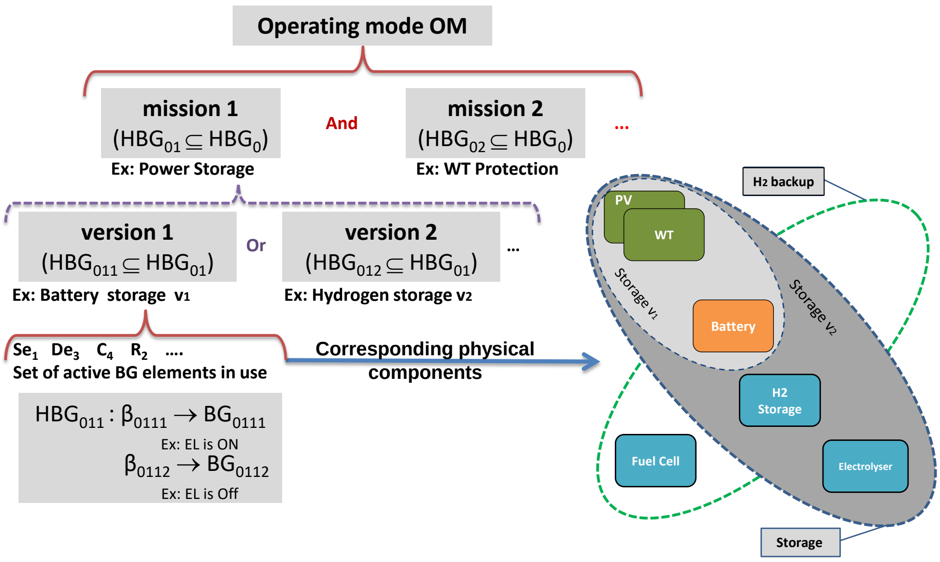

Figure 3.21 – Hierarchical structure between OM and BG elements

to evaluate the possibility to stay in the current OM, with respect to the diagnosis results, by a bottom-up reasoning. This availability evaluation can be used as guard conditions in the automaton for the OMM of both the real system (resp. simulated) and its graphical diagnoser. It rests on the following definitions.

Definition 3.4.1 (Component availability). *Let $BG_i = (\mathcal{E}, \mathcal{A}, \mathcal{J})$ an element of the set of BG $\mathcal{B}$. The availability of an element or component $co \in \mathcal{E}$ is defined by the following map:*

$$
\begin{aligned}
A(co) :& \mathcal{E} \longrightarrow (0,1) \\
co \longmapsto A(co) &= \begin{cases} 0 & \textit{if co is detected as faulty by the diagnoser using } BG_i \\ 1 & \textit{otherwise} \end{cases}
\end{aligned}
\tag{3.22}
$$

Definition 3.4.2 (BG availability). *The availability of a bond graph $BG_i = (\mathcal{E}, \mathcal{A}, \mathcal{J}) \in \mathcal{B}$ is defined by the following map*

$$
\begin{aligned}
A(BG_i) :& \mathcal{B} \longrightarrow (0,1) \\
BG_i \longmapsto & A(BG_i) = \prod A(co) \mid co \in \mathcal{E}
\end{aligned}
\tag{3.23}
$$

Where the operator $\prod$ corresponds to a logical AND.

Definition 3.4.3 (Version availability). *Let V be the set of versions. The availability* *of a version $v_i \in V$ is defined by the following map*

$$\begin{aligned} A(v_i) :& V \longrightarrow (0,1) \\ & v_i \longmapsto A(v_i) = \prod A(BG_j) \mid \quad BG_j \text{ provides the version } v_i \end{aligned} \tag{3.24}$$

Where the operator $\prod$ corresponds to a logical AND.

Definition 3.4.4 (Mission availability)**.** *Let $\mathcal{M}$ be the set of missions. The availability of a mission $m_i \in \mathcal{M}$ is defined by the following map*

$$\begin{aligned} A(m_i) :& \mathcal{M} \longrightarrow (0,1) \\ & m_i \longmapsto A(m_i) = \sum A(v_j) \mid v_j \text{ is a possible version to achieve the mission } m_i \end{aligned} \tag{3.25}$$

Where the operator $\sum$ corresponds to a logical OR.

Definition 3.4.5 (OM availability)**.** *Let $\mathcal{OM}$ be the set of operating modes. The availability of a OM $om_i \in \mathcal{OM}$ is defined by the following map*

$$\begin{aligned} A(om_i) :& \mathcal{OM} \longrightarrow (0,1) \\ & om_i \longmapsto A(om_i) = \prod A(m_j) \mid m_j \text{ is a mission belonging to } om_i \end{aligned} \tag{3.26}$$

Where the operator $\prod$ corresponds to a logical AND.

The OM availability evaluation can be used to check the possibility to stay in the current OM or to switch to another OM according to the diagnosis results. The system can remain in the current mode as long as its availability is equal to one. If this availability turns equal to 0, the system switches to another OM for which the mode domain conditions are true. This implies that the availability of the destination mode must be equal to 1. To avoid deadlock situations, a well-designed automaton has to include a fall-back OM where associated missions aim to ensure the safety of the system and the operators. For example, consider the system represented by [Fig. 3.19] is using both the battery and the EL as a storage mode. If a malfunctioning is detected and isolated as a fault in the active EL, following the Eq. 3.23, the current $BG_{storageH_2}$ will be marked as unavailable $A(EL) = 0 \Rightarrow A(BG_{storageH_2}) = 0$. Since there are two versions, v_1 and v_2 shown in [Fig. 3.20], for the current mission m_{H_2}, the global storage

OM om_{H_2} is still available as seen by Eq. 3.27.

$$\begin{aligned} A(om_{H_2}) = & \quad A(m_{H_2}) \quad \times A(m_2) \times ... \\ = & [\underbrace{A(v_1)}_{0} + \underbrace{A(v_2)}_{1}] \times 1 \times ... = 1 \end{aligned} \tag{3.27}$$

Notice that if the fault is detected in the battery, both v_1 and v_2 are labelled as unavailable. As consequence according to Eq. 3.27 $A(om_{H_2}) = 0$, and the system leaves the current OM to another available OM (backup mode).

The availability notion can be extended to involve the component operational state (see section 2.4.1), for instance the H_2 tank can be marked as unavailable to store hydrogen in case of a leak and in case of reaching full storage capacity.

Remark 3.4.1. *To simplify the annotation of the availability conditions, when a component, mission or OM, denoted by C_K, is available, this availability is expressed by $Av(C_k)$. When it is not, the unavailability is expressed by $\overline{Av}(C_k)$.*

3.4.3 EDHBG for HRES diagnosis and OMM

In general, the OM are defined according to the user objectives, the production demand and the hydrogen storage state. They correspond to the distinct configurations of the different sets of the operating (active) components. Each one of these configurations is expressed by a unique switching vector β_i. The switching conditions between the different OM are defined by the automaton which evaluates continuously the possibilities to stay or not in the current mode. These conditions consider both the user specifications such as covering the demand, and the system component availabilities related to the detected malfunctioning.

In fact, achieving the objectives or the missions intended by the system rests on the services offered by its different components. When the FDI algorithms detect the fault and identify its responsible component source, the service normally provided by this component is no more ensured. As a consequence, some configurations become unavailable or harmful for the system components. In such case, it is convenient to find some configurations that ensure the best service while respecting the safety conditions without using the defective component.

Therefore, the FDI results are included in the switching conditions of the automaton. For the proper functioning of the proposed approach, it is essential to synchronize the diagnoser OM with the real system OM. As shown in [Fig.3.22], the automaton sends

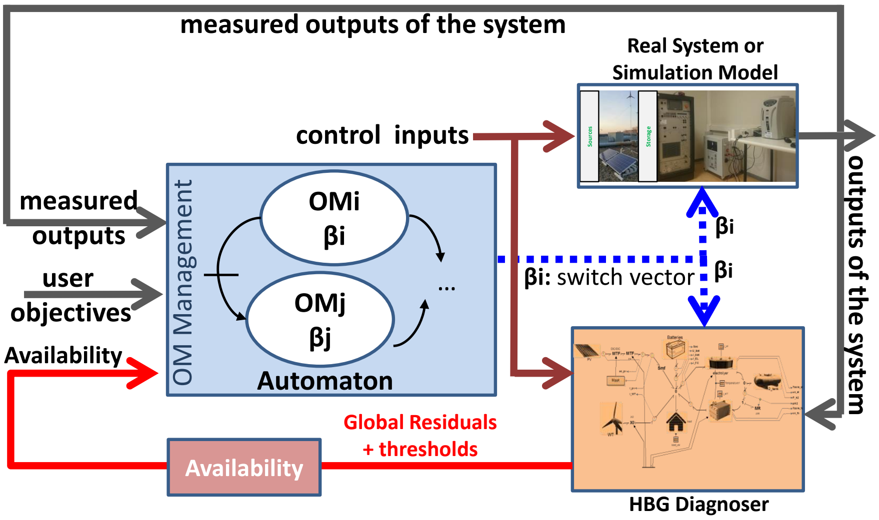

Figure 3.22 – LFT-HBGD synchronized with the real process

the signals included in the vector β_i to activate and deactivate some components of the real system. This vector β_i is shared with the hybrid diagnoser to define the state (ON/OFF) of the controlled junctions. This ensures that the BG, from which the residuals and their thresholds are obtained, is the representation that corresponds to the real system actual configuration. The diagnosis results are sent to the availability block. It evaluates using the diagnsosis result and based on the FSM, the predefined availabilities used in the automaton guard conditions.

3.5 Conclusion

As a well HRES-adapted modelling approach, the EDHBG, offers the possibility to achieve the HRES diagnosis. Using a unique global graphical model along with the implicit consideration of all the switching dynamics and the parameter uncertainties, the FDI is achieved independently from the OM. Same as in the modelling, the integrated automaton handles the OMM while synchronizing both of the diagnoser and the process.

Since the OMM is run independently from the complex dynamic of the system and its residual generation, the diagnosis state can be feed back into the automaton in order to achieve a diagnosis-based OMM. This allows testing different OMM strategies, including protection, safety measures and healthy optimal operating conditions.

Chapter 4

Application: HRES for hydrogen production and storage

4.1 Introduction

The EDHBG developed in chapter II and chapter III serves generally in modelling and diagnosing systems characterized by their switching hybrid dynamics and their multidisciplinary energetic phenomena. HRES fit perfectly under this category. Applied on HRES, a long list of advantages is offered by the proposed approach.

From the modelling perspective, it provides a simple cheap way to design many HRES systems usually composed of very expensive materials. Such digital simulator with available weather data allows performing a better performance and size-cost studies. To refine the design and the size of such system according to the results of such studies, the HRES model is needed to be adjustable. Effectively, the EDHBG constitutes a very adaptable, sizeable and parametrized model (via cells numbers by the amplifiers elements, connected and disconnected sub-models by the controlled junctions, etc.). In addition, it provides an evolutive model which can be easily used in different contexts by adding, modifying or eliminating sub-models. This allows the possibility of establishing some component libraries of configurable sub-models such as FC, EL. Furthermore, the integrated automaton allows defining and simulating different OM. The OMM is made much easier since it is defined and it operates separately from the system dynamic. As a model-based task, the proposed approach allows performing an on-line FDI. Easily derived from the EDHBG model, the graphical EDHBG Diagnoser, developed in chapter III section 3.2.4, can be used to perform redundancy MBD. With the possibility to include the system parametric uncertainties, the diagnoser allows, when needed, a robust fault detection and isolation for all the OM. Benefiting from the BG causal properties, this allows relating the detected fault to the suspected BG element and then its associated physical components.

From the functional point of view, the structured causal model provides a correspondence between the services of the distinct components and their representative sub-models. Having the diagnosis state related to the system functional service map permits obtaining the service operational and functional availabilities. These latter can be used in defining the OM. In order to build and simulate BG models, many BG programming software platforms or simulation environments are available. We mention 20sim®, Symbols Shakti®, MS1® and CAMP-G. For small or medium size systems, BG can be coded in an object-oriented modelling language such as Modelica® .

20sim allows the use of predefined modifiable or entirely new defined BG elements. An interesting feature of 20sim is the automatic causality assignment. This means the user is just needed to "draw" the model structure and entering the parameters and chose the preferred causality model (integral or derivative). On 20sim, a BGD can be also obtained from the associated simulation BG model by simply copying the model and flipping the detectors into sources (dualizing) and following the steps defined in chapter III-section 3.2.4. In fact, generating the BGD from the simulation model is quite easy to be achieved automatically. Using 20Sim 4C, the diagnoser C code can be easily embedded for an on-line use.

In this context, to illustrate the use of the proposed approach, representative HRES is considered and shown in [Fig. 4.1]. The system is composed of two sources PV and WT connected through a common DC bus to the batteries. The DC bus is permanently connected to an electrical load which includes the system operating load. A hydrogen storage (EL/H_2 Tank) unit serves as power storage along with the battery bank. A FC is serving as an application for the stored hydrogen. The EL and a FC, both are connected to hydrogen storage tank. The PV, WT, EL and FC are connected through controlled switches that allow to remotely disconnect, each one independently, from the DC bus. From an energetic point of view, the proposed system fits perfectly with the objectives of this work. It makes up a perfect example of a multi-sources HRES with hydrogen-based multi-storage. The redundancies of the component services manifest the need of the power management and the OMM. The PV, the EL, the FC and the hydrogen tanks constitute perfect modelling subjects of renewable energy systems that present cellular structures.

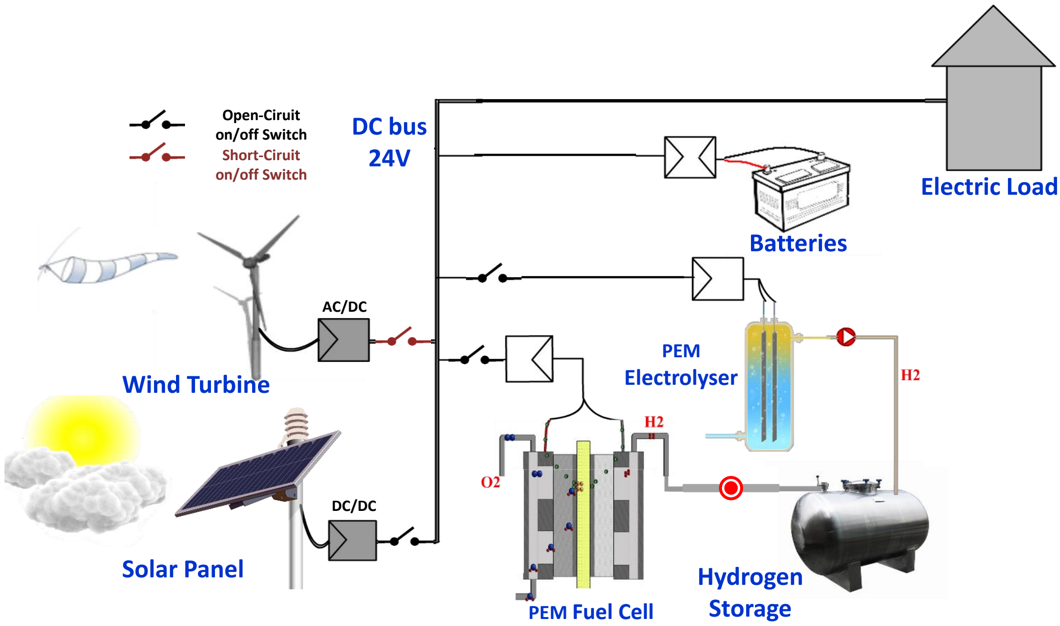

Figure 4.1 – Schema of multi-source with multi-storage HRES

4.2 Design of the simulation BG model

This section, first, presents the experimental HRES platform, then it explains the theory behind the HRES modelling and its assumptions. Then, the BG models are developed and explained for each component separately. Finally, all these components are gathered into one global EDHBG model. The parameters of each sub-models are defined as global variables. They can be defined in two ways, separately for each sub-model aside or globally by an independent block/file that contains all the parameters sorted by their associated component.

4.2.1 Experimental HRES platform

A small size experimental HRES is used to validate the model parameters (mostly given by the manufacturers) and to test the proposed approach. This laboratory set-up is depicted in Fig. 4.2, the system main objective is to produce hydrogen from renewable energy multi-sources.

The system includes:

- ☐ Two PV 200 Watt modules of 54 serial cells each, the two modules are set in parallel electrical configuration. The output of the PV modules is connected to 24 Volt DC bus through a DC/DC converter.

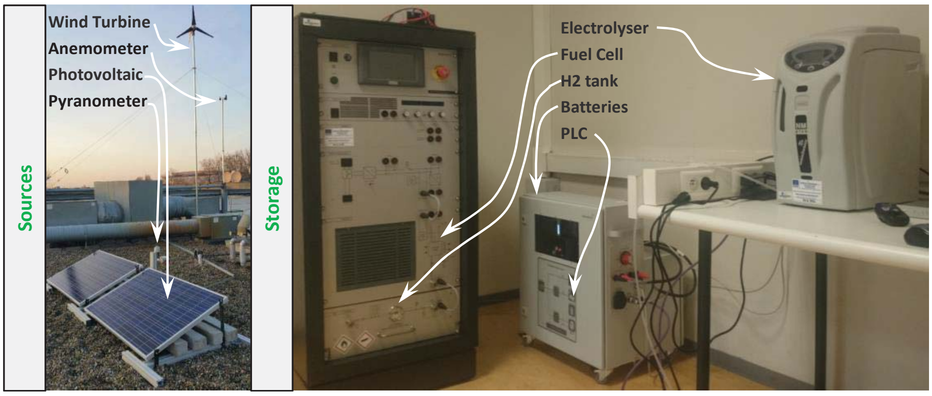

Figure 4.2 – Experimental HRES for hydrogen production and storage

- ☐ A PMG WT with a DC 24 Volt as an output connected to the DC common bus.
- ☐ A battery bank (110 Ah) with DC 24 Volt.
- ☐ A PEM-EL of two cells 30 NL/hour consuming up to max 400 Watt.
- ☐ A PEM-FC of 36 cells generated power up to max 1500 Watt.
- ☐ Hydrogen storage bottles max pressure of 11 bars.
- ☐ A variable resistive load to simulate load profiles.
- ☐ A PLC unit that connects and disconnects the different components from the common DC bus.
- ☐ Weather sensors including anemometer, pyranometer.

Despite the fact that the presented HRES constitutes a perfect example for the purpose of this thesis, working on such experimental set-up is not quite easy and faces many drawbacks. The difficulties that are most likely to encounter the validation of the used approach:

- **Uncontrollable weather conditions:** This limits the real-time validation of the model. The profile of the available power is not controllable, this implies difficulties on checking all the operating modes and power management. For example, it does not allow to verify the high wind with high solar power conditions. Also, for this reason the validation of the systems is done for each of component independently. After the model validation and using real weather data (respectively reconstructed weather data) which are available on-line, the user can use the global model to inspect all the OM.
- **Destructive and dangerous faulty situations:** The set-up is not equipped with faulty modes to test the diagnosis approach. A fault can not be created if it

is not considered in the main design and the safety protocol. In fact, enforcing fault on such experimental system is very difficult for two reasons:

– Due to the harmful nature of the faults that can occur in the system

– Due to the expensive nature of the components

For this reason, pre-registered data from faulty behaviours of a real system can be used to test the diagnoser. Another solution is to use a simulated model of the system with noises, disturbances and uncertainties to imitate the real system behaviour. Using the EDHBG simulation model, the parameters are accessible to imitate any spontaneous or continuous change in the system dynamics. This allows testing the response of the diagnoser to spontaneous faults or continuous degradations.

- **Inaccessible control:** In fact, some components of the experimental set-up are commercial products. Therefore, the used control laws are not accessible nor editable. This complicates the validation and the testing phase.

4.2.2 The theory behind the modelling

4.2.2.1 Photovoltaic panel

[Fig. 4.3] shows a very common one-diode electrical model of the photovoltaic cell. It consists of a current source generating the photo-current I_{ph}. It shares a common

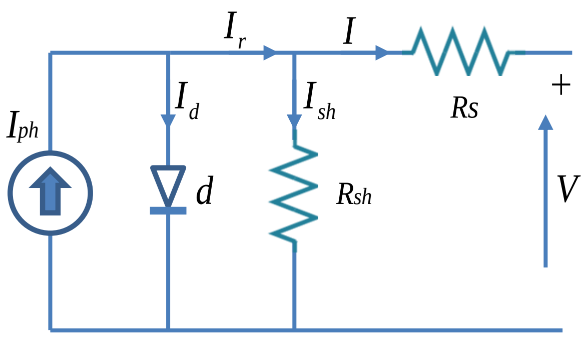

Figure 4.3 – PV cell one-diode electrical model

voltage (mounted in parallel) with a diode d and constant shunt resistance R_{sh} [149]. I_{ph} represents the total electron current mobilized by the sun light. It changes, assumed linearly [10, 150, 151], with the incident solar irradiation and ambient temperature according to the equation expressed by Eq. 4.1.

$$I_{ph} = I_{ph_{[STG]}} + \Delta I_{ph}(G) + \Delta I_{ph}(T) \tag{4.1}$$

where:

- $I_{ph_{[STG]}}$ is given at Standard Temperature and Irradiation (STG) $[STG : T = 25°\text{C}$; $G = 1000W/m^2]$.
- $\Delta I_{ph}(G)$ and $\Delta I_{ph}(T)$ are the photo-current deviations from the STG values, respectively, in function of the actual irradiation and temperature.

Eq.4.2 describes the expression of the photo-current at a given temperature T and the irradiation G [10].

$$I_{ph} = I_{cc}\frac{G}{1000}[\delta l_T(T - 298) + 1] \tag{4.2}$$

I_d stands for the diode reverse leakage current, Eq.4.3 represents its expression in terms of its applied voltage V_d [10, 152].

$$I_d = I_s[e^{\frac{e(V_d)}{aKT}} - 1] \quad \text{with} \quad I_s = I_{0_{ref}}T^3[e^{\frac{-E_g}{KT}}] \tag{4.3}$$

where:

- K is the Boltzmann Constant.
- a is the diode ideality constant, e is the electron charge.
- $\frac{aKT}{e}$ is called the thermal voltage.
- I_s is a temperature T depending on parameter called the saturation current.
- E_g is the band gap of semiconductor material.
- $I_{0_{ref}}$ is the temperature coefficient.

The cell output current I expression is given in Eq.4.4

$$I = I_{ph} - I_d - I_{rsh} \tag{4.4}$$

where I_{rsh} is the shunt resistance current given by Eq.4.5.

$$I_{rsh} = \frac{V + R_s}{R_{sh}} \tag{4.5}$$

Having the relation tying I-U constitutes the statical model of the PV. In fact, the PV by its electronic nature does not show a transient dynamic model. Some have considered the presence of capacitors on the output of the PV. However, the majority of the consulted works have considered the statical behaviour as sufficient.

4.2.2.2 Wind Turbine

The WT extracts part of the kinetic energy of wind and turns it to useful mechanical then electrical energy. In order to continue moving, the wind can never be stripped off of all its kinetic energy. Thus, the WT extracted energy is always partial with theoretical limit of 59% (Betz limit). The ratio between the extracted power P_{mech} relatively to the incident kinetic power of the wind P_{wind} is expressed by Eq. 4.6

$$Cp(\lambda) = \frac{P_{mech}}{P_{wind}} \tag{4.6}$$

where Cp is always less than 0.59 and usually expressed with respect to the tip speed ratio λ defined by Eq. 4.7.

$$\lambda = \frac{wr.r_{wt}}{v_w} \tag{4.7}$$

where:

- wr is the WT rotation speed
- r_{wt} is the rotating radius
- v_w is the wind speed.

Cp is usually obtained by wind tunnel tests and given in lookup tables. In [13, 14], authors presented analytical model of the WT including an empirical parametrized formula of Cp, expressed by Eq 4.8.

$$Cp\left(\lambda', \eta\right) = c_1(\frac{c_2}{\lambda'} - c_3\eta - c_4)e^{-c_5/\lambda'}) + c_6\lambda' \tag{4.8}$$

where:

- $c_i \quad _{i\in\{1,2...6\}}$ are aerodynamic design parameters.
- η represents the pitch angle, $\eta = 0°$ in fixed pitch wind turbine.
- λ' is defined in terms of the tip speed ratio λ and the pitch angle η by Eq. 4.9

$$\frac{1}{\lambda'} = \frac{1}{\lambda + 0.08\eta} - \frac{0.035}{\eta^3 + 1} \tag{4.9}$$

Using Eq. 4.10 where the extracted P_{mech} is written in terms of the mechanical torque T_{mech} and the rotational speed of the WT wr, the expression of Cp can be written in terms of both as shown by Eq. 4.11.

$$P_{mech} = T_{mech} \cdot wr \tag{4.10}$$

$$Cp = \frac{T_{mech}.wr}{P_{wind}} \tag{4.11}$$

where P_{wind} is expressed by Eq. 4.12.

$$P_{wind} = \frac{1}{2} A \rho v_w^3 \tag{4.12}$$

where:

- A is the swept area by the WT
- ρ is the air density.
- v_w is the incident wind speed.

Cp has a maximum at $\lambda_{optimal}$, where the extracted power from the wind is optimal. In order to maintain Cp at its maximum, a MPPT control algorithm is usually needed to drive the WT rotation speed in order to maintain the tip speed ration at $\lambda_{optimal}$.

4.2.2.3 Electroyser and Fuel cell

Thermodynamical Balance

The electrolysis and the FC reaction are multi-domain processes induced by coupled energetic phenomena including: electrical, chemical, thermodynamical and thermal domains.

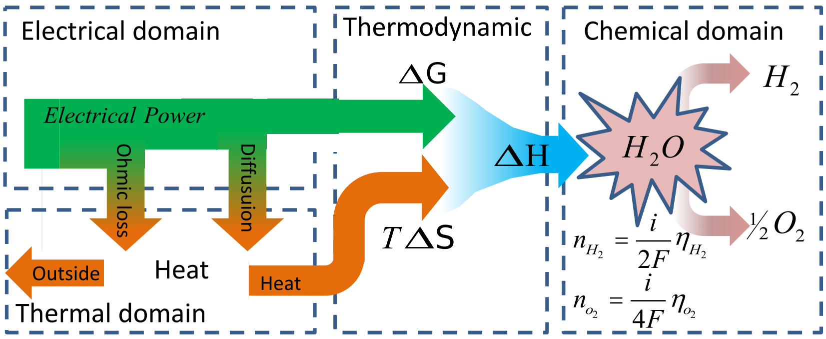

Figure 4.4 – Energy balance of the electrolysis

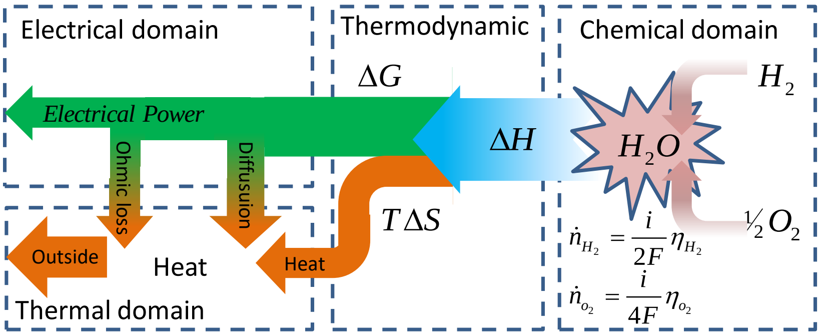

Figure 4.5 – FC energy balance

Thermodynamically, the amount of the energy (per mole) consumed in the electrolysis process or produced in FC, at temperature T, is represented by the enthalpy $\Delta H^0_{(T)}$ (see Fig. 4.4 and Fig. 4.5). This energy is required in the electrolysis (resp. generated in the FC) in both electrical and thermal forms. Eq. 4.13 shows this energy balance:

$$\Delta H^0_{(T)} = \Delta G^0_{(T)} + T\Delta S^0_{(T)} \tag{4.13}$$

where:

- $\Delta G^0_{(T)}$ is called Gibbs free energy or free enthalpy, it represents the amount of the useful reversible energy involved in the thermochemical reaction. In the electrolysis, Gibbs free energy symbolizes the amount of the net electrical energy needed for the chemical process of the electrolysis without counting any losses. In the FC, it represents the very net electrical energy produced before any dissipation.

- $T\Delta S^0_{(T)}$ is the amount of heat (thermal energy) involved in the reactions, it is consumed along with the electrical power in the electrolysis and generated with the electrical power in the FC.

ΔH^0, $\Delta G^0_{(T)}$ and $T\Delta S^0$ are temperature and pressure dependent. In general, ΔH^0 and ΔS^0 are given in lookup tables in standardized conditions (STP) (1 atm 25 C°) called $\Delta H^0_{(298)}$, $\Delta S^0_{(298)}$. Eq. 4.14 and Eq. 4.15 represent the temperature-based approximations of ΔH^0 and $T\Delta S^0$ in the neighbourhood of the temperature T with the thermodynamical parameters defined in Tab. 4.1.

$$\Delta H^0_{(T)} = \Delta H^0_{(298)} + \alpha_{rec}(T - 298) + \frac{\beta_{rec}}{2}(T^2 - 298^2) + \frac{\gamma_{rec}}{3}(T^3 - 298^3) \tag{4.14}$$

$$\Delta S^0_{(T)} = \Delta S^0_{(298)} + \alpha_{rec} \ln(\frac{T}{298}) + \beta_{rec}(T - 298) + \frac{\gamma_{rec}}{2}(T^2 - 298^2) \quad (4.15)$$

The expression of Gibbs free energy $\Delta G^0_{(T)}$ is obtained by replacing Eq. 4.14 and Eq. 4.15 in Eq. 4.13.

	$J.mol^{-1}.K^{-1}$
α_{rec}	-11.5575
β_{rec}	3.9582×10^{-3}
γ_{rec}	3.9582×10^{-6}

Table 4.1 – General Enthalpy coefficient [153]

Since previous approximations Eq. 4.14 and Eq. 4.15 are given at a fixed standard pressure P_0 (1 atm), Eq. 4.16 includes correction terms to obtain ΔG^0 at any pressure [154, 155].

$$\Delta G^0_{(T,P)} = \Delta G^0_{(T,P_0)} + RT \ \ln(\frac{P_{H_2}}{P_0}) + RT \ ln(\frac{P_{O_2}}{P_0})^{0.5} \quad (4.16)$$

Neglecting all form of electrical losses and considering the source of the heat is external (is not electrical), the thermodynamical efficiency of the reaction, at Standard Conditions (STC), can be written in form of Eq. 4.17.

$$Ef_{ther} = \frac{\Delta H^0}{\Delta G^0} \quad (4.17)$$

Noticing that $\Delta H^0 > \Delta G^0$, this means, the electrolysis thermochemical efficiency $Ef_{ther_{EL}}$ is higher than 100% due to the heat contribution and the FC thermochemical efficiency $Ef_{ther_{FC}}$ is lower than 100% due to the heat dissipation.

According to the previous equations, $\Delta H^0_{(T)}$ changes slightly within the temperature range $[0, 100]C^{\circ}$. However, $\Delta G^0_{(T)}$ that represents the contribution of the electrical power in the reaction decreases with higher temperature (see Fig. 4.6). To satisfy the global energy required for the reaction $\Delta H^0_{(T)}$, the decrease in $\Delta G^0_{(T)}$ is compensated by increasing the heat contribution $T\Delta S^0_{(T)}$. This indicates that the higher is the temperature the higher is the heat relative contribution compared to the electrical power in the electrolysis. Therefore, the thermodynamical efficiency $Ef_{ther_{EL}}$ increases with the temperature. This explains the increasing interest in high temperature electrolysis. On the other hand, a higher temperature in FC means the energy balance showed in Fig. 4.5 is shifted to generate more heat, therefore $Ef_{ther_{FC}}$ decreases with high temperature.

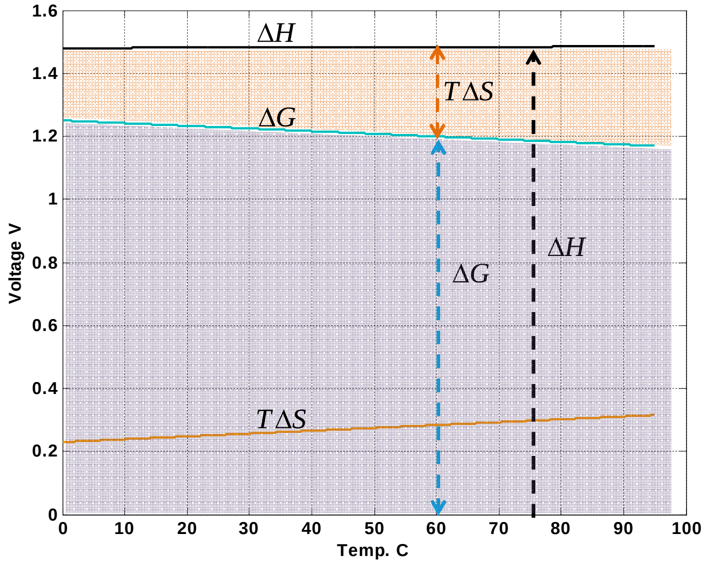

Figure 4.6 – $\Delta H^0_{(T)}$ and $\Delta G^0_{(T)}$ according to the reaction temperature T

Open-circuit voltage

$\Delta H^0_{(T)}$, $\Delta G^0_{(T)}$ and $T\Delta S^0_{(T)}$ represents energy dimensions per mole. In fact, the substance quantities (reactant and products) involved in the reaction is proportional to the total electron charge or the current involved in the reaction according to the Faraday law. Dividing by Faraday constant and the reaction involved electrons number ($2e^-$), the enthalpy and Gibbs free energy can be written in form of electrical potential as shown in Eq. 4.18. The obtained expressions in Eq. 4.19 represent, respectively, the open-circuit electrical potential associated to the standard-pressure $E_{rev(T,P_0)}$ and its correction for any given pressure $\delta E_{rev(P_0,P)}$.

$$E_{rev(T,P)} = \frac{-\Delta G^0_{(T,P)}}{2F} = -\frac{\Delta G^0_{(T,P_0)}}{2F} - \frac{\delta G^0_{(P,P_0)}}{2F} \tag{4.18}$$

$$E_{rev(T,P)} = E_{rev(T,P_0)} + \delta E_{rev(P_0,P)} \tag{4.19}$$

Operating voltage

The reversible power is the net power used directly into the chemical process. In fact, there exist several losses between the electrolysis-applied electrical power (resp. extracted in FC) and the net power involved in the chemical reactions as shown in Fig. 4.4 (resp. Fig. 4.5).

For the same amount of hydrogen rate (related to the consumed current), the losses can be illustrated in form of an increase in the electrolysis electrical voltage (resp. decrease in the FC) between the cathode and the anode. Eq. 4.20 (resp. Eq. 4.21) shows three types of dissipative phenomena during the electrolysis and FC reactions [156, 157, 158].

$$U_{EL\ cell} = E_{rev(T,P)} + |\eta_{act}(i)| + |\eta_{ohm}(i)| + |\eta_{trans}(i)| \tag{4.20}$$

$$U_{FC\ cell} = E_{rev(T,P)} - |\eta_{act}(i)| - |\eta_{ohm}(i)| - |\eta_{trans}(i)| \tag{4.21}$$

$\eta_{act}(i)$, $\eta_{ohm}(i)$ and $\eta_{trans}(i)$ represent the dissipated powers in form of heat.

- The activation losses $\eta_{act}(i) = \frac{RT}{2\alpha_{elec}F}\ \ln(\frac{|i|+I_n}{I_0})$
- The ohmic losses $\eta_{ohm}(i) = R_{ohm}\,|i|$
- The reactant transportation losses $\eta_{trans}(i) = \frac{RT}{2\beta_{elec}F}\ \ln(1 - \frac{|i|}{I_{lim}})$

Thermal dynamic

In the FC the produced heat is dissipated using fans or liquid cooling, to maintain low FC temperature. During the electrolysis, this heat contributes, partially or totally, in the reaction energy balance as shown in Fig. 4.4. In case where the generated heat is as the same amount needed for the electrolysis i.e $|\eta_{act}(i)|+|\eta_{ohm}(i)|+|\eta_{trans}(i)| = T\Delta S^0_{[V]}$, the electrolyser temperature remains stable and the applied electrical voltage is called the thermo-neutral voltage expressed in Eq. 4.22.

$$E_{tn_EL[V]} = \Delta G^0_{[V]} + T\Delta S^0_{[V]} = \Delta H^0_{[V]} \underset{@STC}{\simeq} 1.48V \tag{4.22}$$

When the losses are less than $T\Delta S^0_{[V]}$, the electrolysis process is endothermic and absorbs heat from the ambient medium. This allows a higher efficiency. When the losses are more than $T\Delta S^0_{[V]}$, the electrolysis process starts to be exothermic, emitting heat and/or increasing the electrolyser temperature. The thermal dynamic of the electrolysis and the heat exchanges with the ambient medium are expressed in Eq. 4.23.

$$C_{cal}\frac{dT}{dt} = \sum_{i=1}^{n}\dot{Q}_i - T\Delta S - \dot{Q}_{ex} \tag{4.23}$$

Where:

- C_{cal} represents the global thermal capacity of the cell.
- $\dot{Q}_i$ are the heat fluxes generated by the resistive losses.

- $T\Delta S$ is the heat flux used in the chemical process.
- $\dot{Q}_{ex}$ is the heat flux emitted to the outside medium.

Eq. 4.23 expresses the heat stored as an internal energy (power) $C_{cal}\frac{dT}{dt}$(i.e the temperature variation). It is equal to the difference between, from one side, the generated heat flux from the dissipation $\sum_{i=1}^{n} \dot{Q}_i$ and, from the other side, the re-used part in the reaction $T\Delta S$ and the part exchanged with the external medium $\dot{Q}_{ex}$.

In case of the FC, the dissipated heats $\sum_{i=1}^{n} \dot{Q}_i$ are always positive (released heat). However, unlike the electrolysis $T\Delta S$ is also dissipated i.e positive. Therefore, the thermal dynamic of the FC reaction and the heat exchanges with the external medium are expressed in Eq. 4.24.

$$C_{cal}\frac{dT}{dt} = \sum_{i=1}^{n} \dot{Q}_i + T\Delta S - \dot{Q}_{ex} \tag{4.24}$$

4.2.2.4 H_2 Tanks

The hydrogen is an ideal gas. The storage dynamic is subjected to the thermodynamical law of the ideal gas shown in Eq. 4.25.

$$P_{H_2}.\frac{V_{tank}}{\mathcal{R}.T_{tank}} = n_{H_2} \tag{4.25}$$

Where:

- P_{H_2} is the hydrogen variable storing pressure.
- V_{tank} is the tank volume assumed constant.
- T_{tank} is the tank temperature assumed constant.
- n_{H_2} is the hydrogen quantity in mole.
- $\mathcal{R}$ is the gas constant.

Since we are dealing with the rates (power, mass and molar rates), deriving by the time Eq. 4.25 can be re-written in terms of molar rate $\dot{n}_{H_2}$ as shown in Eq. 4.26 .

$$\dot{n}_{H_2} = \frac{dP_{H_2}}{dt} \cdot \frac{V_{tank}}{\mathcal{R}.T_{tank}} \tag{4.26}$$

Where $\frac{V_{tank}}{\mathcal{R}.T_{tank}}$ can be defined as the capacity of the tank C_{H_2}.

4.2.3 Sub-systems BG models

4.2.3.1 Photovoltaic Model

Fig. 4.7 shows the BG model of PV cell (open voltage). A $MSf : I_{ph}$ is used to generate the photo-current. I_{ph} is obtained in function of the temperature and the irradiation according to Eq.4.2. The diode d can be represented as modulated non-linear resistance MR_d with I-U characteristics represented by Eq.4.3. Since it depends on the ambient temperature, MR_d receives also the T as moulding signal.

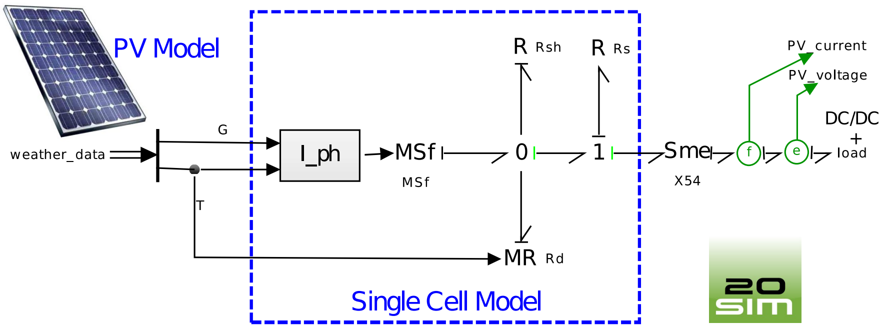

Figure 4.7 – PV Simulation Model on 20Sim

The resistances R_s and R_{sh} are represented by ordinary R BG elements. $MSf : Iph$, R_{sh} and MR_d are sharing same voltage in parallel (common effort), therefore they are connected to the same 0-junction. R_s is in series, it is connected to a 1-junction. This single cell model is connected to the DC/DC model through an effort amplifier Sme with 54 as amplification factor which corresponds to the cell number in the PV model. The symbols ⓕ and ⓔ represent respectively the flow and the effort detector ports.

4.2.3.2 Wind Turbine model

Fig. 4.8 shows a simplified BG model of a PMG wind turbine. $MSf : v_w$ represents the flow source that imposes the incident wind velocity v_w obtained from the data weather file or a real-time sensor output. $MGY : Aero$ represents a virtual gyrator BG element transforming the wind speed into mechanical torque T_{mech}. Classically, the BG gyrator elements MGY transforms the input speed flow f_{wind} into a proportional effort (i.e torque) $T_{mech} = r_{GY}.f_{wind}$. In the WT case, $MGY : Aero$ has a variable $r_{GY} = Cp.P_{wind}/v_w$, this gives that the output power of the gyrator $e_{WT}.f_{WT} = T_{mech}.wr = Cp.P_{wind}$.

In the BG model, $I : m_r$ represents the inertia of the rotor and the equivalent of shaft mass. $R : fr$ represents the viscous friction of the bearings. $TF : Ng$ represents the gear transformation with Ng ratio between the fast and the slow shaft (in this case $Ng = 1$). $MGY : K$ represents the DC generator transformation. $R : d$ represents the stator resistance. The port p represent a sub-model port, it connects the WT sub-model to the rest of the system BG model.

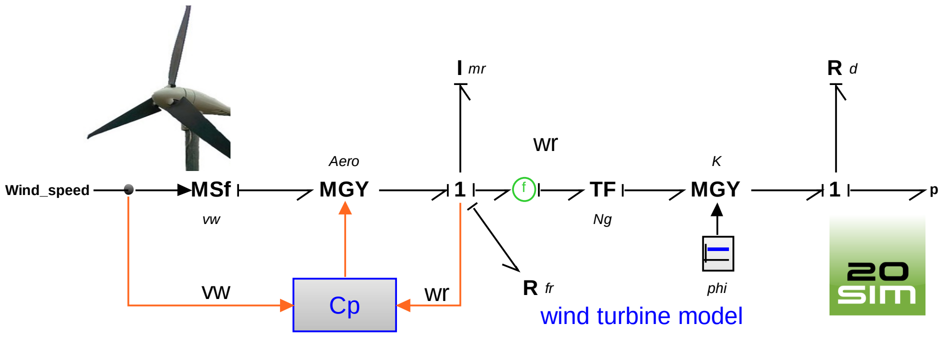

Figure 4.8 – Bond Graph model of the WT

4.2.3.3 Electrolyser and Fuel Cell Model

Externally, an electrolyser is supplied with a controlled input current in order to transform water to hydrogen and oxygen (see Fig. 4.9).

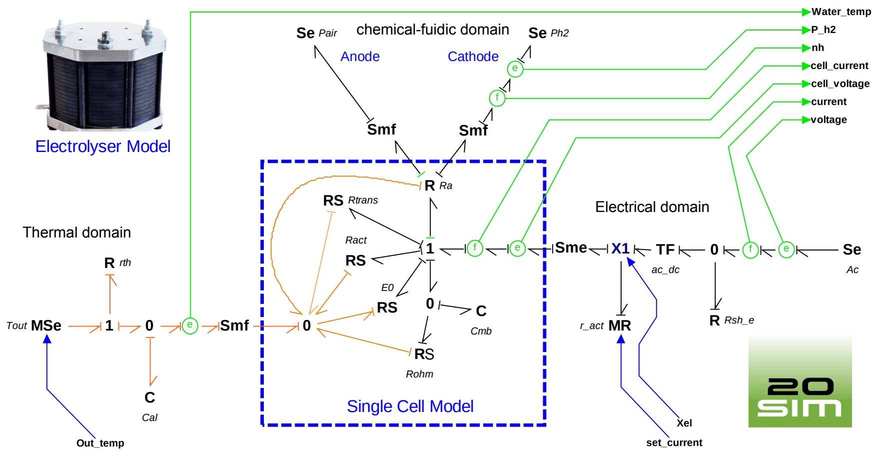

Figure 4.9 – BG model of the electrolyser on 20sim

To provide the controlled input current, an AC source ($Se : Ac$) is used with an AC/DC converter represented by its average model using ($TF : ac/dc$). The converter supplies the electrolyser with the corresponding voltage range. Using an active variable load $MR : r_{act}$, the input current is controlled. The electrolyser external temperature, denoted by T_{out}, is considered constant or controlled. T_{out} is supplied by an effort source $MSe : T_{out}$. The thermal resistance (conductivity) of the electrolyser and the thermal capacity of the water/cells are respectively represented by the BG elements $R : rth$ and $C : Cal$. The inner temperature of the electrolyser (cell+ water temperature) is measured and represented by the effort detector *water_temp*. Oxygen (air) and hydrogen pressures are respectively represented by effort sources ($MSe : Pair$) and ($MSe : Ph2$). These pressures are considered stable and predefined. The hydrogen flow rate is measured by a flow detector n_h. The electrolyser is composed of ns elementary cells mounted in series, this is represented by the effort amplifier element Sme in the electrical sub-model. The flow amplifiers Smf are also used to amplify the oxygen and the hydrogen flow rates and the heat flux according to the cell number. At the cell level, the imposed cell-current is used to provide the thermal and the electrical energies required to perform the chemical reaction. The losses between the applied electrical power and the net power used for the electrolysis, described by Eq.4.20 are represented by BG elements $RS : Ract$, $RS : Rohm$ and $RS : Rtrans$. The open-circuit electrical voltage $E_{rev(T,P)}$ is decomposed, as proposed by Eq. 4.19, into the open-circuit electrical voltage at the standard-pressure $E_{rev(T,P_0)}$ and its correction for any given pressure $\delta E_{rev(P_0,P)}$. These two electrical voltages are respectively represented by the BG elements $RS : E0$ and $R : Ra$.

$R : Ra$ is a 4-port element coupling the chemical model with the electrical and the thermal models. It receives the electrical flow *cell_current* as an input and provides as an output the molar flow rate n_{h_2} and n_{o_2} of the generated hydrogen and oxygen respectively.

The thermal dynamic of the electrolyser [157] is represented by Eq.4.23.

Assuming the temperature of the reaction is homogeneous, a 0-junction is used to balance the generated heat flows (from the electrical losses $RS : Ract$, $RS : Rohm$ and $RS : Rtrans$) with the consumed heat used in the chemical reaction $T\Delta S^0_{[V]}$ and the heat exchanged with the ambient medium.

Through its thermal port, $RS : E0$ absorbs (input power bond) the heat needed for the chemical process $T\Delta S^0$, obtained by Eq. 4.15. In return, the temperature needed to calculate $\Delta G^0_{[V]}$ is communicated through the thermal port as an effort. The consumed electrical power at $R : Ra$ is injected as flow into the thermal model via its thermal bond. In order to calculate $\delta E_{rev(P_0,P)}$, $R : Ra$ needs the water temperature and both hydrogen and oxygen partial pressures. They are communicated as efforts respectively through the thermal, cathode and anode bonds. C_{cal} represent the thermal capacity of the PEM EL with the water, associated to the left part of Eq. 4.23.

C_{mb} represent the electrical capacitor of the PEM. $X1$ represents the controlled junction, it receives n external Xel on/off signal.

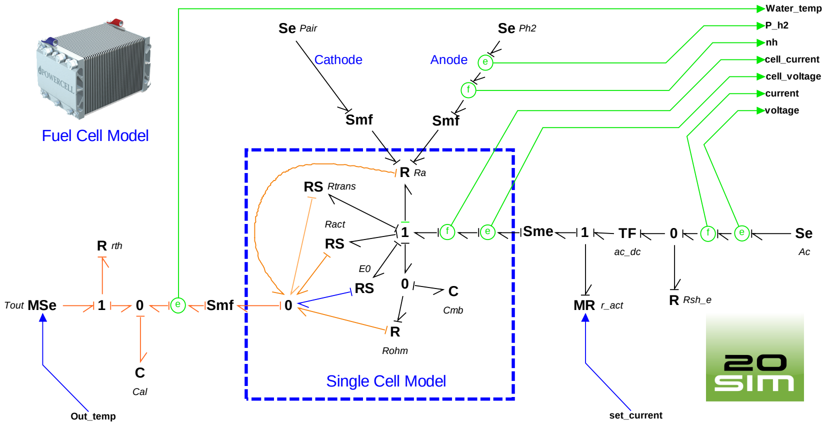

Figure 4.10 – FC energy balance

Fig. 4.10 represents the FC model. In addition to the parameters differences, unlike the electrolyser the $RS : E0$ in the FC injects the generated thermochemical heat into the thermal sub-model along with all the losses as explained in Eq. 4.24. Also, the hydrogen and the oxygen pressure sources are inverted, indicating the consumption of reactant flow rates.

4.2.3.4 H_2 storage tank

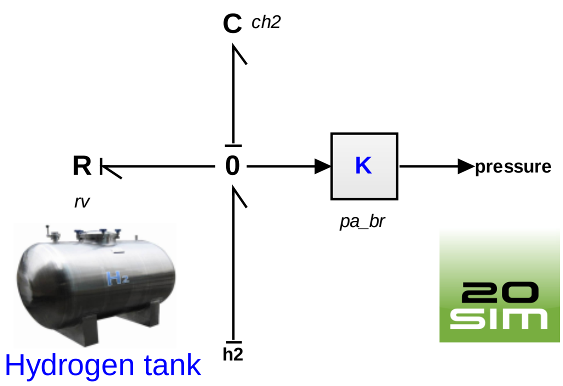

Figure 4.11 – The hydrogen tank linear model

The hydrogen is stored in a tank under max pressure of 10 bars. The tank BG model is showed in Fig. 4.11. The capacity $C : h_2$ is used to represent the storage capacity. It is associated to the dynamic described by the ideal gas law in Eq. 4.26 where $Ch_2 = V_{tank}/(\mathcal{R}.T_{tank})$. The input bond h_2 supplies the storage model with the H_2 molecular flow rate $f_h = \dot{n}_{h_2}$, and returns the effort $e_h = ph_2$, the storage pressure, to the FC/EL sub-models. As noticed $C : Ch_2$ is in integral causality, i.e the storage state ph_2 is obtained according to the integration expressed by Eq. 4.27 which is equivalent to the derivative form of the equation showed by Eq. 4.26.

$$ph_2 = \frac{1}{Ch_2} \int_{t_1}^{t_2} \dot{n}_{h_2} \, dt \tag{4.27}$$

.

$R : rv$ represents the installation leak-tightness resistance usually very high. The tank pressure is measured, k is the gain to obtain the pressures in bars.

4.2.4 Global EDHBG

All the sub-models are connected to the DC common bus represented by the centred 0-junction illustrated in Fig. 4.12. Following the causality strokes, the effort of the DC bus 0-junction i.e voltage is imposed by the batteries-DC/DC. The same voltage propagates to all the sub-models. For the batteries, an effort source $Se : U_{bat}$ is considered, where U_{bat} is a constant voltage. By integrating the output current signal of the batteries, the SoC is estimated according the Eq. 4.28.

$$SoC = SoC_0 - \frac{100}{C_{bat}} \int_{t_0}^{t} i \, dt \tag{4.28}$$

where:

- SoC_0 is the initial state of charge
- C_{bat} is the battery capacity (for example $(55Ah)$)

The EL is connected directly to the storage since its operating pressure range is between 1-10 bars. The FC, in its turn, is connected to the tank through pressure regulator represented by $MR : MR$. The regulator supplies the hydrogen at FC operating rate (0.3 bar).

The PV model is provided with a Mppt control and a Smf to simulate the two PV panels. The automaton used for the OMM is fed with the filtered signals of the measured wind velocity, the total generated power and the storages states (hydrogen pressure and battery SoC).

The switching vector β hands out to each controlled junction the associated corresponding control signal. The FC and the EL controlled junctions $X1$ are in their BG sub-model as showed in Fig. 4.9. The WT is provided with the short-circuit controlled junction $X0$. A fixed load is connected to the DC bus (0 junction), an ordinary BG resistance R is used. The weather data (temperature, solar irradiation and wind velocity) are communicated correspondingly to the PV and WT models.

A parameters block is used. It allows defining all the model parameters sorted by components.

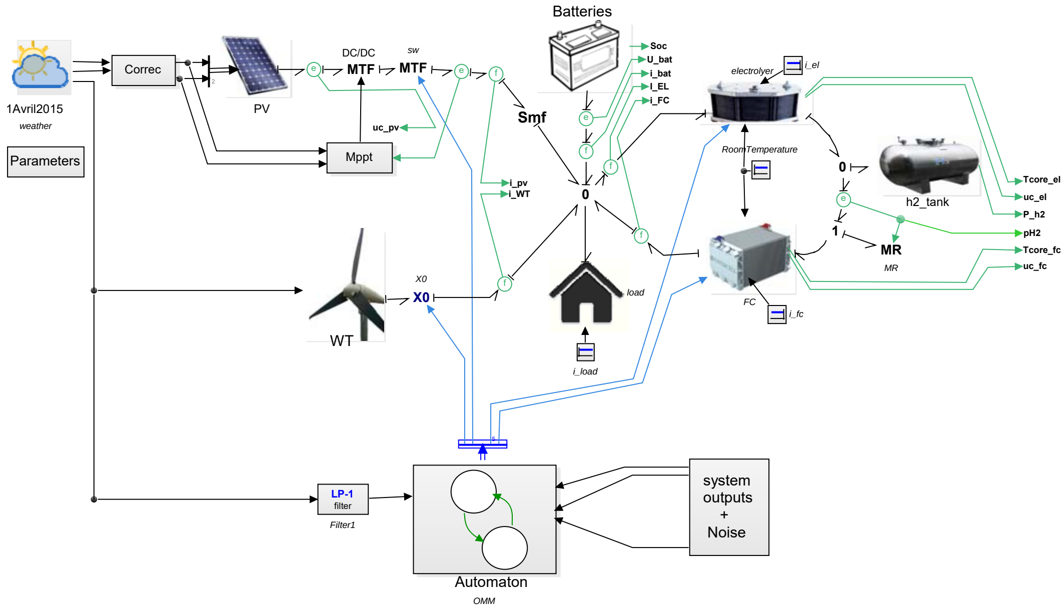

Figure 4.12 – Bond Graph model of the HRES

4.3 Model validation

Each one of the different models of the components (PV, FC and EL) has different set of variables and parameters. For each model, these parameters-variables can be related into two part of the model: static and dynamic. Statical parameters are used in the static model of the components. By adding the dynamical parameters-variables, the dynamical model is found. In this section in order to validate the models, both behaviours statical and dynamical are checked. Some statical parameters were given for some models by the manufacturers (case of the FC and PV). The dynamical models were constructed and identified experimentally. Fig. 4.13 shows the schema of the validation protocol for the dynamical behaviour of the PV. Classically, the model validation consists in comparing the outputs of the model and the real system while both are supplied with the same inputs and under the same operating conditions. A kind of special case for the model of the renewable energy sources (such as PV and WT) is the weather conditions. As the real system harvests power derived from the

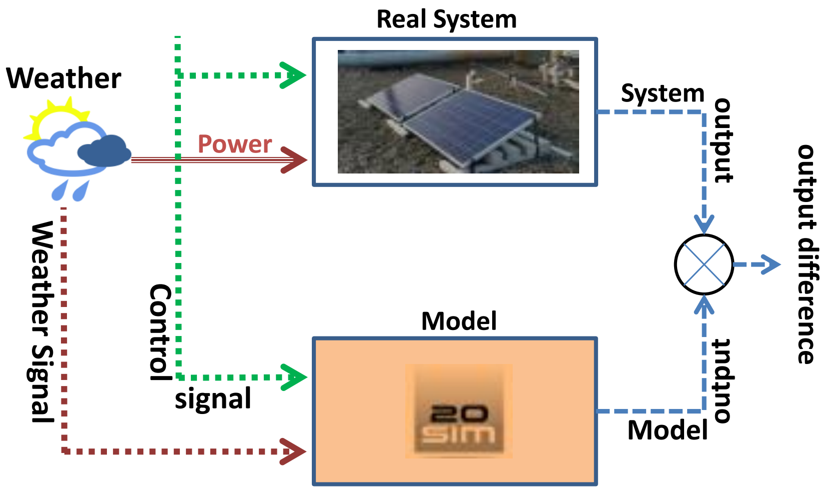

Figure 4.13 – PV model validation schema

weather, this latter is considered here as power inputs (see Fig. 4.13). Nonetheless, the model needs the weather conditions as an input signal to run the simulation. Hence, weather sensors are needed for the simulation model, as shown in Fig. 4.13, regardless if these signals are used or not in the control of the real system.

4.3.1 Wind Turbine

The used WT is PMG small power Primus Air 40 24 V. Specification are showed in Tab. 4.2.

To obtain Cp estimation for all the operating range of the WT : $v_w \in [0 - 25]m/s$, an aero-dynamical analysis through a wind tunnel is needed [159]. Fig. 4.14 shows the Cp variation with respect to the wind speed v_w of the used WT Air40.

Fig. 4.15 shows the output power of the WT Air40 compared to model output with respect to the incident wind speed. The data of the real system are obtained from the manufacturer [159]. The figure illustrates the output of the simulation model matching the output of the real system. The curves show three phases according to the wind

Primus	Air 40 24 V
Rotor Diameter	$1.17m$
Wind Speed	$3.1 - 22m/s$
Alternator	PM brushless
Startup Wind Speed	$3.1m/s$
Voltage	24 VDC

Table 4.2 – WT specifications

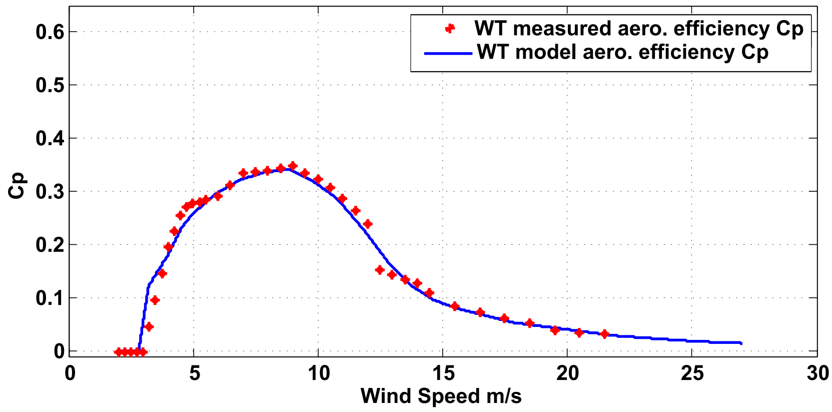

Figure 4.14 – Cp in function of the wind speed

speed ws. First, an increasing power with the increase of $ws \in [3 - 11]m/s$. Then, the optimal wind speed is reached at $ws = 11.3m/s$ where the max power hits $255W$. For $ws \in [15 - 22]m/s$, the WT power is maintained stable $\backsimeq 200W$. At high wind speed $ws > 22m/s$, the WT enters the breaking mode. It is disconnected from DC bus and uses its generator as an electromagnetic breaking to slow down its rotation speed.

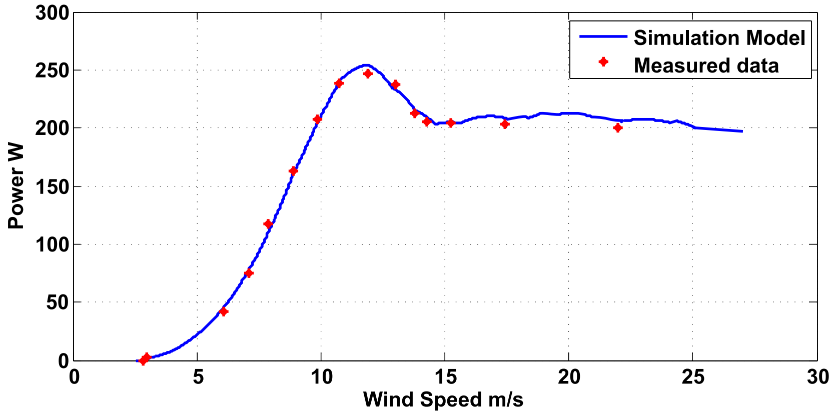

Figure 4.15 – The WT output power according to the incident wind speed

4.3.2 Photovoltaic PV Model

The solar modules are polycrystalline NeMo 54P220 7 from Heckert Solar, they are made out of 54 serial cells each. Tab. 4.3 shows the PV manufacture specifications.

Fig. 4.16 shows the obtained $i(u)$ polarization curve of the simulated model.

			NeMo 54P220 7	
STC	1000 W/m^2,25C°,1.5AM		U_{OC}	33.77V
P_{MPP}	$220Wp(\pm 2.5Wp)$		I_{SC}	8.62A
U_{MPP}	27.54 V		δI_{SC}	0.05%/°K [4.335 10^{-3} A/°K]
I_{MPP}	8.08 A		δU_{OC}	-0.32%/°K [0.108 V/°K]

Table 4.3 – PV specifications

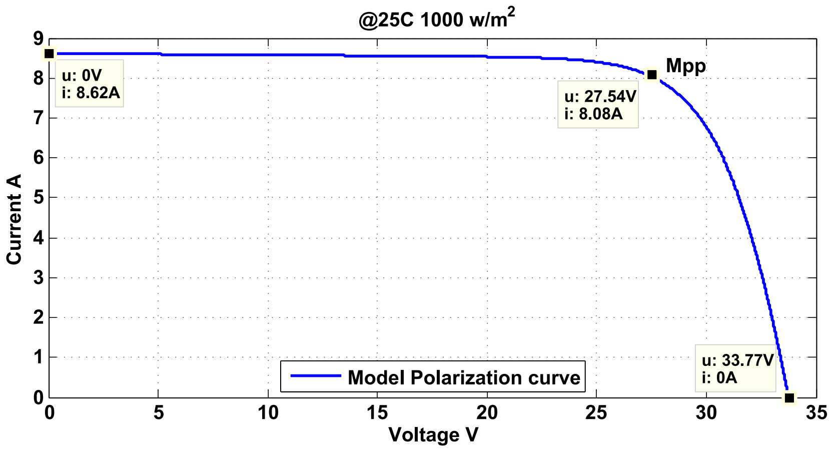

Figure 4.16 – Model polarization curve

The characteristic such as the Maximum Power Point (Mpp), the Open Circuit Voltage (U_{oc}) and the Short Circuit Current (I_{SC}) match the system specifications showed in Tab.4.3. Fig. 4.17 shows the polarization curve under different operating temperatures. As seen, the Open-Circuit Voltage U_{oc} shifts down by approximately $1.1V$ for every $10°K$ of temperature increase, this approximately corresponds to the $\delta U_{oc} = -0.32\%/°K$ showed in Tab.4.3. The short-circuit current I_{SC} shows a less sensibility to the temperature $\delta I_{SC} = 0.05\%/°K << -\delta U_{oc} = 0.32\%/°K$.

Fig. 4.18 shows the increase in the power (Mpp included) with lower temperatures. The Maximum power is 221 W at $STC = [25°\text{C}, 1000W/m^2]$. For an increase of $10°K$, the Mpp decreases about 10 W. This result is in accordance with the given specifications in Tab.4.3.

Since the generated power depends on the incident irradiation, Fig. 4.19 shows the polarization curve at different irradiation rates. The results illustrate that the increasing

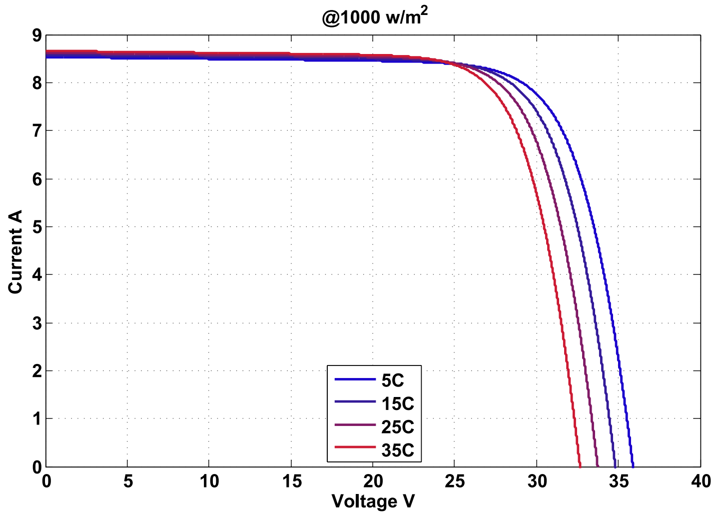

Figure 4.17 – Model polarization curve at different temperatures

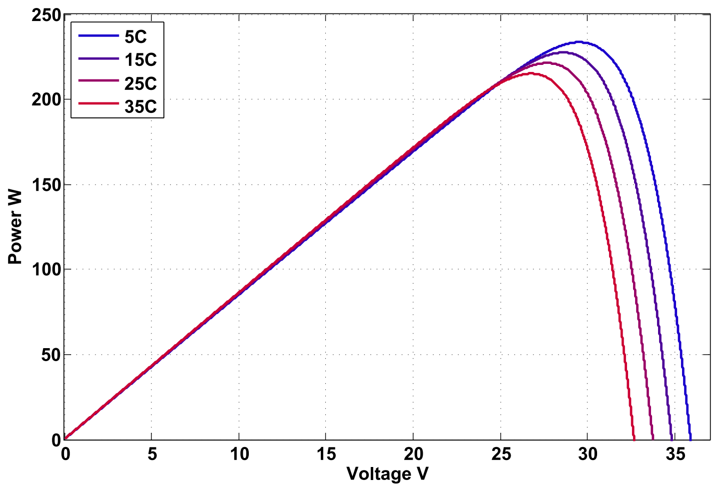

Figure 4.18 – Power P(u) at different temperatures

irradiation increases mainly the current output. Fig. 4.20 shows the increase of the generated power $P(u)$ with the increasing of irradiation.

The previous results validate the static model of the PV. To validate the transient behaviour of the model, the measured output of two PV connected in parallel is compared to the model output in Fig. 4.21. The results show that the estimated power of the model matches the real measured power. The figure shows also the incident irradiation on the PV plan in W/m^2.

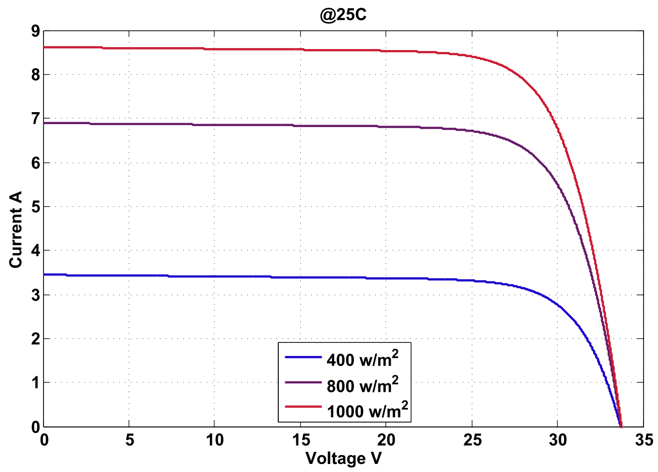

Figure 4.19 – Model polarization curve at different irradiations

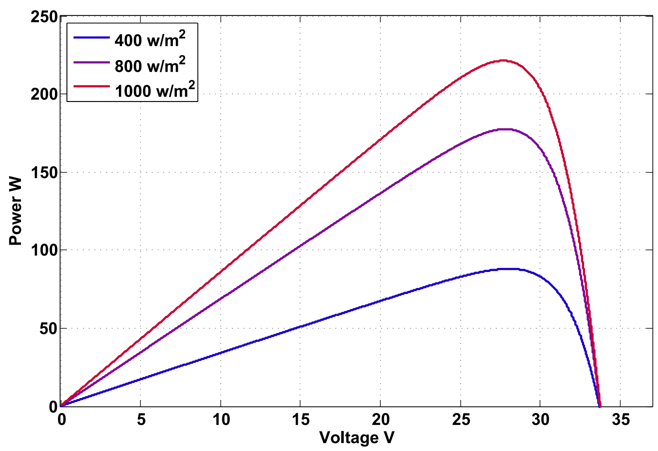

Figure 4.20 – Power P(u) at different irradiations

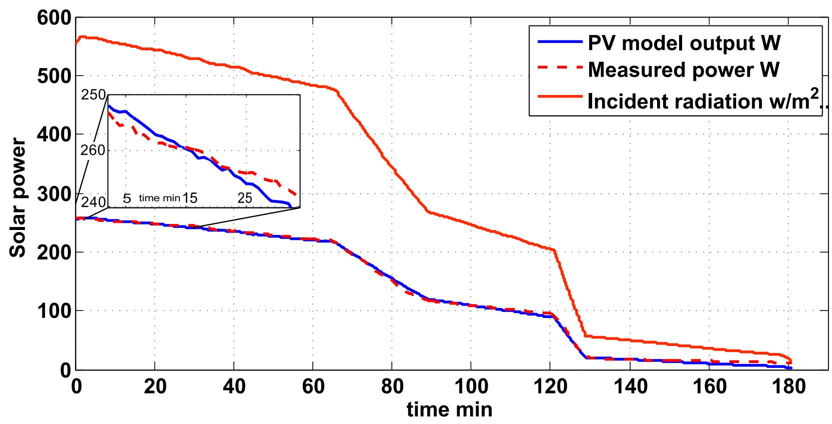

Figure 4.21 – PV output compared to model output

4.3.3 Electrolyser and Fuel cell

Tab. 4.4 shows the EL and the FC specifications.

Electrolyser		FC	
Hydrogen flow rate STP (20 C, 1bar)	Model NMH2 Plus 500 0-500 cc/min at STP	FC Model	Nexa 1.2kW
Max outlet pressure	11 bar	H_2 pressure	0.3- 0.5 bar
Power consumption	350 W	Power	1200 W
Input voltage	110-230 V/ 50- 60Hz Max	Output voltage	40-20 V/ DC

Table 4.4 – Electrolyser and Fuel Cell specifications

Fig. 4.22 shows the obtained polarization curve of the simulated model in comparison with the two-cell electrolyser measured output.

Fig. 4.23 shows the relatively small error in Volt between the model and the real output in function of the current. The simulated model is less accurate at the low current range. This is due to the modelling assumptions in the activation losses.

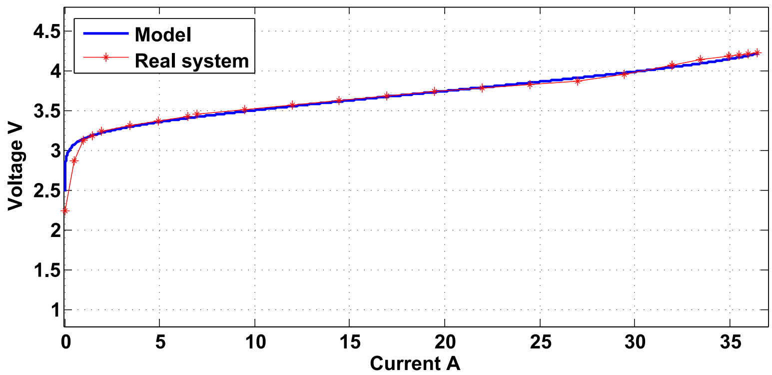

Figure 4.22 – EL polarization curve Simulation EL Model Vs real System

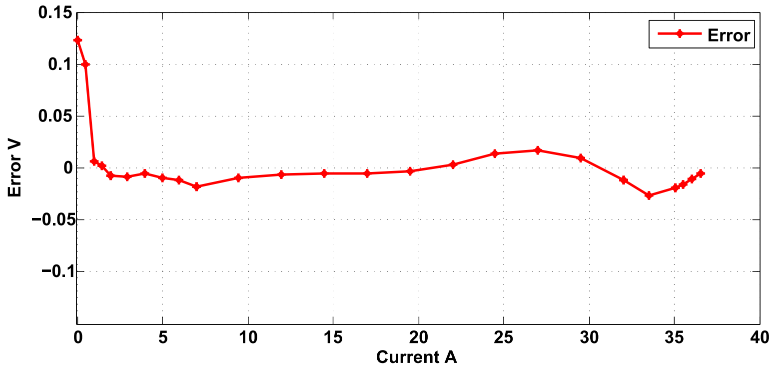

Figure 4.23 – Model Simulation error

Using the model, Fig. 4.24 shows, with respect to the current, the different phenomenon contributions in the electrolysis energetic balance. The losses due to the activation process represent the major contributor in increasing the voltage i.e lowering the efficiency. As Fig. 4.24 shows, while the ohmic losses are more or less proportional to the current, the activation losses increases significantly in the low current range to stabilize at the medium-high current range. The transportation losses are more significant at the higher current range.

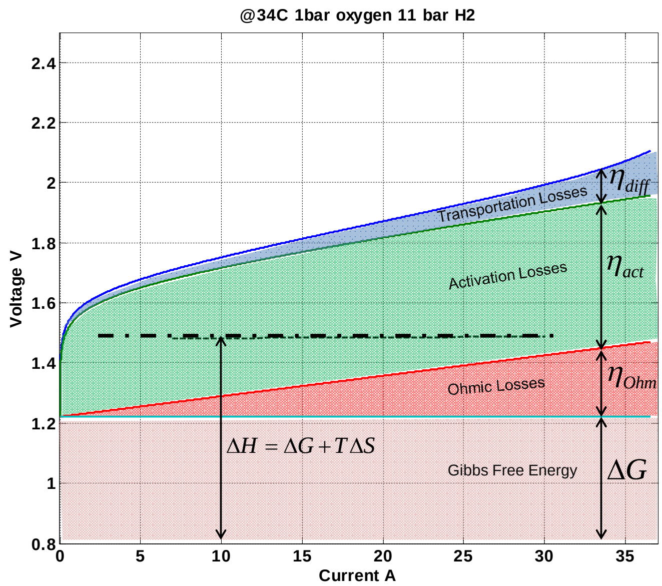

Figure 4.24 – Electrical losses in the electrolyser

Fig. 4.25 shows the effect of temperature on a single cell, the figure shows the polirazition curve at 34°C, 50°C and 80°C. For a constant current, the electrolysis voltage decreases with the increasing temperature. In other terms, for the same hydrogen production rate associated to same current i, a higher temperature leads to lower operating voltage. Consequently, less power is needed and higher efficiency is provided. The consumed power per cell at 34°C with respect to the current is represented by Fig. 4.26.

The cell efficiency of the electrolyser is represented in Fig. 4.27. Since higher current evokes more dissipative phenomena. The efficiency decreases at higher current range. Noticing that at the low current range the efficiency can be as high as 120%. The 100% is attended when the current corresponds to the thermoneutral voltage 1.48 V. In this condition of very low current, the hydrogen flow rate is very low (stoichiometric ratio or Faraday law). Despite the cells relatively high efficiency 70%, the global efficiency is

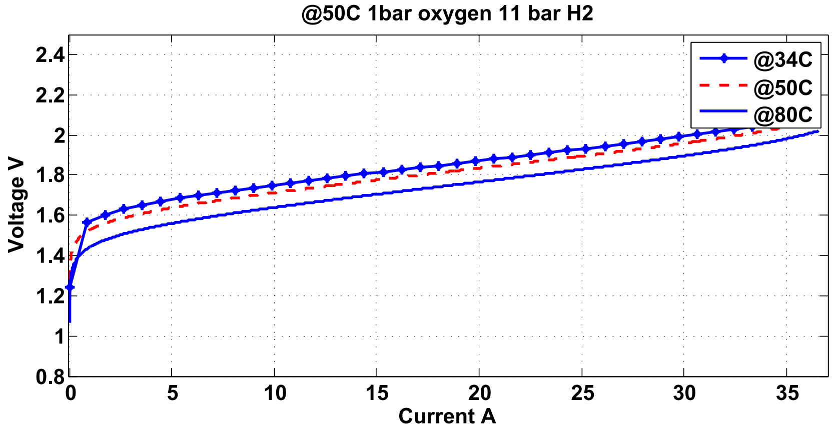

Figure 4.25 – Model Simulation under different temperatures

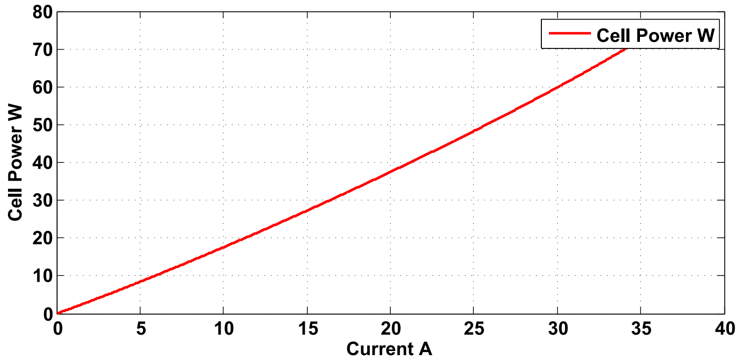

Figure 4.26 – The consumed power per cell

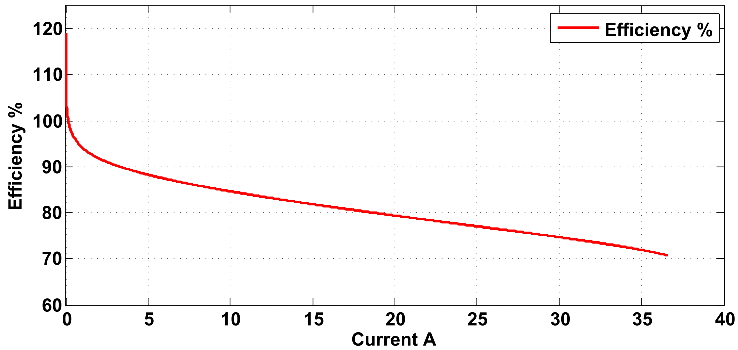

Figure 4.27 – The electrolysis cell efficiency

reduced significantly by the auxiliary part down to 40%. Fig. 4.28 shows the dynamical validation where the total power consumption of electrolyser (2 cells and auxiliary loads) is compared to the model. The figure also shows the net power used in the electrolyser core (just the model, and the net power stored as hydrogen). At high current, about more than the half of the consumed power is dissipated in the process.

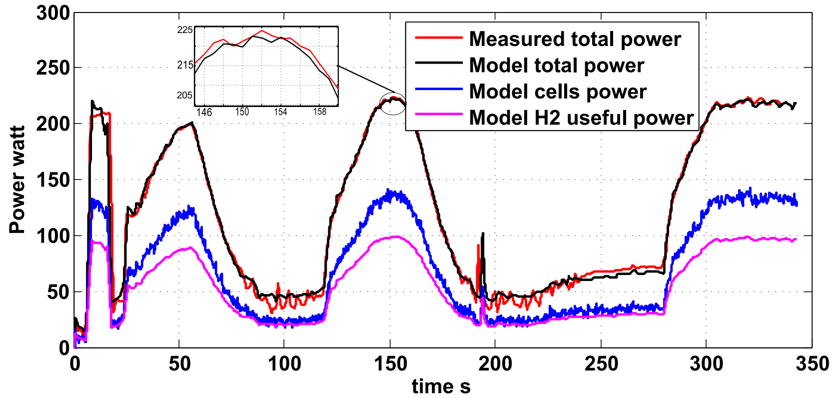

Figure 4.28 – Consumed power EL BG Model Vs real System

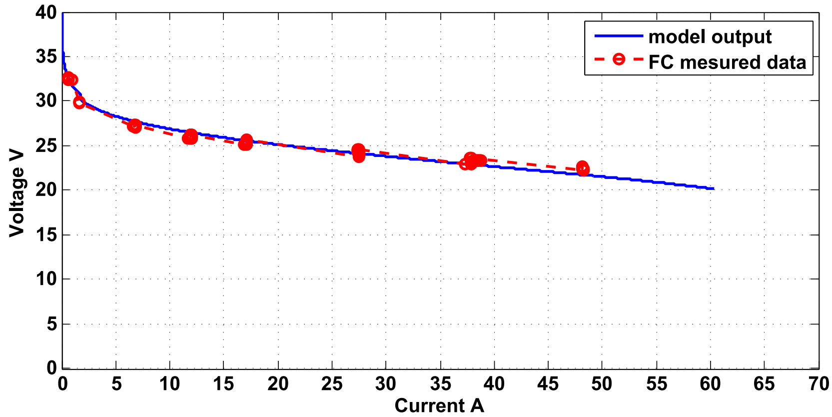

Figure 4.29 – FC measured and simulated U-I curve

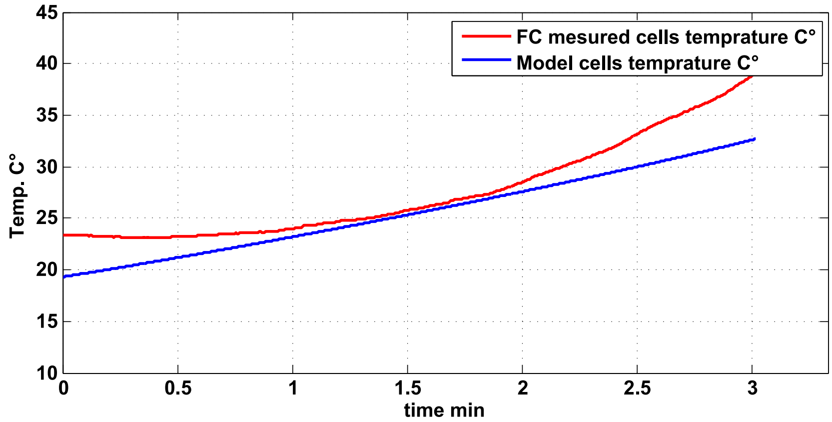

Figure 4.30 – FC measured and simulated cells temperature

Similarly for the FC, model and the measured polarization curve are represented in Fig. 4.29. Fig. 4.30 shows the measured and the model temperature compared. The temperature inaccuracy is due to the fact the FC uses a controlled fan for an air forced cooling. The model, however, uses linearised average heat transfer sub-model (i.e r_{cal} is constant in the FC BG model).

4.4 Graphical EDHBG Diagnoser

4.4.1 Introduction

In this section, we apply the proposed diagnosis approach on the same small size experimental HRES. The diagnoser is obtained from the EDHBG model as described in chapter III. Here, the developed procedure is applied on each part of the EDHBG. When assembled together along with the automaton, the EDHBG Diagnoser is build.

4.4.2 Graphical diagnosis models

4.4.2.1 Graphical PV diagnoser

[Fig. 4.31] shows the dualized BGD of the PV panel. Both sensors (voltage and current) of the PV panel are replaced respectively by source of effort **MSe** and flow **MSf**. On the dualizing bonds, the flow sensors ⓕ and the effort sensors ⓔ provide the evaluation of the nominal residual.

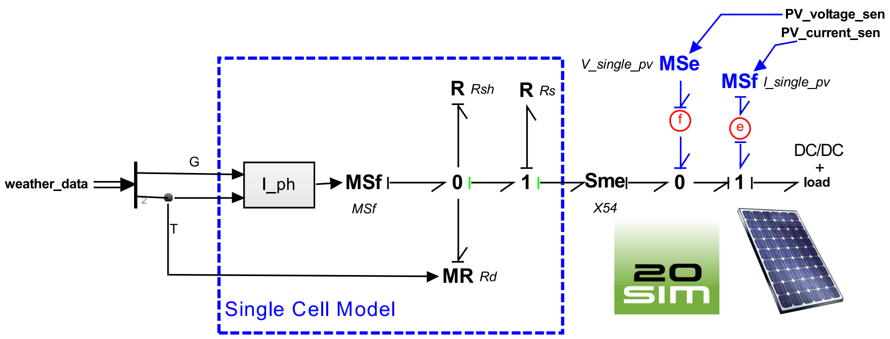

Figure 4.31 – Solar panel BGD

4.4.2.2 Graphical EL & FC diagnoser

In Chapter III, [Fig. 3.14] shows the nominal BGD of the diagnoser. [Fig.3.18] and [Fig.3.17] show the LFT-HBGD of the electrolyser. This allows obtaining the robust residuals with their dynamical thresholds. The FC diagnoser is obtained similarly.

4.4.2.3 Graphical H_2 tank diagnoser

[Fig. 4.32] shows the BGD of the hydrogen tank. The effort detector in the simulation model showed in Fig. 4.11; that represents the pressure sensor in the real system which is replaced with an effort source MSe fed with the measured hydrogen pressure inside of the real process tank. Notice that the $C : ch_2$ flips to derivative causality. A flow detector ⓕ implemented on the bond of the added effort source allows to collect the residual evaluation.

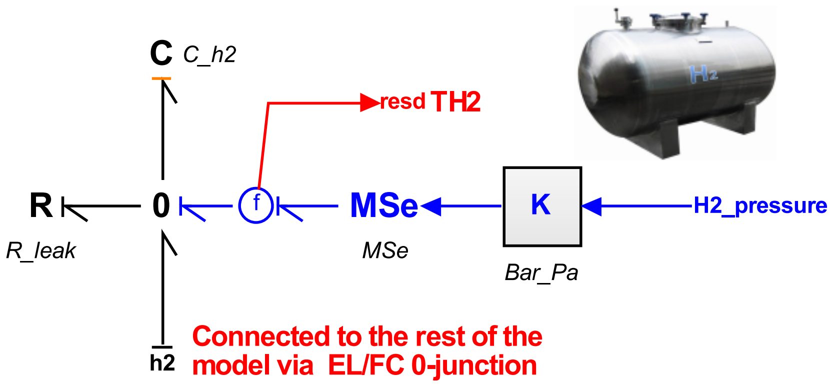

Figure 4.32 – Hydrogen tank BGD

4.4.2.4 WT diagnoser

Actually, the WT has only one current sensor at the output. The rotation speed is estimated and not measured therefore the rotation speed sensor in the model can not be dualized (missing the measured signal).

In [Fig. 4.33], the global HBGD of the system is depicted.

4.5 Operating Mode Management

The automaton depicted in [Fig. 4.34] achieves the OMM, three OM are distinguished.

- OM_1: **Low power** This mode is accessed when the power generated by the renewable sources does not cover the demand. In this case, the batteries are drained at first and then eventually the FC is triggered to use the stored hydrogen as a power back-up and prevent the power shortage.

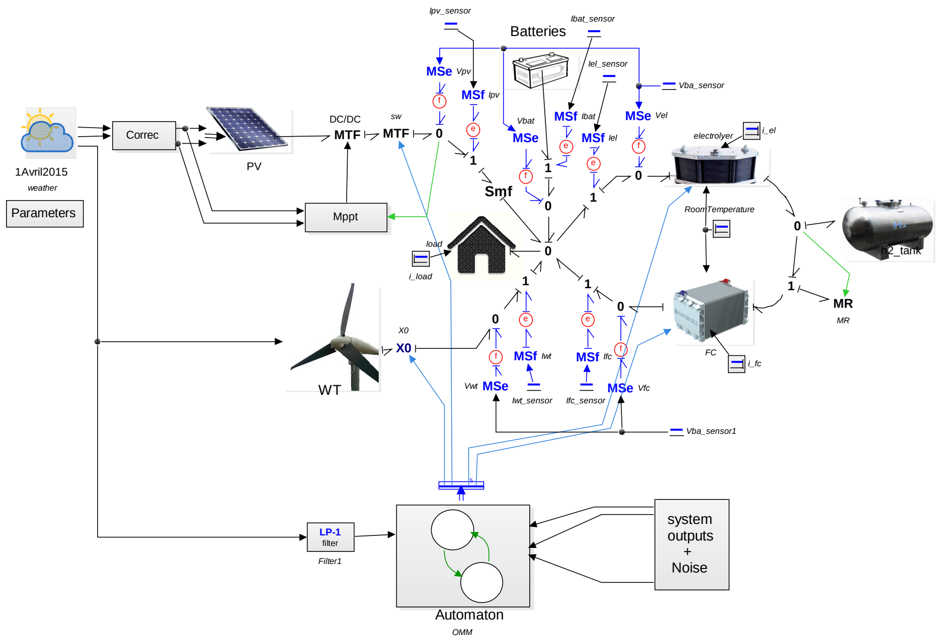

Figure 4.33 – EDHBG Diagnoser of the HRES

- OM_2: **High power** This mode is activated when the power generated by the renewable sources overcomes the required load. The power surplus is then stored as hydrogen using the EL or/and as electricity using the batteries.
- OM_3: **Safe power** This mode is activated when the system fails to provide the required power or when one or more faults occur which make some critical components to be unavailable.

In the present application, the load is considered to be the system self-operating load which is constant (around 100W). To maximise the harvested power, the sources, when active, are always operating following the Mppt algorithm. The condition to access OM_1 is that the generated power by the sources, denoted P_r, is less than 100 W. The system is maintained in this mode until the P_r reaches 200W. To access OM_2, the power P_r must be more than 200W. The system is maintained in OM_2 until the generated power drops to 100W. The safe mode OM_3 is triggered from OM_1 when this latter is no more available due to component failure $\overline{Av}(OM_1)$ or due to power shortage $(P_r < 100W) \wedge (SoC < 30\%) \wedge (P_{H_2} < 1bar)$. From OM_2, OM_3 is activated when the mode is not available due to a fault $\overline{Av}(OM_2)$ or due to the saturation of all the storage units $(P_r > 200W) \wedge (SoC > 95\%) \wedge (P_{H_2} > 10bar)$.

Remark 4.5.1. *For a better explanation, let the Operating Condition (OC) be the domain condition associated to each mode or version, the system stays in the associated* *configuration as long as this condition is maintained true. It worth to note that the OC represents the opposite of the exit conditions from the concerned domain.*

The missions associated to each mode and the different versions that allow achieving each mission are listed below according to the priority order, where for each version a list of the needed hardware resources and the OC are showed.

$$a_{wt1} = (v_w < 20m/s) \wedge (Av(V^1_{M11}))$$
$$d_{wt1} = (v_w > 22m/s) \vee (\overline{Av}(V^1_{M11}))$$
$$a_{fc} = (Soc < 30\%) \wedge (Av(V^2_{M21}))$$
$$d_{fc} = (Soc > 80\%) \vee (\overline{Av}(V^2_{M21}))$$
$$a_{wt2} = (v_w < 20m/s) \wedge (P_r < 200W) \wedge (Av(V^1_{M11}))$$
$$d_{wt2} = (v_w > 22m/s) \vee (P_r > 450W) \vee (\overline{Av}(V^1_{M11}))$$
$$d_{EL} = (p_{h_2} > 10bar) \vee (Pr < 200W) \vee (\overline{Av}(V^2_{M22}))$$
$$a_{EL} = (p_{h_2} < 9bar) \wedge (Pr > 300W) \wedge (Av(V^2_{M22}))$$
$$as_{OM_1} = \overline{Av}(OM_1) \vee (P_r < 100W) \wedge (SoC < 30\%) \wedge (P_{H_2} < 1bars)$$
$$as_{OM_2} = \overline{Av}(OM_2) \vee (P_r > 200W) \wedge (SoC > 95\%) \wedge (P_{H_2} > 10bar)$$

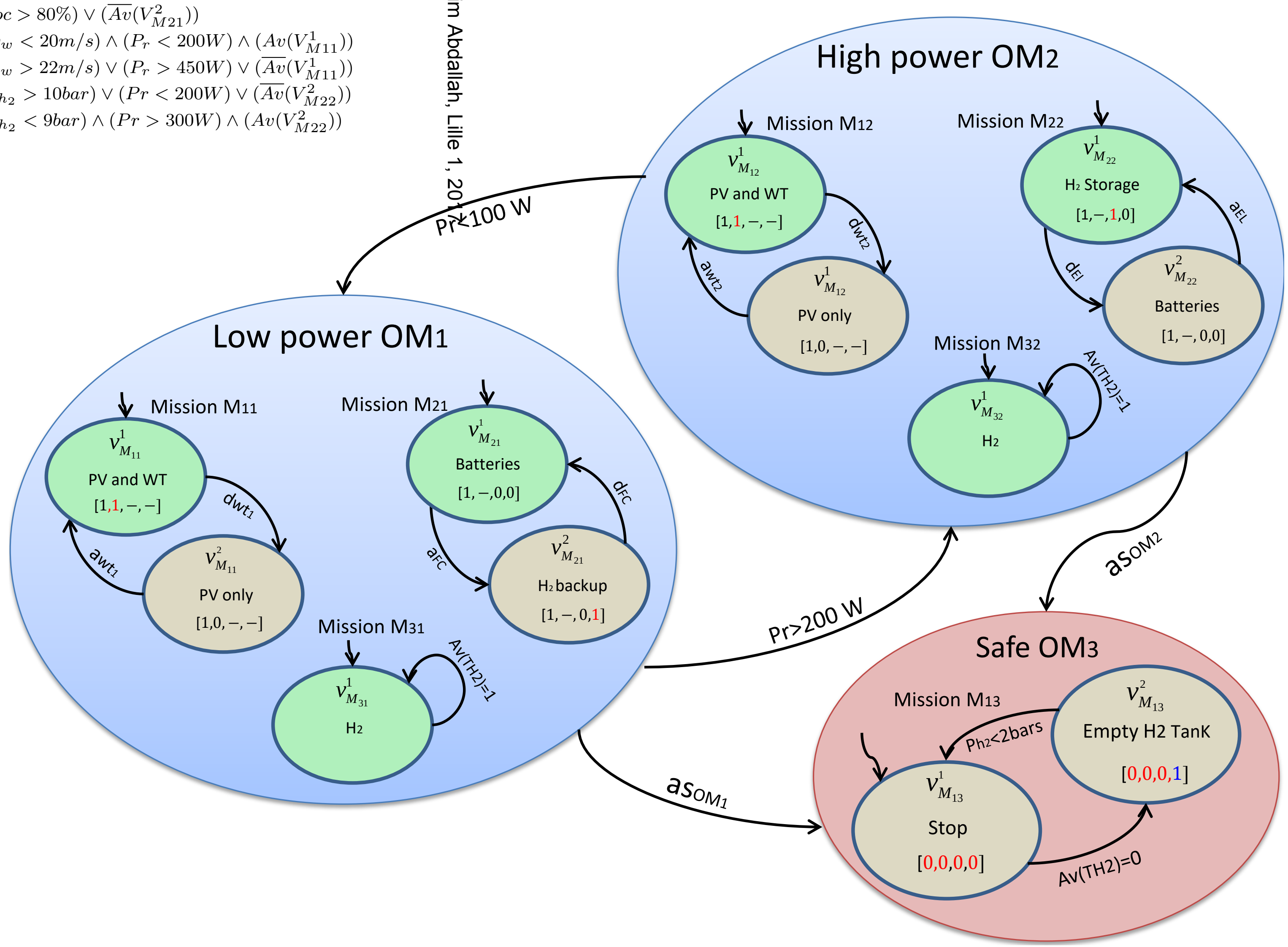

Figure 4.34 – The automaton OMM

- OM_1**: Low power** This OM is associated with 3 missions to be fulfilled:
  - **mission M_{11}: Harvest power**
    There exist three versions to achieve this mission, listed in operational priority:
    - $V^1_{M11} = \{WT, PV\}$
      OC: $(v_w < 22m/s) \wedge Av(WT)$ where:
      v_w is the wind speed
      $Av(WT)$ is the operational availability of the WT.
      This means that, by default, both sources are used unless in case of high wind speed or fault detection related to the WT.
    - $V^2_{M11} = \{PV\}$
      OC: $(v_w > 20m/s) \vee (\overline{Av}(WT))$
      The PV is considered as the primary source which is not to be disconnected. The system recovers from this single source mode if the wind speed is within the WT operating range and this latter is not marked faulty.
  - **mission M_{21}: Use stored power**
    There exist three versions to achieve this mission, listed in operational priority:
    - $V^1_{M21} = \{Batteries\}$
      OC: $(SoC > 30\%) \wedge Av(Batteries)$ where:
      SoC is the batteries state of charge
      $Av(Batteries)$ is the operational availability of the batteries.
      This version uses only the batteries as backup storage, it is chosen by default. The system stays using it as long as the batteries are not drained out to less than 30% and the batteries are not detected faulty.
    - $V^2_{M21} = \{Batteries, FC\}$
      OC: $(SoC < 80\%) \wedge (P_{H_2} > 1bar) \wedge Av(FC) \wedge Av(Batteries)$ where:
      P_{H_2} is the stored hydrogen pressure
      $Av(FC)$ is the FC operational availability.
      This version uses both the FC and the batteries to supply power, it maintains operational the time needed to recharge the batteries up to 80% and as long as there is enough hydrogen and both the FC and the batteries are healthy.

- **mission M_{31}: Secure H_2**

  There is only one version to achieve this mission:

  * $V^1_{M31} = \{H_2Tank\}$
    OC: $Av(TH_2)$ where:
    $Av(TH_2)$ is the operational availability of the hydrogen tank.
    This version is achievable as long as the tank is healthy.

- OM_2: **High power** This OM is associated with 3 missions to be fulfilled:

  - **mission M_{12}: Harvest power**

    There exist three versions to achieve this mission, listed in operational priority:

    * $V^1_{M12} = \{WT, PV\}$
      OC: $(v_w < 22m/s) \wedge (P_r < 450W) \wedge Av(WT)$ where:
      $P_r = 450W$ is the power limit of the different component.
      As before, this version uses both sources, it is activated by default and is maintained operational as long as the wind are not very high ($v_w < 22m/s$), the WT is healthy and the generated power is less the maximum power limits of the system components (450W).
    * $V^2_{M12} = \{PV\}$
      OC: $(v_w > 20m/s) \vee (P_r > 200W) \vee (\overline{Av}(WT))$
      This version uses only the PV as a source, it is set active as long as the wind speed or the generated power are relatively high ($v_w > 20m/s$, $P_r > 200W$) or as long as the WT is faulty.

  - **mission M_{22}: Store the surplus power**

    There exist three versions to achieve this mission, listed in operational priority:

    * $V^1_{M22} = \{Batteries, EL\}$
      OC: $(P_{H_2} < 10bar) \wedge Av(Batteries) \wedge Av(EL)$ where:
      $Av(EL)$ is the operational availability of the EL.
      By default, this version uses both the batteries and the EL to store power, it is maintained active as long as the hydrogen pressure in the tank is less than the max capacity 10 bar and as long as both the batteries and the EL are healthy.
    * $V^2_{M22} = \{Batteries\}$
      OC: $(SoC < 80\%) \wedge Av(Batteries)$

This version uses only the batteries as storage solution. It is maintained active as long as the batteries are not full and there not faulty.

– **mission M_{31}: Secure H_2**

There is only one version to achieve this mission:

∗ $V^1_{M31} = \{H_2Tank\}$
OC: $Av(TH_2)$ where:
$Av(TH_2)$ is the operational availability of the hydrogen tank.
This version is achievable as long as the tank is healthy.

• OM_3: **Safe mode** It constitutes one mission of securing the system which is achievable through two versions

– **mission M_{13}: Secure the system**

∗ $V^1_{M31} = \{\Phi\}$
All the components are stopped.

∗ $V^2_{M31} = \{FC\}$
OC: $Av(FC)$ where, in case of hydrogen leak, the FC is started in order to consume and evacuate the hydrogen in the tank.

As shown in [Fig. 4.34], in each of the Lower power OM_1 and High power OM_2 there is three sub-automaton evolving in parallel. Each sub-automata is set to achieve one mission related to the concerned OM. The automaton generates the vector β_i which control the switching state of the different components. The general form of the vector is $\beta_i = [X_{PV}, X_{WT}, X_{EL}, X_{FC}]$. In OM_1 and OM_2 when the two missions M_{1i}, M_{2i}, are executed in parallel, they define, each, a part of β_i as shown in [Fig. 4.34].

Suppose for example, the mission M_{11} of OM_1 is been fulfilled according to the version $V^1_{M_{11}}$ and simultaneously the required mission M_{21} is been fulfilled according to the version $V^1_{M_{21}}$. The generated vector is, then:

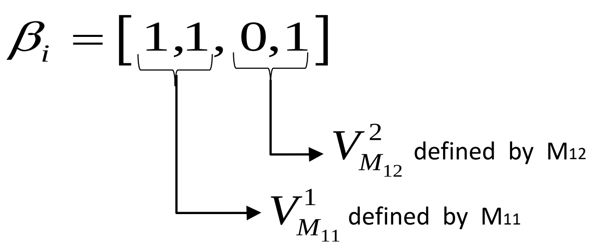

4.6 Results

The availability of the hardware resources, used in each version, for each mission and then for each mode are evaluated as showed in chapter 3. In this part, we represent multiple scenarios, the first consists of normal operation, the others consider faulty situations (hydrogen leak and faulty EL conditions).

4.6.1 Scenario 1: Normal faultless behaviour

[Fig. 4.35], [Fig. 4.36], [Fig. 4.37] and [Fig. 4.38] illustrate the normal faultless behaviour of the system. The simulation uses 24 hours weather data of a sunny, average winds day[1]. The batteries are initially charged at 32% and the hydrogen pressure is about 93% of the maximum capacity of the tank.

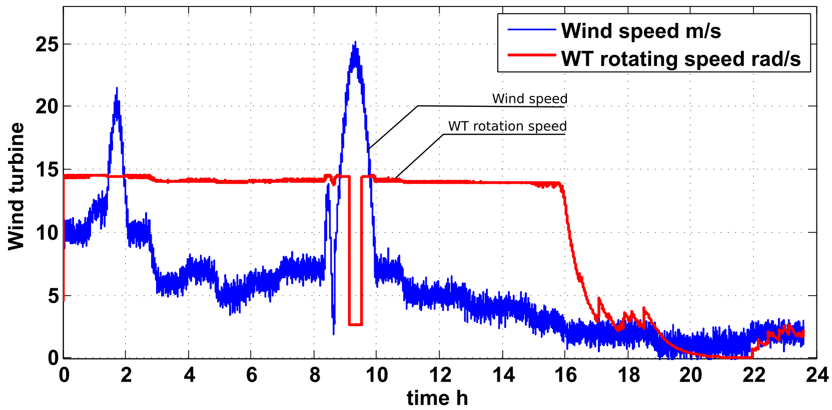

Figure 4.35 – Wind speed and WT rotation speed.

[Fig. 4.35] shows the wind speed and the WT rotation speed. [Fig. 4.36] shows the WT output power which increases in high wind conditions. Following the versions associated to the mission M_{11} (resp. M_{12}) of the OMM, the WT, as expected, brakes when the wind speed exceed the operation limit 22m/s i.e between t=[9:05; 9:30]h. [Fig. 4.36] adds to the WT generated power, the power generated by the PV which follows a sunshine cycle in a cloudless day. The sum of these two generated powers is also showed in the figure.

Between t=[00:00h] and t=[11:45h], the sum of both wind and the solar powers P_r were more than enough to satisfy the load $P_r > 200W$. The system starts then in OM_2: High power. The surplus is stored as hydrogen and electricity using both the EL and

[1]data of: 1, April, 2015

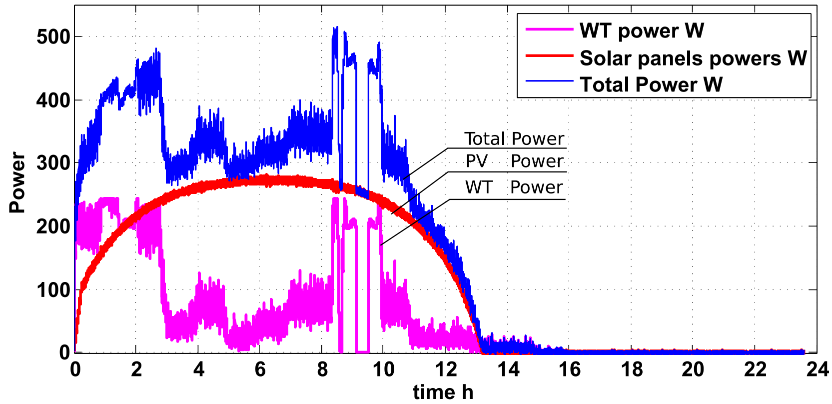

Figure 4.36 – The generated powers

the batteries according to the default version of the power storage mission $M_{22} : V^1_{M22}$. The EL is normally allowed to be maintained active as long as the hydrogen pressure in the tank is less than the maximum limit 10bar (see [Fig. 4.37] and [Fig. 4.38]).

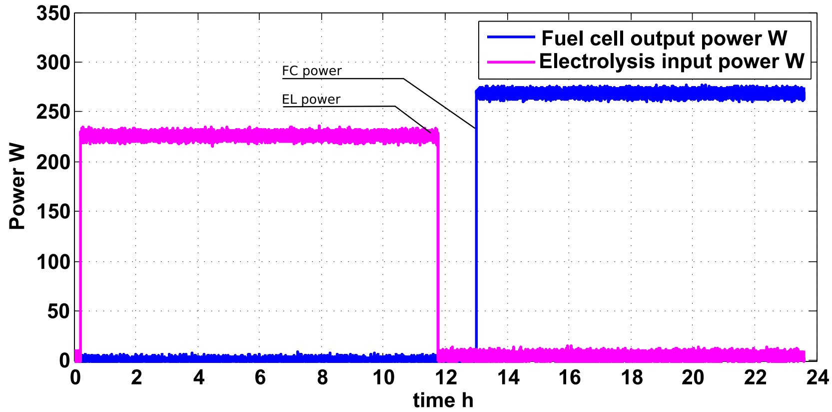

Figure 4.37 – The Hydrogen in and out power

Between t=[11:45]h and t=[13:02h], the generated power of the sources drops but still more than the load demand $100W < P_r < 200W$. The system still operating in OM_2, the activation condition d_{EL} is then satisfied, as a result, the EL is deactivated and only the batteries are used to store power according to V^2_{M22}.

Following the OMM, when the generated power is not enough to cover the load, the system switches to the Low power OM_1 where the batteries are used at first to cover the load power, then when the SoC of the batteries becomes very low, the FC is activated to back up the system. **After t=[13:02h]**, the generated power of the sources drops to less than load required power $P_r < 100W$. As a consequence, the system switches to Low power: OM_1. Because of the low SoC of the batteries $SoC < 30\%$, the system

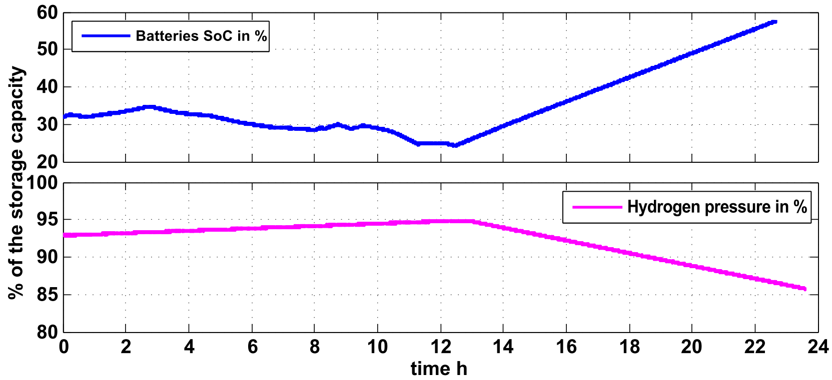

Figure 4.38 – The storage states

switches directly from the default version V^1_{M21} (only batteries) to V^2_{M21} where the FC is activated to back up the sources and the batteries. [Fig. 4.37] and [Fig. 4.38] shows respectively the FC power (260W) and the hydrogen pressure drops due to the FC consumption. The SoC of the batteries rises as the most of the FC power is used to recharge the batteries.

Fig. 4.39 gives the sequence of the activated OM, the missions, the consulted versions, the triggering events and the switching vector β_i for each case.

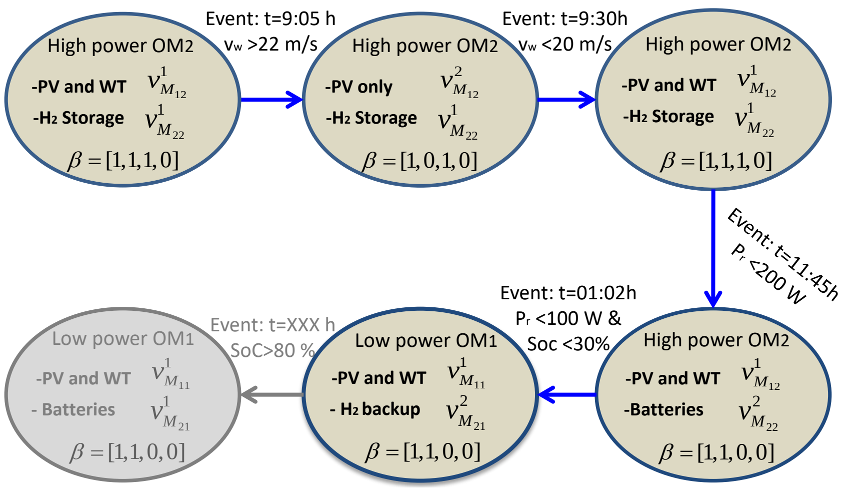

Figure 4.39 – The simulation normal sequence of events and OM trajectory

4.6.2 Scenario 2: Leak in the Hydrogen tank

In addition to the same simulation conditions of scenario 1 in this scenario, we consider a leak in the hydrogen tank between t=[10:30; 12:30]h. The system, as before, starts in OM_2, missions M_{12}, M_{22} are fulfilled according the versions $V^1_{M_{12}}$, $V^1_{M_{22}}$ respectively.

[Fig. 4.40] shows the hydrogen tank residual output of the graphical diagnoser. In the absence of the leak between t=[00:00; 10:30]h, the residual obtained by the diagnoser is contained within the thresholds. The system follows the same expected behaviour as in the normal faultless scenario 1. [Fig. 4.41], [Fig. 4.42], [Fig. 4.43] and [Fig. 4.44] illustrate the normal behaviour before the leak. When the leak occurs at t=[10:30; 12:30]h, the residual overpasses the thresholds indicating the leak detection.

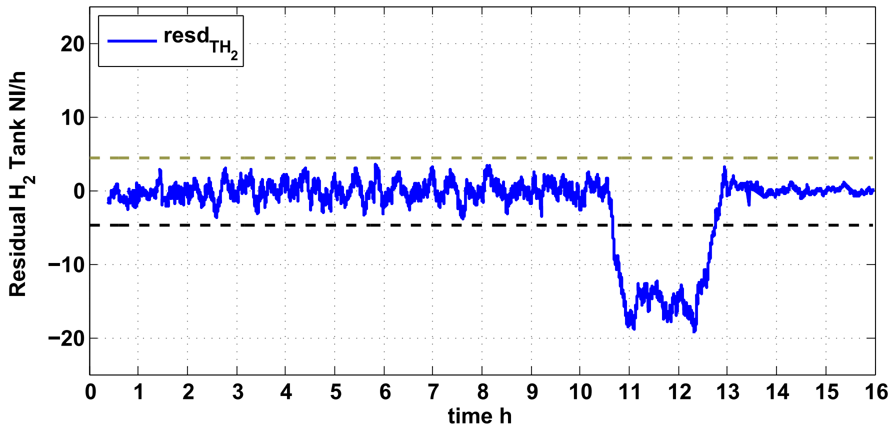

Figure 4.40 – Hydrogen tank residual, a leak scenario between [10:30 12:30]h

When the detection occurs at t=[10:30]h the hydrogen tank is marked as unavailable, consequently the unique version of the mission: secure the hydrogen (M_{31} for OM_1) and (M_{32} for OM_2) become unavailable. Consequently, OM_1 and OM_2 become unaccessible. According to the OMM, the system must switch to the safe mode OM_3, more precisely to version $V^2_{M_{13}}$.

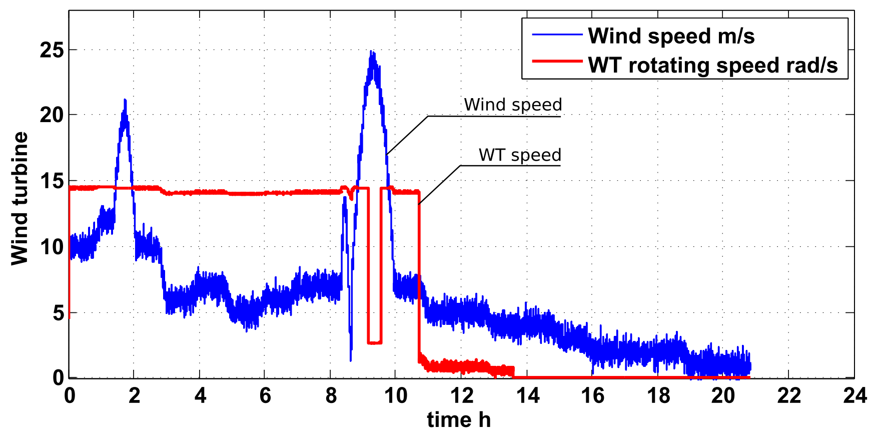

Figure 4.41 – The Wind speed and the WT rotation speed

As shown in the faultless scenario 1, in normal case, the wind turbine would be maintained operational until it stops at t=[16:00]h due to insufficient wind speed

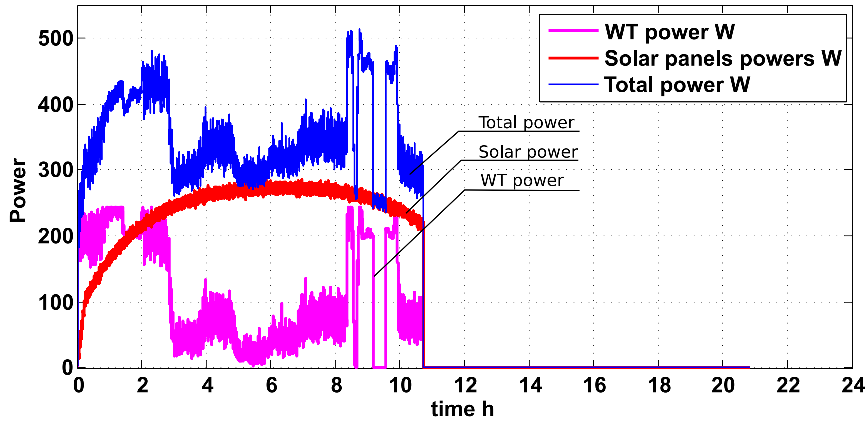

Figure 4.42 – PV, WT and total powers

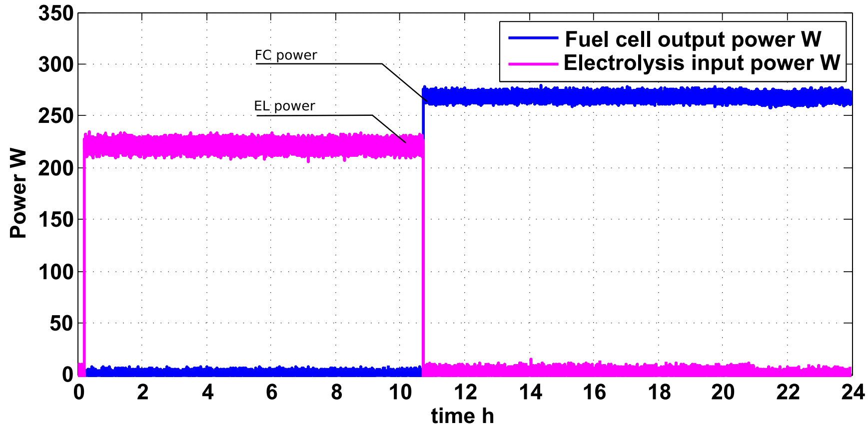

Figure 4.43 – The Hydrogen storage units powers

$v_w < 3m/s$. Although, [Fig. 4.41] and [Fig. 4.42] shows, at t≃[10:30]h when the H_2 leak occurs and detected both sources are stopped, and their output powers are zero. [Fig. 4.43] illustrates the generated and consumed powers of both the FC and EL. It shows that the EL is also shut-down after the detection, while the FC is activated, at the same time, in order to reduce the hydrogen pressure according to the OMM. [Fig. 4.44], illustrating the hydrogen storage and the battery SoC, shows the hydrogen pressure drops after the FC is activated.

[Fig. 4.45] shows the sequence of the active OM, the occurring events and transitions superposed on the previous faultless ones. Because the Safe OM is a blocking mode, after the detection the systems maintains in this mode until a user intervention to reset the OMM is performed.

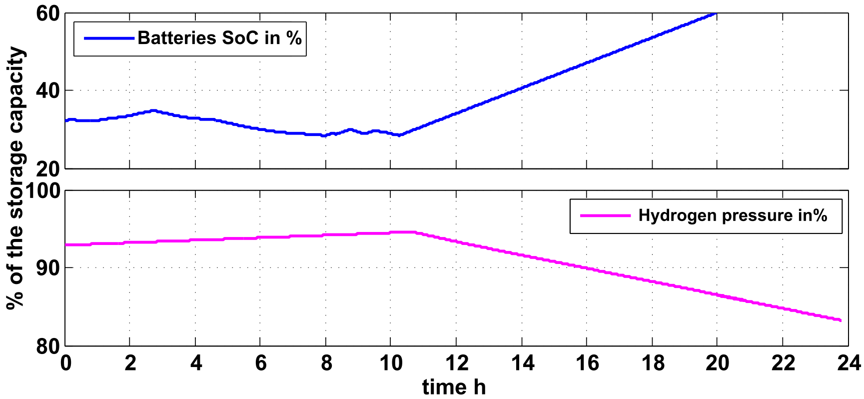

Figure 4.44 – The storage state: SoC batteries and hydrogen pressure

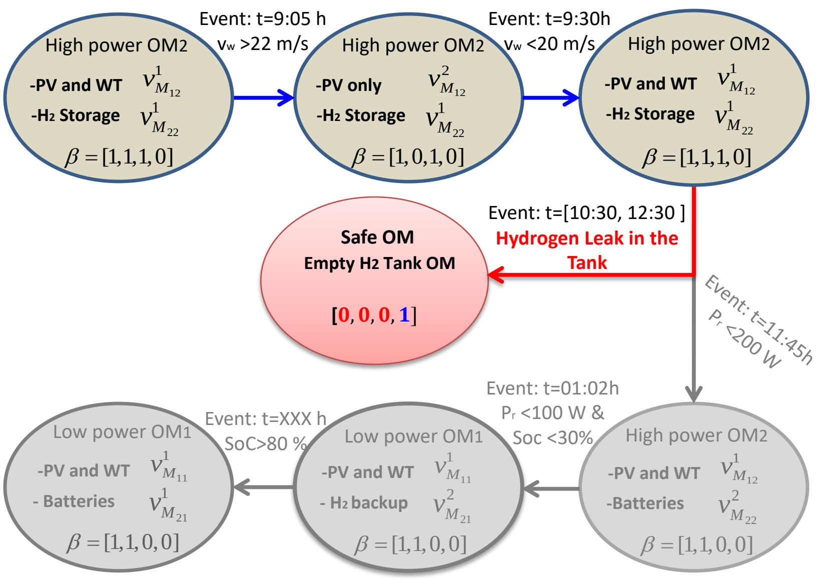

Figure 4.45 – The simulation sequence of events and transitions

4.6.3 Scenario 3: Electrolyser under undesirable conditions

In this scenario, we consider an unexpected increase in the ohmic resistance of the EL PEM membrane. This can be due to an insufficient water supply to the EL i.e water starvation [160]. [Fig. 4.46a] shows the electrolyser residuals with their dynamical thresholds in healthy case. The residuals are maintained between the thresholds.

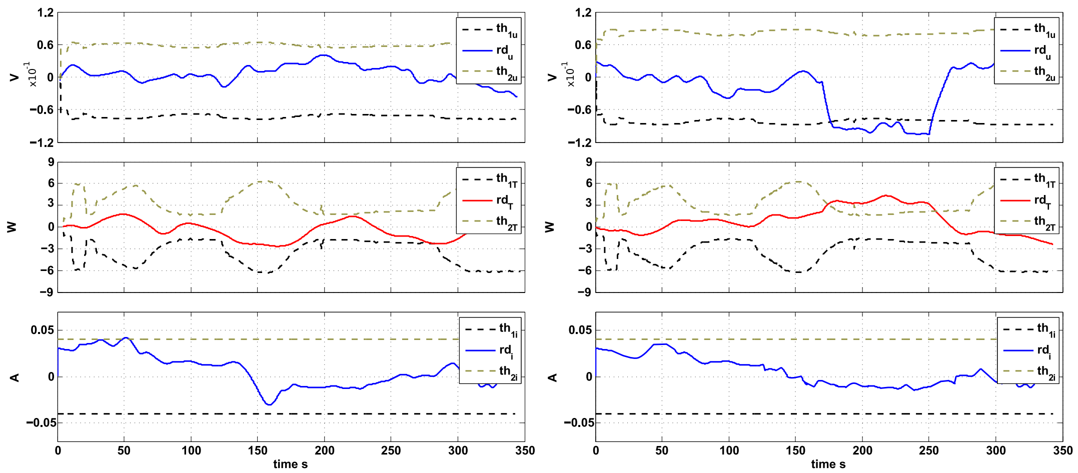

(a) Normal case (b) Membrane drying between [175-250]s

Figure 4.46 – The electrolyser HBGD residuals

Independently from the OMM for the moment, in case of membrane drying i.e water starvation between t=[175;250]s, [Fig. 4.46b] shows the residual detection. Both of the thermal and the voltage residuals are affected and overpass their thresholds. This comes in convenience with the FSM. The first residual marks an increase in the operating voltage due to the resistance increase. The second residual indicates the increase in the consumed power (the sign of the residual reflects the variations according to the half arrows direction in the diagnoser).

Remark 4.6.1. *In case of the detection within the OMM, the detection will take place just for slight moment before the system switches off the EL.*

In the next simulation, we consider the fault in the EL occurs at t=[8:20]h in the OMM context showed by [Fig. 4.34]. The system, as before, starts in OM_2, missions M_{12}, M_{22} are fulfilled according to the versions $V^1_{M_{12}}, V^1_{M_{22}}$ respectively. In the absence of the EL fault between t=[00:00; 8:20]h, the system follows the same expected behaviour as in normal faultless scenario 1. [Fig. 4.47], [Fig. 4.48], [Fig. 4.49] and [Fig. 4.50] illustrate a normal behaviour before the fault detection.

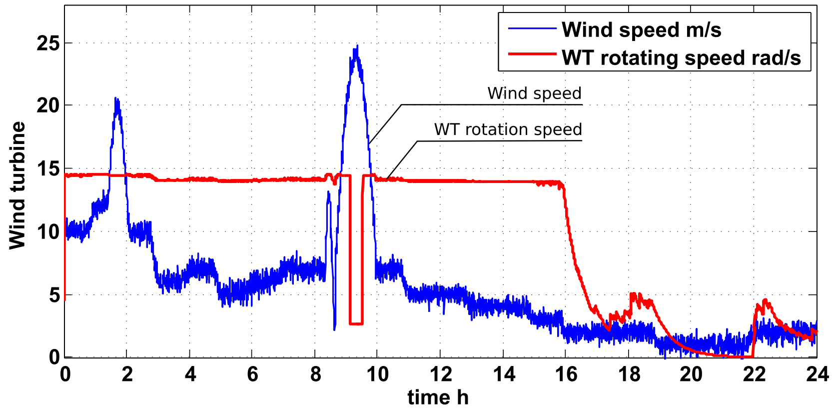

Figure 4.47 – The Wind speed and the WT rotation speed

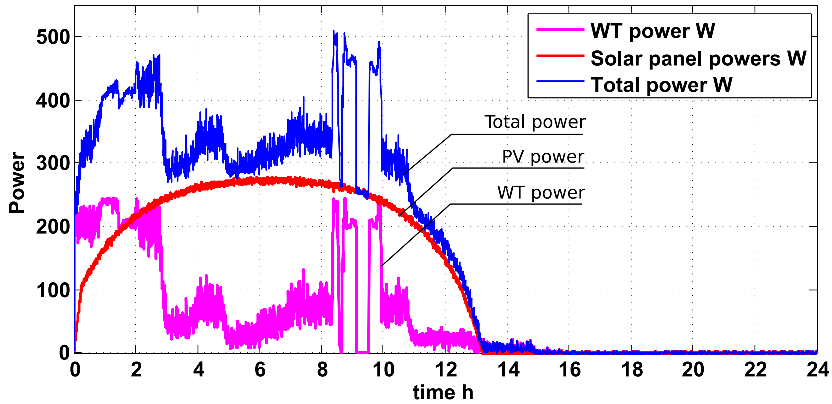

Figure 4.48 – PV, WT and total powers

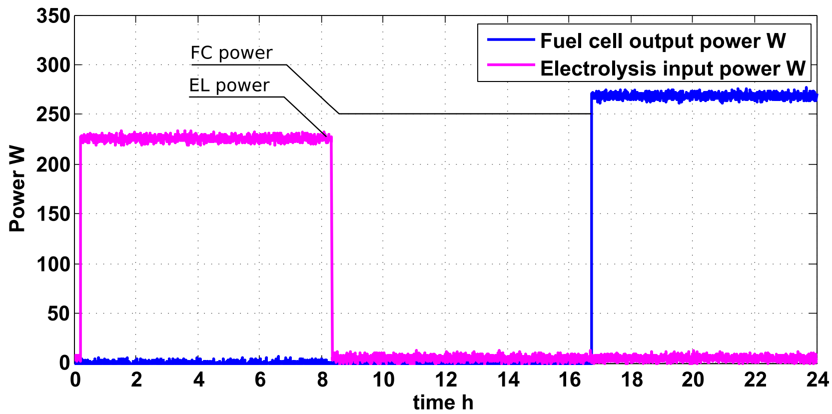

Figure 4.49 – The Hydrogen storage units powers

Since the mission M_{12} (harvest power) does not dependent on the EL health state, after the detection at t=[8:20]h, [Fig. 4.47] and [Fig. 4.48] show that the source behaviours are not affected by the fault.

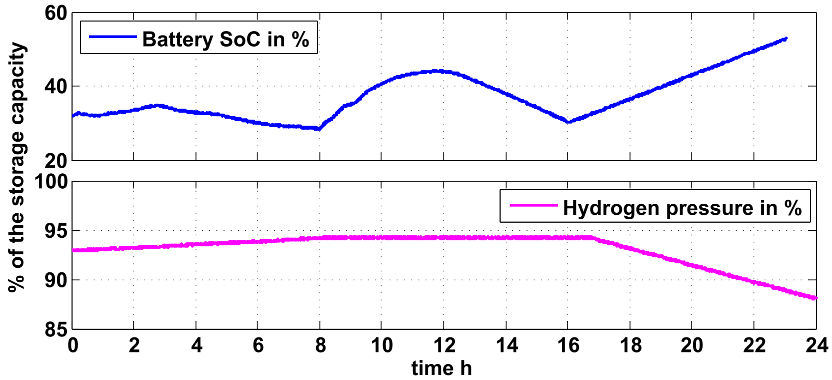

Figure 4.50 – The storage state: SoC batteries and hydrogen pressure

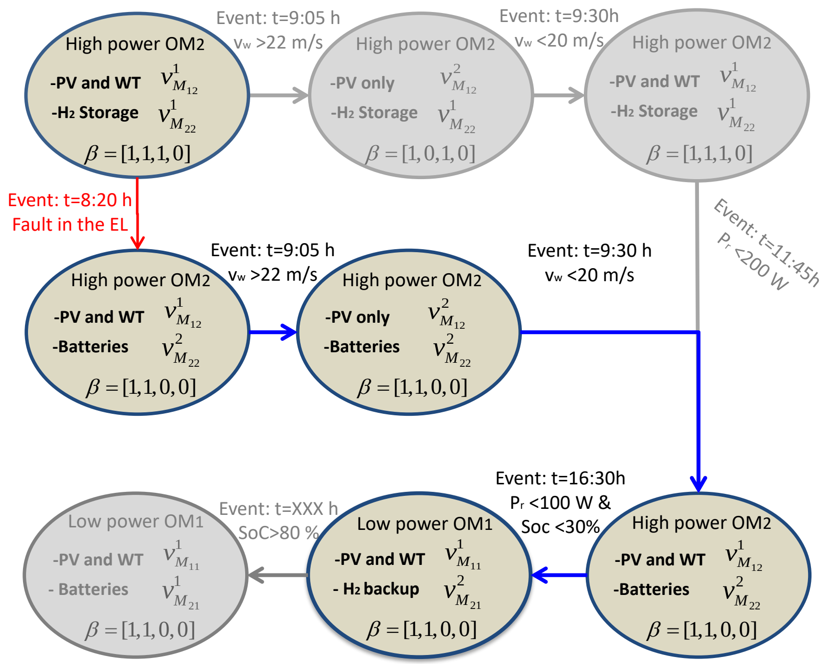

Figure 4.51 – The simulation sequence of events and transitions

In faultless conditions, between t=[8:20; 11:45]h, the system would be still operating in OM_2 according to $V^1_{M_{22}}$ where the EL and the batteries are used to store power. Instead, in this scenario, after the detection $V^1_{M_{22}}$ becomes unavailable, the system switches to $V^2_{M_{22}}$ where the batteries are used as single storage unit. [Fig. 4.49] shows that the EL is set off at t=[8:20]h, [Fig. 4.50] shows the hydrogen pressure stabilized after the detection and the battery SoC increases. At t=[01:02]h, the system enters the Low power OM_1 after the generated power becomes low $P_r < 100W$. Between t=[01:02; 16:30]h M_{11} and M_{21} are achieved according to versions $V^1_{M_{11}}$ and $V^1_{M_{21}}$ respectively. Thus, the batteries are still the only storage unit in use.

At t=[16:30]h, the batteries SoC drops to less than 30%, this triggers the FC to back up the system according to $V^2_{M_{21}}$. [Fig. 4.49] shows the FC initiates at t=[16:30]h where the hydrogen pressure starts decreasing (see [Fig. 4.50]).

[Fig. 4.51] shows the new sequence of the active OM, the occurring events and transitions superposed on the expected faultless ones.

4.7 Conclusion

As the results show, the proposed approach offering a valuable asset in modelling and diagnosing the HRES. It yields a graphical diagnoser simply issued from the simulation model. The global graphical model along with the implicit consideration of all the switching dynamics and the parameters uncertainties, achieves the FDI independently from the OM. The integrated automaton handles the OMM while synchronizing both of the diagnoser and the process. In the light of the diagnosis results, the EDHBG allows achieving the OMM. In addition to the power management, the OMM is based on both the operational and the functional availabilities of the components allowing to exploit many mode management strategies such as the system reconfiguration, safety measures, optimal operating conditions and fault tolerant operating strategies. This offers a more secure and reliable HRES.

Chapter 5

General Conclusion

5.1 Summary and outcome of the thesis

In the context of the engagement against the climate change and the pollution, HRES for the green hydrogen production constitute a strategic asset to win the trade between the energy dependency and the environmental restrictions. The stored hydrogen represents a very precious energy carrier. It can play a double role as large-scale long-term power storage and/ or as green emission-less fuel replacing the fossil fuel. Due to the countless different components and the different configurations that can be used in the HRES, many designs and system architectures are possible. These are chosen and designed according to the user objectives, the user budget, the geographical location of the system, etc. In this context, modelling the HRES is very crucial task that allows to decide the optimal configuration, the type and the size of the different components, and more specially to test the long-term reliability of such system. Other tasks are based on the model such as the continuous control, the prediction, the model-based diagnosis, etc.

By consulting the state of art of the published works related to the HRES, it was obvious the need for a clear dynamical modelling approach that allows the multidisciplinary modelling, and covers the dynamical switching behaviour along with the need to test various OMM. From theoretical point of view, the method must be flexible with the model-based tasks without the need to consult or change the modelling representation. At the end of the first chapter, the HBG was found as the best potential candidate to replace the equation-based modelling methodologies. Beside the great suitability to represent the multidisciplinary and the global dynamic of the HRES, HBG was found unable to express the behaviour of the discrete state associated to the selected OM. This problematic is solved in the second chapter where a simple state-machine (automaton) is defined and integrated to the HBG. It allows a simple easy definition of the OMM independent from the description of the dynamical model. Moreover, some specific characteristics of some HRES components were not included in the BG methodology such as the non-linear dissipative coupled phenomena, the cellular structures of the PV, FC, EL, battery. In the second chapter, the classical BG theory is also adapted to respond to these modelling criteria.

By the end of chapter II, the proposed BG model represents a good solution for the modelling and simulating multidisciplinary switching dynamical systems, specially the HRES. Yet, on the other hand, the developed approach still suffers from the inability to achieve the model-based tasks. As these are normally achievable through the equation-based models, those later are still advantageous. For instance, to achieve a robust model-based diagnosis using the BG the user classically was supposed to recover the analytical equation of the model. This inconsistency between the modelling approach and the model-based diagnosis is solved in the chapter III. The state of art shows an absence of the diagnosis for the HRES as whole system, this applies also on the reconfiguration and the protection measures ignored in the OMM. Chapter III develops the techniques allowing, based on the proposed approach, to implement an on-line diagnoser. It explains also how to integrate the diagnosis outputs in the OMM to perform protection-based or fault-tolerant reconfiguration strategies. The proposed methods are applied in chapter IV on a small-size experimental set-up. The results are shown for two scenario-cases: The first considers normal OMM without fault using the proposed modelling technique. The second considers OMM that includes the reconfiguration based on the online diagnosis where two faulty scenarios are animated. Chapter IV includes also the details of the EDHBG modelling of the PV/WT/battery/EL/FC HRES. It shows also the derivation and the synthesis of the global diagnoser model.

The obtained results demonstrate the strength of the proposed approach not just as a unified modelling approach that covers all the concerned physical domains and the OM but also as unified multi-task approach that allows the OMM and the online robust diagnosis implementations.

5.2 Perspective

- **HRES-specific perspectives**
  - **Model-prediction-based OMM:** Nowadays, predicted weather data are widely available. They can be used along with the model to forecast and optimise the component status used to define more reliable OMM.
  - **Model-based graphical prognosis:** In addition, since most of the HRES suffers from degradations, it is possible to extend the graphical proposed approach used for the diagnosis to perform a health prognosis. Until now, these kinds of studies are done analytically by using the obtained results of the equation-based diagnosis through estimating the component parametric variation.

- **General perspectives**
  - **Graphical global system representation:** These results can enable a new interpretation of the graphical modelling as a powerful alternative user-friendly paradigm to model the concerned systems. Similar to the analytical approaches, it guarantees performing many other tasks more simply and effectively.
  - **Toward an automatic modelling and diagnosis:** Recent interesting industrial works are in progress suggesting the automatic derivation of the BG model from the CAD drawing. Part of the thesis constitute the bridge permitting the following extraction of the model-based diagnoser. This allows a full automation of the two tasks.

Bibliography

[1] Eurostat Statistic Explained. *Air pollution by industries and households.* 2016.

[2] http://www.deule-climat.net/2014.htm.

[3] Pierre Hollmuller et al. "Evaluation of a 5 kW p photovoltaic hydrogen production and storage installation for a residential home in Switzerland". In: *International Journal of Hydrogen Energy* 25.2 (2000), pp. 97–109.

[4] Jeremy Lagorse, Damien Paire, and Abdellatif Miraoui. "Sizing optimization of a stand-alone street lighting system powered by a hybrid system using fuel cell, PV and battery". In: *Renewable Energy* 34.3 (2009), pp. 683–691.

[5] Agata Godula-Jopek, Walter Jehle, and Jörg Wellnitz. *Hydrogen storage technologies: new materials, transport, and infrastructure.* John Wiley & Sons, 2012.

[6] A Yilanci, I Dincer, and HK Ozturk. "Performance analysis of a PEM fuel cell unit in a solar–hydrogen system". In: *International Journal of Hydrogen Energy* 33.24 (2008), pp. 7538–7552.

[7] M.H. Nehrir et al. "A Review of Hybrid Renewable Alternative Energy Systems for Electric Power Generation: Configurations, Control, and Applications". In: *Sustainable Energy, IEEE Transactions on* 2.4 (Oct. 2011), pp. 392–403. ISSN: 1949-3029.

[8] Prabodh Bajpai and Vaishalee Dash. "Hybrid renewable energy systems for power generation in stand-alone applications: a review". In: *Renewable and Sustainable Energy Reviews* 16.5 (2012), pp. 2926–2939.

[9] V. Tamrakar, S. C. Gupta, and Y. Sawle. "Study of characteristics of single and double diode electrical equivalent circuit models of solar PV module". In: *2015 International Conference on Energy Systems and Applications.* Oct. 2015, pp. 312–317.

[10] M. G. Villalva, J. R. Gazoli, and E. R. Filho. "Comprehensive Approach to Modeling and Simulation of Photovoltaic Arrays". In: *IEEE Transactions on Power Electronics* 24.5 (May 2009), pp. 1198–1208. ISSN: 0885-8993.

[11] Chihchiang Hua and Chihming Shen. "Study of maximum power tracking techniques and control of DC-DC converters for photovoltaic power system". In: *Power Electronics Specialists Conference, 1998. PESC 98 Record. 29th Annual IEEE.* Vol. 1. May 1998, 86–93 vol.1.

[12] M. Dahmane, J. Bosche, and A. El-Hajjaji. “Power management strategy for renewable hybrid stand-alone power system”. In: *2015 4th International Conference on Systems and Control (ICSC)*. Apr. 2015, pp. 247–254.

[13] O.C. Onar, M. Uzunoglu, and M.S. Alam. “Dynamic modeling, design and simulation of a wind fuel cell ultra-capacitor-based hybrid power generation system”. In: *Journal of Power Sources* 161.1 (2006), pp. 707–722. ISSN: 0378-7753.

[14] Pragya Nema, R.K. Nema, and Saroj Rangnekar. “A current and future state of art development of hybrid energy system using wind and PV-solar: A review”. In: *Renewable and Sustainable Energy Reviews* 13.8 (2009), pp. 2096–2103. ISSN: 1364-0321.

[15] K.W.E. Cheng et al. “Review of the wind energy generating system”. In: *Advances in Power System Control, Operation and Management (APSCOM 2009), 8th International Conference on*. Nov. 2009, pp. 1–7.

[16] S. Muller, M. Deicke, and R.W. De Doncker. “Doubly fed induction generator systems for wind turbines”. In: *Industry Applications Magazine, IEEE* 8.3 (May 2002), pp. 26–33. ISSN: 1077-2618.

[17] D. Das et al. “An optimal design of a grid connected hybrid wind photovoltaic fuel cell system for distributed energy production”. In: *Industrial Electronics Society, 2005. IECON 2005. 31st Annual Conference of IEEE*. Nov. 2005.

[18] M.A. Abdullah et al. “A review of maximum power point tracking algorithms for wind energy systems”. In: *Renewable and Sustainable Energy Reviews* 16.5 (2012), pp. 3220–3227. ISSN: 1364-0321.

[19] A.M. Bhandare, P.J. Bandekar, and S.S. Mane. “Wind energy maximum power extraction algorithms: A review”. In: *Energy Efficient Technologies for Sustainability (ICEETS), 2013 International Conference on*. Apr. 2013, pp. 495–500.

[20] Marcelo Carmo et al. “A comprehensive review on PEM water electrolysis”. In: *International journal of hydrogen energy* 38.12 (2013), pp. 4901–4934.

[21] Loc Nguyen Khanh et al. “Power-Management Strategies for a Grid-Connected PV-FC Hybrid System”. In: *Power Delivery, IEEE Transactions on* 25.3 (July 2010), pp. 1874–1882. ISSN: 0885-8977.

[22] A Yilanci, I Dincer, and HK Ozturk. “A review on solar-hydrogen/fuel cell hybrid energy systems for stationary applications”. In: *Progress in Energy and Combustion Science* 35.3 (2009), pp. 231–244.

[23] Di Lu et al. “Design of a power management system for an active PV station including various storage technologies”. In: *Power Electronics and Motion Control Conference, 2008. EPE-PEMC 2008. 13th*. Sept. 2008, pp. 2142–2149.

[24] G. Zini and P. Tartarini. “Hybrid systems for solar hydrogen: A selection of case-studies”. In: *Applied Thermal Engineering* 29.13 (2009), pp. 2585–2595. ISSN: 1359-4311.

[25] Tao Zhou et al. "Modeling and Control Design of Hydrogen Production Process by Using a Causal Ordering Graph for Wind Energy Conversion System". In: *Industrial Electronics, 2007. ISIE 2007. IEEE International Symposium on*. June 2007, pp. 3192–3197.

[26] R Logesh et al. "Resources, configurations, and soft computing techniques for power management and control of PV/wind hybrid system". In: *Renewable and Sustainable Energy Reviews* 69 (2017), pp. 129–143.

[27] P. Garcia et al. "ANFIS-Based Control of a Grid-Connected Hybrid System Integrating Renewable Energies, Hydrogen and Batteries". In: *Industrial Informatics, IEEE Transactions on* 10.2 (May 2014), pp. 1107–1117. ISSN: 1551-3203.

[28] A. Bouharchouche, E.M. Berkouk, and T. Ghennam. "Control and energy management of a grid connected hybrid energy system PV-wind with battery energy storage for residential applications". In: *Ecological Vehicles and Renewable Energies (EVER), 2013 8th International Conference and Exhibition on*. Mar. 2013, pp. 1–11.

[29] R.F. Coelho, L. Schimtz, and D.C. Martins. "Grid-connected PV-wind-fuel cell hybrid system employing a supercapacitor bank as storage device to supply a critical DC load". In: *Telecommunications Energy Conference (INTELEC), 2011 IEEE 33rd International*. Oct. 2011, pp. 1–10.

[30] Józef Paska, Piotr Biczel, and Mariusz Kłos. "Hybrid power systems–An effective way of utilising primary energy sources". In: *Renewable Energy* 34.11 (2009), pp. 2414–2421.

[31] Caisheng Wang and M.H. Nehrir. "Power Management of a Stand-Alone Wind/Photovoltaic/Fuel Cell Energy System". In: *Energy Conversion, IEEE Transactions on* 23.3 (Sept. 2008), pp. 957–967. ISSN: 0885-8969.

[32] W. Gao et al. "PV - wind - fuel cell - electrolyzer micro-grid modeling and control in Real Time Digital Simulator". In: *Clean Electrical Power, 2009 International Conference on*. June 2009, pp. 29–34.

[33] K. Agbossou, M.L. Doumbia, and A. Anouar. "Optimal hydrogen production in a stand-alone renewable energy system". In: *Industry Applications Conference, 2005. Fourtieth IAS Annual Meeting. Conference Record of the 2005*. Vol. 4. Oct. 2005, pp. 2932–2936.

[34] Nooshin Bigdeli. "Optimal management of hybrid PV/fuel cell/battery power system: A comparison of optimal hybrid approaches". In: *Renewable and Sustainable Energy Reviews* 42 (2015), pp. 377–393.

[35] Sihem Nasri, Ben Slama Sami, and Adnane Cherif. "Power management strategy for hybrid autonomous power system using hydrogen storage". In: *International Journal of Hydrogen Energy* 41.2 (2016), pp. 857–865.

[36] Laith M Halabi et al. "Performance analysis of hybrid PV/diesel/battery system using HOMER: A case study Sabah, Malaysia". In: *Energy Conversion and Management* 144 (2017), pp. 322–339.

[37] Zhenhua Jiang. "Power management of hybrid photovoltaic - fuel cell power systems". In: *Power Engineering Society General Meeting, 2006. IEEE*. 2006,

[38] Paddy Finn and Colin Fitzpatrick. "Demand side management of industrial electricity consumption: promoting the use of renewable energy through real-time pricing". In: *Applied Energy* 113 (2014), pp. 11–21.

[39] Erkan Dursun and Osman Kilic. "Comparative evaluation of different power management strategies of a stand-alone PV/Wind/PEMFC hybrid power system". In: *International Journal of Electrical Power & Energy Systems* 34.1 (2012), pp. 81–89. ISSN: 0142-0615.

[40] Arnau González et al. "Optimal sizing of a hybrid grid-connected photovoltaic and wind power system". In: *Applied Energy* 154 (2015), pp. 752–762.

[41] Hocine Belmili et al. "Sizing stand-alone photovoltaic–wind hybrid system: Techno-economic analysis and optimization". In: *Renewable and Sustainable Energy Reviews* 30 (2014), pp. 821–832.

[42] Juan P Torreglosa et al. "Control based on techno-economic optimization of renewable hybrid energy system for stand-alone applications". In: *Expert Systems with Applications* 51 (2016), pp. 59–75.

[43] Abdolvahhab Fetanat and Ehsan Khorasaninejad. "Size optimization for hybrid photovoltaic–wind energy system using ant colony optimization for continuous domains based integer programming". In: *Applied Soft Computing* 31 (2015), pp. 196–209.

[44] Dimitris Ipsakis et al. "Power management strategies for a stand-alone power system using renewable energy sources and hydrogen storage". In: *International Journal of Hydrogen Energy* 34.16 (2009). 4th Dubrovnik Conference 4th Dubrovnik Conference, pp. 7081–7095. ISSN: 0360-3199.

[45] Bahram Panahandeh et al. "Simulation of PV–wind-hybrid systems combined with hydrogen storage for rural electrification". In: *International Journal of Hydrogen Energy* 36.6 (2011), pp. 4185–4197.

[46] E. Ahmed and S. Yuvarajan. "Hybrid Renewable Energy System Using DFIG and Multilevel Inverter". In: *Green Technologies Conference, 2012 IEEE*. Apr. 2012, pp. 1–6.

[47] FJ Vivas et al. "H2RES2 simulator. A new solution for hydrogen hybridization with renewable energy sources-based systems". In: *International Journal of Hydrogen Energy* 42.19 (2017), pp. 13510–13531.

[48] Pablo García et al. "Optimal energy management system for stand-alone wind turbine/photovoltaic/hydrogen/battery hybrid system with supervisory control based on fuzzy logic". In: *International Journal of Hydrogen Energy* 38.33 (2013), pp. 14146–14158.

[49] José L Bernal-Agustín and Rodolfo Dufo-Lopez. "Simulation and optimization of stand-alone hybrid renewable energy systems". In: *Renewable and Sustainable Energy Reviews* 13.8 (2009), pp. 2111–2118.

[50] Diego Feroldi, Lucas Nieto Degliuomini, and Marta Basualdo. "Energy management of a hybrid system based on wind–solar power sources and bioethanol". In: *Chemical Engineering Research and Design* 91.8 (2013), pp. 1440–1455.

[51] Adel Brka, Ganesh Kothapalli, and Yasir M Al-Abdeli. "Predictive power management strategies for stand-alone hydrogen systems: Lab-scale validation". In: *International Journal of Hydrogen Energy* 40.32 (2015), pp. 9907–9916.

[52] C.M. Colson and M.H. Nehrir. "A review of challenges to real-time power management of microgrids". In: *Power Energy Society General Meeting, 2009. PES '09. IEEE.* July 2009, pp. 1–8.

[53] A. Ghazanfari et al. "Active Power Management of Multihybrid Fuel Cell/Supercapacitor Power Conversion System in a Medium Voltage Microgrid". In: *Smart Grid, IEEE Transactions on* 3.4 (Dec. 2012), pp. 1903–1910. ISSN: 1949-3053.

[54] B. Davat et al. "Fuel cell-based hybrid systems". In: *Advanced Electromechanical Motion Systems Electric Drives Joint Symposium, 2009. ELECTROMOTION 2009. 8th International Symposium on.* July 2009, pp. 1–11.

[55] A. Etxeberria et al. "Hybrid Energy Storage Systems for renewable Energy Sources Integration in microgrids: A review". In: *IPEC, 2010 Conference Proceedings.* Oct. 2010, pp. 532–537.

[56] Robert H. Lasseter. "Microgrid and Distributed Generation". In: *journal of energy engineering* (2007).

[57] V. Prema and K.U. Rao. "Predictive models for power management of a hybrid microgrid 2014; A review". In: *Advances in Energy Conversion Technologies (ICAECT), 2014 International Conference on.* Jan. 2014, pp. 7–12.

[58] Cinda Sandoval et al. "Energy management control strategy to improve the FC/SC dynamic behavior on hybrid electric vehicles: A frequency based distribution". In: *Renewable Energy* 105 (2017), pp. 407–418.

[59] Keyu Chen, Alain Bouscayrol, and Walter Lhomme. "Energetic macroscopic representation and inversion-based control: Application to an electric vehicle with an electrical differential". In: *Journal of Asian Electric Vehicles* 6.1 (2008), pp. 1097–1102.

[60] K. Rajashekara. "Hybrid fuel-cell strategies for clean power generation". In: *Industry Applications, IEEE Transactions on* 41.3 (May 2005), pp. 682–689. ISSN: 0093-9994.

[61] Andres Hernandez, Daniel Hissel, and Rachid Outbib. "Modeling and fault diagnosis of a polymer electrolyte fuel cell using electrical equivalent analysis". In: *IEEE Transactions on Energy Conversion* 25.1 (2010), pp. 148–160.

[62] D Rowel. "Linear graph modeling: state equation formulation". In: *Massachusetts Institute of Technology Department of Mechanical Engineering* (2004).

[63] KS Agbli et al. "Multiphysics simulation of a PEM electrolyser: Energetic Macroscopic Representation approach". In: *international journal of hydrogen energy* 36.2 (2011), pp. 1382–1398.

[64] Henry M Paynter. *Analysis and design of engineering systems*. MIT press, 1961.

[65] Jean Thoma and B Ould Bouamama. *Modelling and simulation in thermal and chemical engineering: A bond graph approach*. Springer Science & Business Media, 2013.

[66] Peter J Gawthrop. "Bond-Graph Modelling and Causal Analysis of Biomolecular Systems". In: *Bond Graphs for Modelling, Control and Fault Diagnosis of Engineering Systems*. Springer, 2017, pp. 587–623.

[67] Dhafer Mezghanni et al. "Bond graph modelling of a photovoltaic system feeding an induction motor-pump". In: *Simulation Modelling Practice and Theory* 15.10 (2007), pp. 1224–1238.

[68] Abd Essalam Badoud et al. "Bond graph modeling and optimization of photovoltaic pumping system: Simulation and experimental results". In: *Simulation Modelling Practice and Theory* 36 (2013), pp. 84–103.

[69] Tore Bakka and Hamid Reza Karimi. "Bond graph modeling and simulation of wind turbine systems". In: *Journal of Mechanical Science and Technology* 27.6 (2013), pp. 1843–1852.

[70] Rémi Saisset et al. "Bond Graph model of a PEM fuel cell". In: *Journal of Power Sources* 156.1 (2006), pp. 100–107.

[71] Xavier Roboam X. and Stéphan Astier. "Graphes de liens causaux pour systèmes à énergie renouvelable (partie 1)". In: *Techniques de l'ingénieur Systèmes électriques pour énergies renouvelables* ref. article : d3970 (2006).

[72] Xavier Roboam X. and Stéphan Astier. "Graphes de liens causaux pour systèmes à énergie renouvelable (partie 2)". In: *Techniques de l'ingénieur Systèmes électriques pour énergies renouvelables* ref. article : d3971 (2006).

[73] Ching Chuen Chan, Alain Bouscayrol, and Keyu Chen. "Electric, hybrid, and fuel-cell vehicles: Architectures and modeling". In: *IEEE transactions on vehicular technology* 59.2 (2010), pp. 589–598.

[74] R. Andouisi et al. "Bond graph modelling and dynamic study of a photovoltaic system using MPPT buck-boost converter". In: *IEEE International Conference on Systems, Man and Cybernetics*. Vol. 3. Oct. 2002, p. 6.

[75] AH Abdol Rahim et al. “An overview of polymer electrolyte membrane electrolyzer for hydrogen production: Modeling and mass transport”. In: *Journal of Power Sources* 309 (2016), pp. 56–65.

[76] Ahmad Haddad. “Modèle dynamique non linéaire de la pile à combustible du type PEM: application à la régulation de l’humidité dans la membrane électrolytique”. PhD thesis. Université de Technologie de Belfort-Montbeliard, 2009.

[77] Guillaume Fontès. “Modélisation et caractérisation de la pile PEM pour l’étude des interactions avec les convertisseurs statiques”. In: (2005).

[78] Samer Rabih. “Contribution à la modélisation de systèmes réversibles de types électrolyseur et pile à hydrogène en vue de leur couplage aux générateurs photovoltaïques”. PhD thesis. 2008.

[79] Haluk Görgün. “Dynamic modelling of a proton exchange membrane (PEM) electrolyzer”. In: *International journal of hydrogen energy* 31.1 (2006), pp. 29–38.

[80] SA Grigoriev et al. “Mathematical modeling and experimental study of PEM electrolysis”. In: *Proc. seventh European symp. on electrochemical engineering. Toulouse, France*. 2005, pp. 3–5.

[81] Daniel Hissel et al. “A review on existing modeling methodologies for PEM fuel cell systems”. In: *Fundamentals and developments of fuel cells cenference* (2008).

[82] Caisheng Wang, M. H. Nehrir, and S. R. Shaw. “Dynamic models and model validation for PEM fuel cells using electrical circuits”. In: *IEEE Transactions on Energy Conversion* 20.2 (June 2005), pp. 442–451. ISSN: 0885-8969.

[83] Ozcan Atlam and Mohan Kolhe. “Equivalent electrical model for a proton exchange membrane (PEM) electrolyser”. In: *Energy Conversion and management* 52.8 (2011), pp. 2952–2957.

[84] C. Martinson et al. “Equivalent electrical circuit modelling of a Proton Exchange Membrane electrolyser based on current interruption”. In: *2013 IEEE International Conference on Industrial Technology (ICIT)*. Feb. 2013, pp. 716–721.

[85] Pierre Olivier. “Modélisation et analyse du comportement dynamique d’un système d’électrolyse PEM soumis à des sollicitations intermittentes: Approche Bond Graph”. PhD thesis. Lille 1, 2016.

[86] Dimitris Ipsakis et al. “The effect of the hysteresis band on power management strategies in a stand-alone power system”. In: *Energy* 33.10 (2008), pp. 1537–1550.

[87] G Bruni et al. “Energy management in a domestic microgrid by means of model predictive controllers”. In: *Energy* 108 (2016), pp. 119–131.

[88] M. Dahmane et al. “Renewable energy management algorithm for stand-alone system”. In: *2013 International Conference on Renewable Energy Research and Applications (ICRERA)*. Oct. 2013, pp. 621–626.

[89] Moamar Sayed Mouchaweh. “Diagnostic des Systèmes dynamiques hybrides (SDH)”. In: *Techniques de l’ingénieur Méthodes de production* ref. article : ag3542 (2016).

[90] Michel Bertrand, Claude Iung, and Janan Zaytoon. “Systemes dynamiques hybrides Modelisation et simulation”. In: *Techniques de l’ingénieur Modélisation et analyse de systèmes asservis* ref. article : s7105 (2015).

[91] Wolfgang Borutzky. *Bond Graph Model-based Fault Diagnosis of Hybrid Systems.* Springer, 2015.

[92] Latéfa Ghomri and Alla Hassane. “Continuous Petri Nets and Hybrid Automata for the analysis of manufacturing systems”. In: *IFAC-PapersOnLine* 48.3 (2015), pp. 1024–1029.

[93] Zhiwei Gao, Carlo Cecati, and Steven X Ding. “A survey of fault diagnosis and fault-tolerant techniques—Part I: Fault diagnosis with model-based and signal-based approaches”. In: *IEEE Transactions on Industrial Electronics* 62.6 (2015), pp. 3757–3767.

[94] Rajeev Alur et al. “The algorithmic analysis of hybrid systems”. In: *Theoretical computer science* 138.1 (1995), pp. 3–34.

[95] J. Lygeros et al. “Dynamical properties of hybrid automata”. In: *Automatic Control, IEEE Transactions on* 48.1 (Jan. 2003), pp. 2–17.

[96] A. Schwarze et al. “Modelling driving behaviour using hybrid automata”. In: *IET Intelligent Transport Systems* 7.2 (June 2013), pp. 251–256. ISSN: 1751-956X.

[97] David Rene and Alla Hassane. “Discrete, continuous, and hybrid Petri Nets”. In: *NY: Springer-Verlag* (2005).

[98] C. Valentin and C. Rimlinger. “Control verification of a chemical automated process by mixed Petri nets”. In: *Robotics and Automation, 2002. Proceedings. ICRA ’02. IEEE International Conference on.* Vol. 1. 2002, 84–89 vol.1.

[99] Pieter J Mosterman and Gautam Biswas. “Modeling discontinuous behavior with hybrid bond graphs”. In: *Proc. of the Intl. Conference on Qualitative Reasoning, Amsterdam, the Netherlands.* 1995, pp. 139–147.

[100] Wassim M Haddad, Sergey G Nersesov, and VijaySekhar Chellaboina. “Energy-based control for hybrid port-controlled Hamiltonian systems”. In: *Automatica* 39.8 (2003), pp. 1425–1435.

[101] R. Goebel, R.G. Sanfelice, and A. Teel. “Hybrid dynamical systems”. In: *Control Systems, IEEE* 29.2 (Apr. 2009), pp. 28–93.

[102] H. Alla and L. Ghomri. “Modeling and simulation by hybrid Petri nets”. In: *Proceedings of the 2012 Winter Simulation Conference (WSC).* Dec. 2012, pp. 1–8.

[103] David Harel. “Statecharts: A visual formalism for complex systems”. In: *Science of computer programming* 8.3 (1987), pp. 231–274.

[104] Yonit Kesten and Amir Pnueli. "Timed and hybrid statecharts and their textual representation". In: *International Symposium on Formal Techniques in Real-Time and Fault-Tolerant Systems*. Springer. 1992, pp. 591–620.

[105] K. Tsuda et al. "Reconfiguration strategies for hybrid systems". In: *Proceedings of the 2001 American Control Conference. (Cat. No.01CH37148)*. Vol. 2. 2001, 868–873 vol.2.

[106] S. Yin et al. "Data-Based Techniques Focused on Modern Industry: An Overview". In: *IEEE Transactions on Industrial Electronics* 62.1 (Jan. 2015), pp. 657–667. ISSN: 0278-0046.

[107] S. Shenghao et al. "The fault element diagnosis model of weighed directed bipartite graph based on Bayesian suspected degree". In: *2015 IEEE Advanced Information Technology, Electronic and Automation Control Conference (IAEAC)*. Dec. 2015, pp. 748–752.

[108] Pierpaolo Polverino et al. "Model-based diagnosis through Structural Analysis and Causal Computation for automotive Polymer Electrolyte Membrane Fuel Cell systems". In: *Journal of Power Sources* 357 (2017), pp. 26–40.

[109] Enno Ruijters and Mariëlle Stoelinga. "Fault tree analysis: A survey of the state-of-the-art in modeling, analysis and tools". In: *Computer science review* 15 (2015), pp. 29–62.

[110] Venkat Venkatasubramanian et al. "A review of process fault detection and diagnosis: Part I: Quantitative model-based methods". In: *Computers & chemical engineering* 27.3 (2003), pp. 293–311.

[111] B Ould Bouamama et al. "Graphical methods for diagnosis of dynamic systems: Review". In: *Annual Reviews in Control* 38.2 (2014), pp. 199–219.

[112] Mogens Blanke et al. *Diagnosis and fault-tolerant control*. Vol. 2. Springer, 2006.

[113] Nathalie Verdiere, Carine Jauberthie, and Louise Trave-Massuyes. "Functional diagnosability and detectability of nonlinear models based on analytical redundancy relations". In: *Journal of Process Control* 35 (2015), pp. 1–10.

[114] Marcel Staroswiecki and G Comtet-Varga. "Analytical redundancy relations for fault detection and isolation in algebraic dynamic systems". In: *Automatica* 37.5 (2001), pp. 687–699.

[115] Chang Boon Low et al. "Causality Assignment and Model Approximation for Hybrid Bond Graph: Fault Diagnosis Perspectives". In: *Automation Science and Engineering, IEEE Transactions on* 7.3 (July 2010), pp. 570–580. ISSN: 1545-5955.

[116] B Ould-Bouamama et al. "Bond graphs for the diagnosis of chemical processes". In: *Computers & chemical engineering* 36 (2012), pp. 301–324.

[117] W Borutzky. "Fault indicators and adaptive thresholds from hybrid system models". In: *IFAC Proceedings Volumes* 45.2 (2012), pp. 392–397.

[118] Sanjoy K Ghoshal, Subrata Samanta, and Arun K Samantaray. "Robust fault detection and isolation of hybrid systems with uncertain parameters". In: *Proceedings of the Institution of Mechanical Engineers, Part I: Journal of Systems and Control Engineering* 226.8 (2012), pp. 1013–1028.

[119] H. Al-Sheikh and N. Moubayed. "Fault detection and diagnosis of renewable energy systems: An overview". In: *2012 International Conference on Renewable Energies for Developing Countries (REDEC)*. Nov. 2012, pp. 1–7.

[120] RF Mesquita Brandão, JA Beleza Carvalho, and FP Maciel Barbosa. "Application of neural networks for failure detection on wind turbines". In: *PowerTech, 2011 IEEE Trondheim*. IEEE. 2011, pp. 1–6.

[121] Abd Badoud et al. "Bond Graph Algorithms for Fault Detection and Isolation in Wind Energy Conversion." In: *Arabian Journal for Science & Engineering (Springer Science & Business Media BV)* 39.5 (2014).

[122] B. Lu et al. "A review of recent advances in wind turbine condition monitoring and fault diagnosis". In: *2009 IEEE Power Electronics and Machines in Wind Applications*. June 2009, pp. 1–7.

[123] Kuei-Hsiang Chao, Sheng-Han Ho, and Meng-Hui Wang. "Modeling and fault diagnosis of a photovoltaic system". In: *Electric Power Systems Research* 78.1 (2008), pp. 97–105.

[124] Yuchuan Wu, Qinli Lan, and Yaqin Sun. "Application of BP neural network fault diagnosis in solar photovoltaic system". In: *Mechatronics and Automation, 2009. ICMA 2009. International Conference on*. IEEE. 2009, pp. 2581–2585.

[125] Abdel Aitouche, Quan Yang, and B Ould Bouamama. "Fault detection and isolation of PEM fuel cell system based on nonlinear analytical redundancy-An application via parity space approach". In: *The European Physical Journal Applied Physics* 54.2 (2011), p. 23408.

[126] N Yousfi Steiner et al. "Model-based diagnosis for proton exchange membrane fuel cells". In: *Mathematics and Computers in Simulation* 81.2 (2010), pp. 158–170.

[127] ME Lebbal and Stéphane Lecœuche. "Identification and monitoring of a PEM electrolyser based on dynamical modelling". In: *International journal of hydrogen energy* 34.14 (2009), pp. 5992–5999.

[128] I. F. Daniel et al. "Monitoring and diagnosis of the inverter from a renewable energy system". In: *2012 International Conference and Exposition on Electrical and Power Engineering*. Oct. 2012, pp. 167–171.

[129] Liyan Zhang and Alex Q Huang. "Model-based fault detection of hybrid fuel cell and photovoltaic direct current power sources". In: *Journal of Power Sources* 196.11 (2011), pp. 5197–5204.

[130] P. J. Gawthrop and G. P. Bevan. "Bond-graph modeling". In: *IEEE Control Systems* 27.2 (Apr. 2007), pp. 24–45. ISSN: 1066-033X.

[131] Wolfgang Borutzky. *Bond graph methodology: development and analysis of multidisciplinary dynamic system models*. Springer Science & Business Media, 2009.

[132] C Sueur and G Dauphin-Tanguy. "Structural controllability/observability of linear systems represented by bond graphs". In: *Journal of the Franklin Institute* 326.6 (1989), pp. 869–883.

[133] Controllab. *20sim*. Version 4.6.

[134] B Ould-Bouamama et al. "Model builder using functional and bond graph tools for FDI design". In: *Control Engineering Practice* 13.7 (2005), pp. 875–891.

[135] Diogo MF Santos, César AC Sequeira, and José L Figueiredo. "Hydrogen production by alkaline water electrolysis". In: *Química Nova* 36.8 (2013), pp. 1176–1193.

[136] Belkacem Ould Bouamama and Geneviève Dauphin-Tanguy. "Modélisation par bond graph: application aux systèmes energétiques". In: *Techniques de l'ingénieur. Génie énergétique* BE8281 (2006).

[137] Matías A Nacusse and Sergio J Junco. "Switchable structured bond: A bond graph device for modeling power coupling/decoupling of physical systems". In: *Journal of Computational Science* 5.3 (2014), pp. 450–462.

[138] W Borutzky. "Discontinuities in a bond graph framework". In: *Journal of the Franklin Institute* 332.2 (1995), pp. 141–154.

[139] Geneviève Dauphin-Tanguy and Christian Rombaut. "Why a unique causality in the elementary commutation cell bond graph model of a power electronics converter". In: *Systems, Man and Cybernetics, 1993.'Systems Engineering in the Service of Humans', Conference Proceedings., International Conference on*. IEEE. 1993, pp. 257–263.

[140] Yew Chai Paw and Gary J Balas. "Parametric uncertainty modeling for LFT model realization". In: *Computer-Aided Control Systems, 2008. CACSD 2008. IEEE International Conference on*. IEEE. 2008, pp. 834–839.

[141] Mohand Arab Djeziri et al. "LFT Bond Graph Model-Based Robust Fault Detection and Isolation". In: *Bond Graph Modelling of Engineering Systems*. Springer, 2011, pp. 105–133.

[142] Mohand Arab Djeziri et al. "Robust fault diagnosis by using bond graph approach". In: *IEEE/ASME Transactions on Mechatronics* 12.6 (2007), pp. 599–611.

[143] Mohand Arab Djeziri. "Diagnostic des Systèmes Incertains par l'Approche Bond Graph". PhD thesis. Ecole Centrale de Lille, 2007.

[144] Ibrahim Abdallah, Anne-Lise Gehin, and Belkacem Ould Bouamama. "Functional Hybrid Bond Graph for Operating Mode Management". In: *IFAC-PapersOnLine* 49.5 (2016), pp. 327–332.

[145] B. Ould Bouamama et al. “Fault detection and isolation of smart actuators using bond graphs and external models”. In: *Control Engineering Practice* 13.2 (2005), pp. 159–175. ISSN: 0967-0661.

[146] M Khemliche, B Ould Bouamama, and H Haffaf. “Sensor placement for component diagnosability using bond-graph”. In: *Sensors and Actuators A: Physical* 132.2 (2006), pp. 547–556.

[147] H Mohamed Basri et al. “Fault detection using dynamic parity space approach”. In: *Power Engineering and Optimization Conference (PEDCO) Melaka, Malaysia, 2012 Ieee International.* IEEE. 2012, pp. 52–56.

[148] Anne-Lise Gehin and Marcel Staroswiecki. “Reconfiguration analysis using generic component models”. In: *Systems, Man and Cybernetics, Part A: Systems and Humans, IEEE Transactions on* 38.3 (2008), pp. 575–583.

[149] Yun Tiam Tan, Daniel S Kirschen, and Nicholas Jenkins. “A model of PV generation suitable for stability analysis”. In: *IEEE Transactions on energy conversion* 19.4 (2004), pp. 748–755.

[150] MA Hasan and SK Parida. “An overview of solar photovoltaic panel modeling based on analytical and experimental viewpoint”. In: *Renewable and Sustainable Energy Reviews* 60 (2016), pp. 75–83.

[151] Vun Jack Chin, Zainal Salam, and Kashif Ishaque. “Cell modelling and model parameters estimation techniques for photovoltaic simulator application: A review”. In: *Applied Energy* 154 (2015), pp. 500–519.

[152] B. K. Dey et al. “Mathematical modelling and characteristic analysis of Solar PV Cell”. In: *2016 IEEE 7th Annual Information Technology, Electronics and Mobile Communication Conference (IEMCON).* Oct. 2016, pp. 1–5.

[153] Michael J Moran et al. *Fundamentals of engineering thermodynamics.* John Wiley & Sons, 2010.

[154] Francesco Marangio, Massimo Santarelli, and M Cali. “Theoretical model and experimental analysis of a high pressure PEM water electrolyser for hydrogen production”. In: *International Journal of Hydrogen Energy* 34.3 (2009), pp. 1143–1158.

[155] A Awasthi, Keith Scott, and S Basu. “Dynamic modeling and simulation of a proton exchange membrane electrolyzer for hydrogen production”. In: *International journal of hydrogen energy* 36.22 (2011), pp. 14779–14786.

[156] Marie-Cécile Pera et al. *Electrochemical components.* John Wiley & Sons, 2013.

[157] R García-Valverde, N Espinosa, and A Urbina. “Simple PEM water electrolyser model and experimental validation”. In: *international journal of hydrogen energy* 37.2 (2012), pp. 1927–1938.

[158] Houcheng Zhang et al. “Efficiency calculation and configuration design of a PEM electrolyzer system for hydrogen production”. In: *International Journal of Electrochemical Science* 7.4 (2012), pp. 4143–4157.

[159] Alejandro Lopez Pareja. “Evaluation of Gløshaugen wind conditions”. MA thesis. NTNU, 2016.

[160] Shucheng Sun et al. “Behaviors of a proton exchange membrane electrolyzer under water starvation”. In: *Rsc Advances* 5.19 (2015), pp. 14506–14513.

Event-Driven Hybrid Bond Graph

Application: Hybrid Renewable Energy System for Hydrogen Production and Storage

Abstract

From a general perspective, this research work constitutes a general contribution towards a simpler modelling and diagnosis of the multidisciplinary hybrid systems. Hybrid renewable energy systems where hydrogen, as an energy vector, is used to store the surplus of the renewable power fits perfectly under this description. Such system gathers different energetic components which are needed to be connected or disconnected according to different operating conditions. These different switching configurations generate different operating modes and depend on the intermittency of the primary sources, the production needs, the storage capacities and the operational availability of the different material resources that constitute the system. The switching behaviour engenders a variable dynamic which is hard to be expressed mathematically without investigating all the operating modes. This modelling difficulty is transmitted to affect all the model-based tasks such as the diagnosis and the operating mode management. To solve this problematic, a new modelling tool, called event-driven hybrid bond graph, is developed. Entirely graphic, the proposed formalism allows a multidisciplinary global modelling for all the operating modes of the hybrid system at once. By separating the continuous dynamic driven by the bond graph, from the discrete states modelled by an integrated automaton, the proposed approach simplifies the management of the operating modes. The model issued using this methodology is also well-adapted to perform a robust diagnosis which is achievable without referring back to the analytical description of the model. The operating mode management, when associated with the on-line diagnosis, allows the implementation of reconfiguration strategies and protection protocols when faults are detected. This thesis is written in 5 chapters. After a general introduction that presents the context and the problematic, the first chapter presents the state of art of the modelling and the diagnosis of the multi-sources systems. The proposed event-driven hybrid bond graph is detailed in chapter 2. The third chapter introduces the diagnosis and the operating mode management. Chapter 4 presents the application and chapter 5 is preserved for the general conclusion.

CRIStAL

Centre de Recherche en Informatique, Signal et Automatique de Lille – CNRS UMR 9189 – Avenue Paul Langevin – 59650 Villeneuve d'Ascq

Bond Graph hybride piloté par événements

Application : Système d'énergie renouvelable hybride pour la production et le stockage de l'hydrogène

Résumé

Ce travail de thèse constitue, d'un point de vue général, une contribution à la modélisation et au diagnostic des systèmes multi-domaines hybrides. Il est appliqué à la supervision des systèmes multi-sources de production d'énergie propre où l'hydrogène est utilisé comme moyen de stockage. Un tel système associe des composantes énergétiques de nature différente et fait l'objet de commutations produites par la connexion et la déconnection d'un ou plusieurs composants. Ces commutations génèrent différents modes de fonctionnement et sont liées à l'intermittence des sources primaires, aux besoins de production, aux capacités de stockage et à la disponibilité opérationnelle des ressources matérielles qui constituent le système. La présence de ces commutations engendre une dynamique variable qui est classiquement difficile à exprimer mathématiquement sans exploiter tous les modes. Ces difficultés de modélisation se propagent pour affecter toutes les tâches dépendantes du modèle comme le diagnostic et la gestion de modes de fonctionnement. Pour résoudre ces problématiques, un nouvel outil, appelé, Bond Graph Hybride piloté par événements a été développé. Entièrement graphique, le formalisme proposé permet une modélisation interdisciplinaire globale du système quel que soit son mode de fonctionnement. En séparant la dynamique continue gérée par le Bond Graph Hybride des états discrets modélisés par un automate intégré au formalisme, l'approche proposée simplifie la gestion des modes de fonctionnement. Le modèle issu de cette méthodologie est également bien adapté au diagnostic robuste, réalisable sans recourir aux équations analytiques. Cette gestion des modes de fonctionnement associée au diagnostic robuste permet l'implémentation de stratégies de reconfiguration et de protection en présence de défaillances. Le mémoire de thèse est décomposé en cinq chapitres. Après une introduction générale qui présente le contexte et la problématique, le premier chapitre présente un état de l'art sur la modélisation et la supervision des systèmes multi-sources. Le BGH piloté par événement est détaillé dans le deuxième chapitre. Le troisième chapitre est consacré au diagnostic et à la gestion des modes de fonctionnement. Le quatrième chapitre présente l'application et le cinquième donne une conclusion générale.